

Dissertation
submitted to the
Combined Faculties for the Natural Sciences and for Mathematics
of the Ruperto Carola University of
Heidelberg, Germany
for the degree of
Doctor of Natural Sciences

presented by

Diplom-Physiker **Frank Fleischer**
born in Dortmund

Oral examination: 24/05/2005

Measurement of the
Decay Rate of
the Negative Positronium Ion

Referees: Prof. Dr. Dirk Schwalm
Prof. Dr. Jürgen Kluge

Kurzfassung

Messung der Zerfallsrate des negativen Positronium-Ions

Das aus einem Positron und zwei Elektronen ($e^+e^-e^-$) zusammengesetzte negative Positronium-Ion (Ps^-) stellt eines der einfachsten gebundenen Dreikörpersysteme dar. Es besteht aus stabilen, punktförmigen Teilchen, und wegen der geringen Teilchenmassen ist es weitgehend frei von Störungen durch die starke Wechselwirkung. Diese Eigenschaften sowie das ungewöhnliche Massenverhältnis lassen das Positronium-Ion zu einem interessanten Studienobjekt zur Untersuchung des quantenmechanischen Dreikörperproblems werden. Trotz einer Vielzahl theoretischer Arbeiten beschränken sich die veröffentlichten experimentellen Ergebnisse bislang auf einen Nachweis der Existenz von Ps^- und eine erste Messung seiner Zerfallsrate, deren Fehler mit 4,3% noch eine Größenordnung über der theoretischen Genauigkeit liegt. In der vorliegenden Arbeit wird nach einem kurzen Überblick über die bislang veröffentlichten theoretischen Ergebnisse eine neue Messung der Zerfallsrate vorgestellt. Diese umfasst einerseits ein Testexperiment nach dem schon früher verwendeten Prinzip, andererseits eine präzisere Messung, die auf einer verbesserten Nachweismethode basiert und den experimentellen Fehler auf 0,8% reduziert. Darüberhinaus wird die mit dem vorhandenen Aufbau maximal erreichbare Genauigkeit abgeschätzt, und die Möglichkeiten für weitere Experimente an der neuen, intensiven Positronenquelle NEPOMUC am Forschungsreaktor FRM II in München werden diskutiert.

Abstract

Measurement of the Decay Rate of the Negative Positronium Ion

Consisting of a positron and two electrons ($e^+e^-e^-$), the negative ion of positronium (Ps^-) is one of the simplest three-body systems with a bound state. Its constituents are stable, point-like particles, and due to the small particle masses, it is essentially free from perturbations by strong interaction effects. Together with the rather unique mass ratio, these properties make the Ps^- ion an interesting object for studying the quantum-mechanical three-body problem. Despite numerous theoretical investigations, the published experimental results are so far limited to first observation and a single decay rate measurement. With a precision of 4.3%, its error is still an order of magnitude larger than the theoretical uncertainty. In this thesis, after giving a short review of the currently available theoretical results, a new determination of the decay rate is reported. This includes an exploratory experiment along the lines of the old one and a more precise measurement using an improved detection method. In the latter one, the error has been reduced to 0.8%. Moreover, the maximum precision that can be reached with the current set-up is investigated, and the prospects for further experiments at the new high-intensity positron source NEPOMUC at the FRM II research reactor in Munich are discussed.

Contents

1	Introduction	3
2	Review of Ps^- theory	5
2.1	Ground-state properties of Ps^-	5
2.2	Annihilation and decay rates	12
2.3	Excitation and resonances	17
2.4	Ps^- : Atom or molecule?	22
2.5	Conclusion	23
3	The Heidelberg Ps^- set-up	25
3.1	The positron source	25
3.2	Creating slow positrons by moderation	27
3.3	Magnetic transport and energy selection	29
3.4	Production of positronium negative ions	31
4	Measurement of the decay rate	35
4.1	Principle of the decay rate experiment and set-up	35
4.2	The γ -method	38
4.2.1	The set-up for the γ -method	40
4.2.2	Results	41
4.3	The stripping method	46
4.3.1	The stripping set-up	47
4.3.2	Results	58
4.4	Discussion of systematic errors	68
4.4.1	The low-energy positron beam	68
4.4.2	The acceleration voltages	69
4.4.3	The linear translation stage	69
4.4.4	Field inhomogeneities between the Ps^- foil and the acceleration grid	70

4.5	Conclusion	73
5	Experiments at the NEPOMUC positron source	75
5.1	NEPOMUC: principle of operation and status	75
5.2	A high statistics decay rate measurement	77
5.3	Photodetachment experiments	77
5.4	The $3\gamma/2\gamma$ -branching ratio	80
5.5	Other possible experiments	81
6	Conclusion and outlook	83
	References	85
	Appendix	93
A	Parameters for operating the Ps^- set-up	94
B	Parameters used in the stripping measurement	95
C	Decay rate measurement data	96
C.1	Runs #2 and #4 at $U = 1000\text{ V}$	96
C.2	Run #7 at $U = 1300\text{ V}$	100
C.3	Run #5 at $U = 1900\text{ V}$	104
C.4	Runs #1 and #3 at $U = 3900\text{ V}$	108
C.5	Run #6 at $U = 4000\text{ V}$	112
C.6	Runs #8 and #10 at $U = 4800\text{ V}$	116
C.7	Run #9 at $U = 3900\text{ V}$	120

Chapter 1

Introduction

For several decades it has been known that there is a particle-stable bound state consisting of a positron and two electrons. The first one to discover this was J.A. Wheeler, who calculated a lower limit for its binding energy in 1946 [Whe46], using the variational principle of Ritz with a 3-parameter Hylleraas-type wave function. Obtaining an expectation value of -6.96 eV, he concluded that the second electron is bound by at least 0.19 eV with respect to the ground state of positronium — calculated to have an energy of -6.77 eV in the same paper. For such systems made of electrons and positrons he proposed the name “polyelectrons”. He could not establish the stability of species consisting of more than 3 particles, nevertheless, he suggested that larger clusters of electrons and positrons might explain the nature of the mesons, which had been discovered in the cosmic radiation not long before.

While the two-body polyelectron — today known as positronium — has been the object of intense studies both on the theoretical and experimental side, the three-body polyelectron or positronium ion (Ps^-) almost exclusively found the interest of theoreticians. Up to now, a considerable number of articles covering theoretical calculations of different parameters of the positronium ion have been published. In 1981 A.P. Mills succeeded in producing Ps^- using a beam-foil method [Mil81a]. He identified the ions by the Doppler-shifted annihilation radiation of Ps^- decaying in flight. With the same approach he made a first decay rate measurement of Ps^- in 1983 [Mil83]. So far these two experiments are the only experimental results on the positronium ion which have been published.

Both the neutral positronium atom and the Ps^- ion exhibit a number of attractive features, which also explains the theoretical interest in these systems. According to our present knowledge, their constituents, electrons and positrons, are stable, point-like particles without any structure. To a very good approximation Ps and Ps^- are purely quantum-electrodynamical systems: the contributions of strongly interacting particle loops are negligible because of the small mass. Therefore, neutral positronium offers the ideal testing

ground for QED-based bound-state calculations. Other simple atomic systems like hydrogen have to deal with nuclear size effects; in fact the theoretical prediction of the atomic properties of hydrogen is limited by the poor knowledge of the proton charge radius. By turning the problem around and assuming the validity of bound-state QED, a comparison of higher order calculations and precision measurements of simple atomic systems can be used to determine such nuclear parameters. Obviously this approach excludes a use of the experimental data as a test of QED. As pointed out in [Kar02], positronium (being free from the effects mentioned above) is ideally suited for high precision QED tests. The positronium ion in principle has the same advantages, but due to the complication introduced by the third particle it is less interesting as a high precision QED test. On the other hand it is just the three-body nature of Ps^- which makes this an attractive system to study: with all three constituents having the same mass, the positronium ion has a rather unique mass ratio between H_2^+ and H^- . Therefore, it is intrinsically a three-body problem, and simplifications like the Born-Oppenheimer approximation or the assumption of an infinitely heavy nucleus are not applicable. Lying in the middle between the two extremes of ${}^\infty\text{H}_2^+$ and ${}^\infty\text{H}^-$, Ps^- also allows for a study of the transition from the atomic to the molecular set of quantum numbers. Altogether, it is ideally suited to test the different approaches which have been applied to the solution of the quantum-mechanical three-body problem.

This thesis reports on a new measurement of the decay rate of Ps^- ; it has been written at the Max Planck Institute for Nuclear Physics in Heidelberg in the framework of a project which is aimed at the long overdue experimental investigation of the positronium ion. As it turned out to be difficult to reach a significantly higher precision with the original technique employed in [Mil83], the experiment was performed using an improved approach to the problem of detecting the Ps^- ions. After a short discussion of an exploratory measurement along the lines of Mills's decay rate experiment, the new method is introduced, and the obtained results are presented. In view of a planned continuation of the decay rate experiment at the new high-intensity positron source NEPOMUC at the FRM II research reactor in Munich, the different contributions to the experimental error are investigated in order to assess the limits of precision that can be finally reached. Due to the lack of a review article on the Ps^- theory, also a synopsis of the theory of the positronium ion is given. The thesis concludes with a discussion of further possibilities for experiments on the properties of the positronium ion. With a measurement of the photodetachment cross section to determine the binding energy of Ps^- and to look for the predicted doubly excited resonances or a measurement of the $3\gamma/2\gamma$ branching ratio, they concern parameters for which so far no experimental information has been obtained.

Chapter 2

Review of Ps^- theory

While there has not been much experimental activity regarding the positronium ion, quite some work has been published on the theoretical study of this system. This chapter gives a brief review of the theory of Ps^- and its results. By no means it is claimed to be complete; it is rather a selection. Nevertheless, it will be tried to give an overview of the present knowledge about this exotic ion.

Section 2.1 starts with an overview of the ground-state properties of the positronium ion. Next, section 2.2 summarises the results on the different decay branches, and in section 2.3 excitations and resonances are considered. Finally, the chapter ends with a short discussion of Ps^- from the point of view of general Coulombic three-body systems (section 2.4) and some concluding remarks in sec. 2.5.

2.1 Ground-state properties of Ps^-

Consisting of a positron and two electrons, the positronium ion (Ps^-) represents the probably simplest three-body system. Its constituents are stable, point-like particles and to a very high level of precision the electromagnetic interaction is the only one which contributes significantly to its properties.

As in the case of H^- , the ground state is the only state which is stable against dissociation. In this state the two electrons are in a singlet S-state, the parity is even ($^S L^\pi = ^1 S^e$).

The positronium ion represents a genuine three-body problem, where simplifications like the Born-Oppenheimer approximation or the assumption of an infinitely heavy nucleus cannot be applied. With practically useful analytical solutions of the three-body problem being unavailable, a theoretical treatment is possible only on the basis of numerical approximations.

The Hamiltonian of Ps^- , given in atomic units ($\hbar = e = m_e = 1$), is

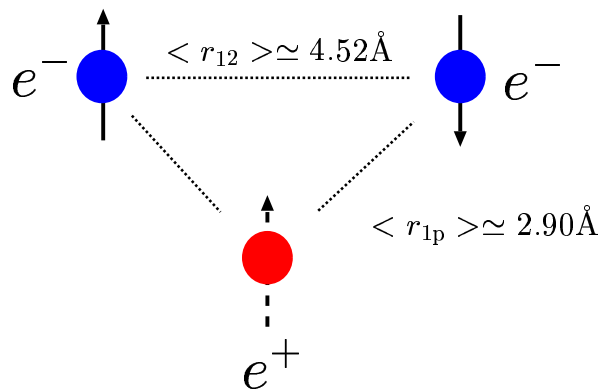


Figure 2.1: Average interparticle distances (cf. tab. 2.1) in the positronium negative ion.

$$H = \frac{\mathbf{p}_p^2}{2} + \frac{\mathbf{p}_1^2}{2} + \frac{\mathbf{p}_2^2}{2} + \frac{1}{|\mathbf{r}_1 - \mathbf{r}_2|} - \frac{1}{|\mathbf{r}_p - \mathbf{r}_1|} - \frac{1}{|\mathbf{r}_p - \mathbf{r}_2|}. \quad (2.1)$$

As a sufficiently precise wavefunction is the necessary prerequisite for all further theoretical considerations, quite a few attempts have been made to calculate this fundamental quantity. Basically, two different approaches have been tried: the majority of the authors presented calculations based on the variational principle of Ritz, others tried to obtain a non-variational solution of the Schrödinger equation by means of a method called ‘correlation function hyperspherical harmonics’ (CFHH) method. Both concepts, as well as the differences between the individual calculations and their results will be discussed in the following.

The variational principle of Ritz is based on the observation that plugging in the ground state wavefunction $|\Psi_0\rangle$ leads to the absolute minimum of the expectation value $\langle \Psi | H \Psi \rangle / \langle \Psi | \Psi \rangle$. Therefore, an arbitrary square-integrable function $|\Phi\rangle$ yields an upper limit to the ground state energy E_0 :

$$E_0 \leq \frac{\langle \Phi | H | \Phi \rangle}{\langle \Phi | \Phi \rangle}. \quad (2.2)$$

Now, a trial function with a number of variational parameters can be chosen and optimized to find the minimum expectation value for E ; sufficiently elaborate trial functions can yield very accurate results. Such variational calculations of the nonrelativistic Ps^- wavefunction have been carried out several times using increasingly sophisticated trial functions and optimization schemes.

Also the first calculations showing the stability of the system [Whe46, Hyl47] were based on this method. In the following, a brief survey of the somewhat more recent variational

calculations — including approximately the last 20 years and not meant to be complete — will be given.

The first work discussed here was published in 1983 by Ho [Ho83b]. He employed a set of Hylleraas-type basis functions

$$\Psi = \sum_{\substack{l \geq m \geq 0 \\ k \geq 0}} C_{klm} \exp[-\alpha(r_{1p} + r_{2p})] r_{12}^k (r_{1p}^l r_{2p}^m + r_{1p}^m r_{2p}^l), \quad (2.3)$$

where r_{12} , r_{1p} and r_{2p} are the interparticle distances between the electrons (1 and 2) and the positron (p), respectively (see fig. 2.1). Summing up to $(k + l + m) \leq \omega = 9$, 125 terms were included in the calculation. In order to facilitate the computation of the energy expectation value (2.2), he expressed the Hamiltonian (2.1) in the distance coordinates given above. By solving for the linear variational coefficients C_{klm} and by optimizing the nonlinear parameter α , an estimate for the ground state energy is obtained.

Bhatia and Drachman followed a similar approach [BD83], using the generalized Hylleraas form

$$\Psi(\mathbf{r}_{p1}, \mathbf{r}_{p2}) = (\sin \theta_{12})^L \sum_{\substack{l \geq L \\ m \geq L \\ n \geq 0}} C_{lmn} \left[r_{p1}^l r_{p2}^m \exp(\gamma r_{p1} + \delta r_{p2}) + (1 \leftrightarrow 2) \right] r_{12}^n \mathcal{D}_L^{0+}. \quad (2.4)$$

Here \mathbf{r}_{pi} are the vectors from the positron to the two electrons, L is the total orbital angular momentum and \mathcal{D}_L^{0+} is a function of the Euler angles to describe the spatial orientation of the vectors \mathbf{r}_{pi} . In the case of the $^1S^e$ ground state of the positronium negative ion, this reduces to

$$\Psi(\mathbf{r}_{p1}, \mathbf{r}_{p2}) = \frac{1}{\sqrt{8\pi^2}} \sum_{l,m,n} C_{lmn} \left[r_{p1}^l r_{p2}^m \exp(\gamma r_{p1} + \delta r_{p2}) + (1 \leftrightarrow 2) \right] r_{12}^n. \quad (2.5)$$

A variational calculation of the ground state was performed both under the restriction of setting the two nonlinear parameters equal ($\gamma = \delta$) and for the more general case, where γ and δ are chosen independently. In the latter case a significant improvement can be achieved. For the optimum choice of parameters one is about twice as large as the other; this reflects the geometrical structure of the positronium ion, which consists of a neutral positronium atom plus a second, loosely bound electron. Up to 220 terms have been included in these computations.

Another set of functions can be found in the work of Petelenz and Smith [PS87]. Their method is equivalent to a variational treatment with the trial function

$$\Psi(r_{1p}, r_{2p}, r_{12}) = \frac{1}{4\pi} \sum_{k=1}^N C_k [\exp(-\alpha_k r_{1p} - \beta_k r_{2p} - \gamma_k r_{12}) + (1 \leftrightarrow 2)]. \quad (2.6)$$

This is an exponential expansion, and only the linear parameters C_k can be obtained by solving the variational equations; the principal problem lies in finding a good strategy to choose the nonlinear coefficients α_k , β_k , γ_k . Here they have been generated in a pseudorandom manner from a set of only six nonlinear parameters. The trial function used contained 150 terms.

Two further steps have been taken by Ho: in 1990 he published a calculation of the same kind as in 1983, now including 946 terms ($\omega = 20$) [Ho90a]; a few years later, in 1993, he extended his method to use a double-basis set of functions like those in (2.3) [Ho93]. By using a sum of two such expansions, therein substituting the exponential factor by $\exp(-\alpha_i r_{1p} - \beta_i r_{2p})$, $i = 1, 2$, respectively, he was able to improve the results again. Physically, this can be understood as a better ability of the two independent function sets to describe the highly correlated inner part of the wavefunction and the outer parts accurately at the same time.

Meanwhile, a new treatment had been published by Frolov et al. They based their efforts on a variational expansion of the form given in (2.6). With up to 700 terms, choosing the nonlinear parameters pseudorandomly, a new record in producing the minimum energy expectation value was set at first [FY89]. But the method could not compete with Ho's double-basis approach [Ho93]. Only after inventing a two-stage strategy for high-precision variational calculations [Fro98], the so far lowest ground-state energy value in literature was obtained [Fro99]. This two-stage strategy splits the exponential variational expansion (2.6) in two parts: a smaller part of 200 terms with very carefully optimized nonlinear parameters and a much larger 1000-term function, whose parameters were only roughly (or even not at all) optimized.

The upper part of table 2.1 summarizes the numerical results of these works; given are the total energy E , the total decay rate Γ and the expectation values of the interparticle distances, $\langle r_{1p} \rangle$ and $\langle r_{12} \rangle$. Note that these results are purely nonrelativistic. Therefore, the binding energy of the second electron in the framework of such a calculation (or, in other words, the stability against dissociation into a neutral Ps atom¹ plus a free electron) can be obtained easily by subtracting the nonrelativistic energy of the positronium ground state,

¹ The absolute ground state of positronium is the ground state of para-Ps (1S_0), in which the electron and the positron are in a singlet spin state. The ortho-Ps ground state is higher in energy by the value of the hyperfine splitting of 203400 MHz (i.e. $8.4 \cdot 10^{-4}$ eV) [BP80]. However, with the calculations of Ps^- being purely nonrelativistic so far, it seems adequate to use the nonrelativistic energy levels of positronium.

Reference	$-E$ [a.u.]	Γ [ns^{-1}]	$\langle r_{1p} \rangle$ [a_0]	$\langle r_{12} \rangle$ [a_0]
[Whe46]	0.256			
[Ho83b]	0.26200490		5.4891	8.5476
[BD83]	0.262005065(2) ^a	2.0861		
[PS87]	0.262005070 ^a			
[Ho90b]	0.26200507021	2.08613	5.48963188	8.54857794
[Ho93]	0.26200507023294(9) ^a	2.0861222(5)	5.489633252	8.548580655
[Fro93]	0.2620050702319	2.086121(1)	5.4896332525	8.5485806553
[Fro98]	0.26200507023297	2.086121(1)	5.4896332525	8.5485806553
[Fro99]	0.262005070232978(4)	2.086122144	5.48963325238	8.54858065516
[HM89c]	0.26200486		5.488352	8.54611129
[KHM93]	0.26200467	2.08610(6)	5.28881	8.54699

^a The marked values have been obtained by extrapolation, therefore they may be lower than the exact value.

Table 2.1: Overview of the theoretical results regarding the total nonrelativistic ground state energy E , the total decay rate Γ and the average interparticle distance. The upper part of the table lists a number of variational calculations, the lower part two nonvariational treatments. The errors, if indicated, are those given in the respective references. Concerning the energy values one should keep in mind that these are purely nonrelativistic results. Due to the missing relativistic corrections, the physical precision is much lower (about five digits). More details can be found in the text.

$E_{\text{Ps}} = 0.25$ a.u., from the listed energy values. For the most precise calculation [Fro99], for example, this leads to $E_B = 0.0120050702329757$ a.u. = 0.326674721317821 eV. Here, as in [Fro99], a conversion factor of 27.2113961 eV/a.u. was used.

While it is easy to compare the success of different functions with respect to the ground state energy, there are no simple criteria to test the quality of the numerical wavefunctions obtained by this approach; in the end only the comparison of predicted quantities with experimental data allows to draw conclusions about the accuracy of the results. The minimum energy value alone does not give a reliable indication if the system is well described by the computed wavefunction. Especially it can be seen easily that the variational approach only tests the integral characteristics of the function. As there are regions which contribute very little to the expectation value of the Hamiltonian, this obviously does not necessarily require an adequate point-wise approximation of the true ground-state wavefunction. Furthermore, it is an inherent feature of the Ritz variational method that the wavefunction estimate is less precise than the energy estimate. It can be shown (see,

Reference	$\nu_{12} [a_0^{-1}]$	$\nu_{1p} [a_0^{-1}]$
[Ho83b]	0.4971	-0.4991
[BD83]	0.49508	-0.50000
[PS87]	0.4991688867	-0.4999877805
[Ho90b]	0.49968	-0.50002
[Ho93]	0.4999773	-0.5000020
[Fro93]	0.4999293	-0.49999708
[Fro98]	0.499972144320	-0.4999997640218
[Fro99]	0.499983153136046	-0.499999795011881

Table 2.2: Numerical values for the two-particle cusps ν_{12} (electron-electron) and ν_{1p} (electron-positron) as computed by the different authors. The exact values are $+0.5$ and -0.5 , respectively. More details can be found in the text.

for example, [Sch98]) that an error of $\mathcal{O}(\epsilon)$ in the wavefunction shows up only as an error of the order $\mathcal{O}(\epsilon^2)$ in the energy. Therefore, it is desirable to find other ways to check the accuracy of a numerically computed wavefunction. For systems interacting by Coulomb forces, a widely used test is provided by the evaluation of the so-called two-particle cusps

$$\nu_{ij} = \frac{\langle \Psi | \delta(r_{ij}) \frac{\partial}{\partial r_{ij}} | \Psi \rangle}{\langle \Psi | \delta(r_{ij}) | \Psi \rangle}, \quad (2.7)$$

with r_{ij} representing the distance between the particles i and j . The exact values of these cusps are

$$\nu_{ij} = q_i q_j \mu_{ij}, \quad (2.8)$$

where the q_i are the charges and μ_{ij} is the reduced mass of the particles i and j [Kat57]. Thus, in atomic units, $\nu_{12} = +0.5$ and $\nu_{1p} = -0.5$. This allows for an independent and, most importantly, local test of the wavefunction. Especially the regions of vanishing interparticle distances, which are crucial for any decay rate calculation, are probed. Again, we cannot expect this alone to be a sufficient condition for good-quality wavefunctions; indeed, it is possible to construct a trial function which reproduces the exact cusp values without providing accurate predictions of the bound-state properties [Fro99]. Table 2.2 lists the respective numerical values of ν_{ij} obtained in the variational works.

In order to resolve these problems, direct solutions of the three-body Schrödinger equation have been sought for. The mathematical framework for these endeavours was the so-called correlation function hyperspherical harmonic (CFHH) method, a multidimen-

sional generalization of the approach used in three-dimensional two-body problems (for a short summary and further references, see [HM89b, HM89a]). After separation of the centre-of-mass motion, the remaining $3N - 3$ spatial coordinates of an N -body system are transformed into one hyperradius R and $3N - 4$ dimensionless ‘hyperangles’ with a finite range of values. Now, the imposition of periodic boundary conditions allows for expressing functions of these coordinates in terms of discrete series, and this finally reduces the partial differential equation to a set of coupled ordinary differential equations. As the discretization for the two-body problem leads to the spherical harmonics, the hyperangular functions are called ‘hyperspherical harmonics’. In practical calculations, this method suffers from the problem that several important features of atomic wavefunctions cannot be adequately described by a small number of continuous hyperspherical harmonics. Examples are cusps at vanishing interparticle distances, where the potential is singular. Because of the consequent slow convergence, these calculations could not compete with the most advanced variational approaches. Haftel and Mandelzweig [HM89b, HM89a] proposed to separate the wavefunction into a product of two factors $\psi = \phi\chi$, where χ , the so-called correlation function, is chosen to account for the basic analytic structure. The remaining function ϕ should display a rather smooth behaviour, thus one can hope for a rapidly convergent expansion into hyperspherical harmonics.

The method has been applied to the positronium negative ion [HM89c], using the simple correlation function

$$\chi = \exp(-\gamma(r_{1p} + r_{2p}) - \delta r_{12}). \quad (2.9)$$

There are several meaningful possibilities to choose the parameters γ and δ , depending on which analytical feature of the wavefunction is given priority. Haftel and Mandelzweig tried four obvious parametrizations; the best results they obtained for their so-called ‘uncorrelated cusp parametrization’ ($\gamma = MZ/(M + 1) = 0.5$, $\delta = 0$), which takes the singularity of the Coulomb potential between electron and positron into account, while the one between the two electrons is neglected. The electron-positron cusp is especially important for the calculation of the decay rate, where a precise knowledge of the wavefunction at this singular point is needed.

A second investigation following this path can be found in [KHM93]. Setting out from the observation that the correlation function (2.9) could only reproduce the electron-positron cusp, they employed a more elaborate function to take into account all the cusps and the asymptotic behaviour of the wavefunction. Indeed, this refinement of the technique lead to a significant improvement in accuracy. The numerical results of both CFHH calculations are listed in the lower part of table 2.2. As they are based on a direct solution of the

Schrödinger equation, also these computations are purely nonrelativistic.

Concerning the binding energy, the large number of significant figures in the more precise of the results is somewhat misleading. As a physical quantity (as opposed to a mathematical measure of the properties of the trial function), it is certainly not meaningful without consideration of relativistic effects or QED contributions. A complete calculation of the lowest-order relativistic corrections has not yet been published. A partial evaluation can be found in [BD98]. There Bhatia and Drachman again applied their approach from 1983, this time including up to 615 terms in the expansion. More importantly, they considered the relativistic corrections to the energy and started to compute the relevant expectation values. Though not yet being complete, their results give an indication of the size of the relativistic effects: the so-far calculated terms lower the total energy by $3.38 \cdot 10^{-6}$ a.u. Also Frolov [Fro99] discusses the relativistic corrections, but an evaluation of the necessary expectation values is still missing. Accordingly, a calculation of these contributions would be the logical next step in the theoretical investigation of the Ps^- ground-state energy. Putting the so far published results together, one can adopt a theoretical best value of $E = -0.262008(5)$ a.u., the uncertainty being due to the incomplete knowledge of the relativistic contributions.

Another characteristic parameter of a bound state is the expectation value of the interparticle distances. Looking at the values $\langle r_{1p} \rangle$ and $\langle r_{12} \rangle$ in table 2.1, the rather large size of the positronium negative ion is remarkable: the two electrons are separated by a distance of several Ångström. It should be kept in mind, however, that the basic structure of the positronium negative ion is not that of an equilateral triangle; the two electron-positron distances are rather different. In fact, the system can be crudely described as a positronium atom plus a second, loosely bound electron [BD83].

2.2 Annihilation and decay rates

Although being stable against dissociation, the positronium ion has a rather short lifetime: it decays via electron-positron annihilation. Many aspects of the Ps^- decays can be understood in terms of the corresponding decay channels of neutral positronium. Given the above-mentioned geometrical structure, this is not too surprising: as a first approximation, the decay of the positronium negative ion can be considered as a positronium decay plus a spectator electron.

In the case of neutral positronium, there are two distinct spin states, depending on the relative spin orientation of the electron and the positron: on the one hand there is the singlet state 1S_0 (para-Ps), on the other the triplet state 3S_1 (ortho-Ps). Both decay by



Figure 2.2: The two lowest-order Feynman diagrams contributing to the 2γ decay amplitude $\mathcal{M}(e^+e^- \rightarrow n\gamma)$.

electron-positron annihilation, but due to their different behaviour under CP transformation, they differ in the possible numbers of final-state photons. While the singlet state ($\Gamma(\text{Ps}, {}^1S_0) = 7990.9(17) \mu\text{s}^{-1}$ [ARG94]) can decay only into an even number of photons, for the triplet state ($\Gamma(\text{Ps}, {}^3S_1) = 7.0404(10)(8) \mu\text{s}^{-1}$ [VZG03]) only odd numbers are possible. The situation in the Ps^- ion is different. The two electrons are in a relative singlet spin state, and as this is a spherically symmetric configuration, there is no preferred orientation of the positron spin. Therefore, either combination of electron and positron spins can occur, and a positronium ion may decay into any number of photons. With the presence of a third particle to help ensuring the energy-momentum conservation, even the one-photon decay is possible.

As expected, the total rate is by far dominated by the 2γ decay. The three-gamma decay and all channels involving more photons are higher-order effects in the QED perturbation expansion, and the one-gamma decay requires a three-body interaction, which is extremely unlikely. Already the crude picture of a Ps atom plus a spectator electron is able to explain some of the results; the $3\gamma/2\gamma$ branching ratio, for example, essentially reflects the ratio of the triplet and singlet positronium decay rates, weighted by their respective multiplicity: $\Gamma_{3\gamma}/\Gamma_{2\gamma} \approx 3\Gamma(\text{Ps}, {}^3S_1)/\Gamma(\text{Ps}, {}^1S_0)$

The first theoretical calculation of the (2γ and 3γ) decay rates has been given by Ferrante [Fer68], analogous to the corresponding computation for positronium (cf. [JR76]). The starting point is the matrix element $\mathcal{M}(e^+(\mathbf{p})e^-(\mathbf{q}) \rightarrow n\gamma)$ for free-particle states of electron and positron (with momentum \mathbf{p} and \mathbf{q} , respectively) annihilating into n photons. As the typical momenta in an atomic system are small compared to mc , the expression can be simplified by taking the nonrelativistic limit; expanding the matrix element in powers of \mathbf{p}/mc , this means that only the terms of zeroth order in the three-momentum are kept. Thus, the initial four-momentum is of the form $p^\mu = (m, 0, 0, 0)$. If the effects

of the (atomic-scale) binding energy are neglected, the decay amplitude simply has to be integrated over the momentum distribution in the bound state. In other words, one considers the bound state $|B\rangle$ as a linear superposition of states with definite momentum. The weight is given by $\tilde{\psi}(\mathbf{p}_i)$, the Schrödinger wavefunction in momentum space:

$$|B\rangle = \mathcal{N} \int \frac{d^3p_1 d^3p_2 d^3p_p}{(2\pi)^9} \tilde{\psi}(\mathbf{p}_p, \mathbf{p}_1, \mathbf{p}_2) |e^+, \mathbf{p}_p; e^-, \mathbf{p}_1; e^-, \mathbf{p}_2\rangle, \quad (2.10)$$

where \mathcal{N} is a normalization constant (spins have not been written down explicitly in this equation). Now, the expression for the bound-state annihilation amplitude is given by the corresponding superposition of decay amplitudes:

$$\begin{aligned} \mathcal{M}(|B\rangle \rightarrow n\gamma) &= \mathcal{N} \int \frac{d^3p_1 d^3p_2}{(2\pi)^9} \tilde{\psi}(\mathbf{p}_p, \mathbf{p}_1, \mathbf{p}_2) \\ &\quad \times [\mathcal{M}(e^+(-\mathbf{p}_1 - \mathbf{p}_2) e^-(\mathbf{p}_1) \rightarrow n\gamma) \delta^{(3)}(\mathbf{p} + \mathbf{p}_2) + (1 \leftrightarrow 2)] \end{aligned} \quad (2.11)$$

Here it was assumed that the centre-of-momentum system is used ($\mathbf{P} = \sum \mathbf{p}_i = 0$, therefore $\mathbf{p}_p = -\mathbf{p}_1 - \mathbf{p}_2$). $\mathbf{p} = \sum \mathbf{k}_i$ is the sum of the final-state photon momenta. The two terms describe the annihilation with each of the two electrons, respectively. The delta functions ensure the overall momentum conservation, i.e. the sum of the outgoing photon momenta must be equal and opposite to the final-state electron momentum. The decay rate can be calculated from the squared amplitude $|\mathcal{M}|^2$. As we are not interested in spin- and polarization-dependent results, the appropriate averaging over the initial spin states and the summation over all possible photon polarizations finally leads to the desired result.

Using this method, the rates for all decay channels can be computed from the corresponding Feynman diagrams. As an example, fig. 2.2 shows the two graphs contributing in lowest order to the two-gamma decay. In the nonrelativistic approximation discussed above (i.e. setting the 4-momenta of the electron and the positron to $(m, 0, 0, 0)$), the matrix element \mathcal{M} turns out to be independent of the initial momenta. Therefore, the integration in eq. (2.11) gives a factor of $\psi(0)$, the position-space Schrödinger wavefunction at zero electron-positron distance.

There is also a more general work by Chang Lee, who considered the problem of positron annihilation in a many-electron system [Lee58] from a quite universal point of view — without applying his approach to the special case of Ps^- . For this, his method is more or less equivalent to the approach discussed above.

As a result of these calculations, the two-gamma decay rate (in atomic units) in lowest order is given by

$$\Gamma_{2\gamma}^{(0)} = 2\pi\alpha^4 \frac{c}{a_0} \langle \delta(r_{\mathbf{1p}}) \rangle. \quad (2.12)$$

As it turns out, the expression — apart from the wavefunction-dependent expectation value — only differs by a factor of 1/2 from the one for the decay of 1S_0 positronium². This simply reflects the availability of a second electron and the different probabilities to find the electron-positron pair in a singlet state. In other words, there is no qualitative difference between the two decays in our approximation.

Ferrante also published numerical values for the 2γ - and 3γ -annihilation rates [Fer68], based on the approach just described. He obtained a value of $\Gamma_{2\gamma} = 1.99 \text{ ns}^{-1}$ (using a six-parameter variational wavefunction) for the 2γ -decay rate; in the case of the 3γ decay, he seems to have missed the statistical weight given by the different multiplicities of the spin states.

Experimentally it is difficult to make an accurate measurement of the decay rate for a single branch. The most obvious quantity to measure in this context is the total decay rate $\Gamma = \Gamma_{1\gamma} + \Gamma_{2\gamma} + \Gamma_{3\gamma} + \dots$, summing up the contributions from all possible branches. Approximately, the total decay rate is given by

$$\Gamma = 2\pi\alpha^4 \frac{c}{a_0} \left[1 - \alpha \left(\frac{17}{\pi} - \frac{19\pi}{12} \right) \right] \langle \delta(r_{\mathbf{1p}}) \rangle. \quad (2.13)$$

This is the dominating 2γ decay rate (2.12), multiplied by a factor $(1 + \eta_1 + \eta_2)$ to correct for the additional possibility of 3γ decays ($\eta_1 = \Gamma_{3\gamma}/\Gamma_{2\gamma} = \alpha/\pi(4\pi^2/3 - 12)$) and the leading radiative corrections to the two-gamma decay rate ($\eta_2 = \alpha/\pi(5 - \pi^2/4)$). The three-gamma correction η_1 was taken from the work of Ore and Powell [OP49], who calculated the probability of 3γ decays (in lowest order) for the case of neutral positronium. Likewise, Harris and Brown originally investigated the radiative correction η_2 to the annihilation amplitudes for free particles and positronium atoms [HB57]. Bound-state effects are therefore still missing, and some contributions of order α are not included [BD83]. Unfortunately, no estimates of the size of the missing contributions can be found in the literature. They define the theoretical uncertainty of eq. (2.13). As a conservative estimate, we can assume that they are at most of a magnitude comparable to the corrections η_1 and η_2 ; accordingly we estimate the uncertainty to be roughly $3 \cdot 10^{-3}$.

The numerical value of the total decay rate has been calculated from eq. (2.13) by several authors. As already discussed above, this requires the knowledge of the wavefunction,

² There one obtains $\Gamma(^1S_0) = 4\pi\alpha^4 \frac{c}{a_0} |\Psi(0)|$.

more precisely of the expectation value $\langle \delta(r_{1\mathbf{p}}) \rangle$. Accordingly, virtually all authors who published a numerical result for the wavefunction, also plugged in their results into the formula (2.13). The respective values they obtained are listed in table 2.1. Considering our guess for the theoretical uncertainty, the calculated total decay rate is given by

$$\Gamma = 2.086(6) \text{ ns}^{-1}. \quad (2.14)$$

By the way, it may be remarked that the total decay rate is the only property of the positronium negative ion which has been measured so far. The experimental value of $2.09(9) \text{ ns}^{-1}$ agrees very well with the theoretical predictions, but the error is too large to test the theory critically. Even the simple model of a positronium atom plus a loosely bound electron leads to a decay rate still in accordance with experiment [BD83].

Regarding the 3γ decay rate (or equivalently, the $3\gamma/2\gamma$ branching ratio), the published investigations confined themselves to using the already mentioned approximate relation $\Gamma_{3\gamma}/\Gamma_{2\gamma} \approx 3\Gamma(\text{Ps}, {}^3S_1)/\Gamma(\text{Ps}, {}^1S_0)$, which also forms the basis of the three-gamma correction to the total decay rate (see above).

The second parameter concerning the decays of Ps^- which stimulated theoretical interest is the one-photon decay rate $\Gamma_{1\gamma}$. As already discussed above, this is a genuine three-body effect. Regarding the evaluation of the relevant contributions to the one-gamma rate in order to derive an analytical expression, two works are publicly available. Chu and Pönisch have calculated it for the $e^+e^+e^-$ system [CP86], and their results should be valid for Ps^- , too. Second, there is an investigation of the 1γ rate by Kryuchkov [Kry94], where he for the first time included all lowest-order Feynman diagrams contributing to the process. He arrived at the expression

$$\Gamma_{1\gamma}^{(0)} = \frac{64\pi^2}{27} \alpha^3 m^{-5} |\Psi(0, 0, 0)|^2, \quad (2.15)$$

proportional to the probability density to find all three particles at the same point (this is again brought about by neglecting the comparably small atomic momenta, leaving only the zeroth-order term proportional to m). The result from [CP86] is larger by a factor $9/4$, which is attributed to the fact that only 4 of 8 diagrams have been considered in this calculation [Kry94]. Numerical results can be found in a few papers: in [CP86], Chu and Pönisch used their result (which, according to [Kry94], is wrong by a factor of $9/4$) and several published values of $|\Psi(0, 0, 0)|^2$ to compute a result of about $8.8 \cdot 10^{-2} \text{ s}^{-1}$. The other references based their results on the formula from [Kry94]; they obtained $\Gamma_{1\gamma} = 3.92 \cdot 10^{-2} \text{ s}^{-1}$ [Kry94], $\Gamma_{1\gamma} = 3.82271 \cdot 10^{-2} \text{ s}^{-1}$ [Fro98] and $\Gamma_{1\gamma} = 3.82340 \cdot 10^{-2} \text{ s}^{-1}$ [Fro99], respectively.

In connection with the decays, there are also other parameters to be mentioned, of course. Interesting are not only the decay rates, but also the photon energies and the angular correlations. Considering a positronium ion at rest — or equivalently, viewing it in its centre-of-momentum system, the sum of all final-state momenta has to be zero. As one would expect from the $\text{Ps} + e^-$ picture, a large momentum transfer to the second electron is quite unlikely. Therefore, the two gamma rays from a two-photon decay have an energy of about $m_e c^2 = 511 \text{ keV}$ each, and their momenta are approximately equal and opposite. [Ho83b] calculated the corresponding angular correlation function, which turns out to be narrower than its equivalent for neutral positronium. This is in accordance with what one would expect in a loosely bound system: as the particles are less strongly confined in position, their momentum distribution becomes narrower. In the case of the three-gamma decay, the situation is less simple; while it is still true that the second electron to a good approximation remains unaffected, there are now three photons to share the energy and the momentum. For this reason, the gamma energies are not fixed, but they vary continuously. In any case, they have to sum up to a total energy of $2m_e c^2 = 1022 \text{ keV}$ and a total momentum of $\mathbf{P} = 0$. The one-gamma decay gives rise to a free electron and a photon, both of them having fixed energies. As a simple relativistic kinematics calculation shows, the electron gains a kinetic energy of $2/3 \cdot m_e c^2 = 341 \text{ keV}$, and a 681 keV photon is emitted. In the initial Ps^- rest frame, these two are sent out in exactly opposite directions.

Annihilation into four or more gamma rays is suppressed by additional factors of α . Because of the very small contribution of these decays, none of them seems to have been investigated in more detail.

2.3 Excitation and resonances

All the properties discussed so far refer to the ground state of the positronium negative ion. As mentioned in the beginning, this is the only state which is stable against dissociation. Nevertheless, Ps^- features a number of doubly excited autodissociative states, which show up as resonances in electron-Ps scattering or in the Ps^- photodetachment cross section. These have been the subject of several theoretical investigations.

In this context, also the question of a $^3P^e$ metastable state has to be mentioned. Such a state is known to exist in H^- [Mil81b], and it would be experimentally interesting because of its comparably long lifetime: if energetically lower than the Ps ($n = 2$) threshold, it cannot decay by autodissociation, there are no dipole-allowed transitions to the ground state, and direct annihilation is strongly suppressed by the form of the wavefunction. The

first one to point out this possibility and its consequences was Mills [Mil81b]. Using a 70-term Hylleraas wavefunction for this triplet state, he tried to establish its stability against dissociation, but he could not obtain a binding energy below the $n = 2$ threshold of neutral positronium. Furthermore, he investigated the stability for different H^- -like ions as a function of the mass ratio m/M , m being the mass of the unlike particle, M the total mass of the system.

A problem closely related to the investigation of the resonances is the calculation of the photodetachment cross section. Experimentally, photodetachment measurements are the most promising means of accessing the predicted resonances. The relevant process can be described as



Regarding the spin state of the so-produced neutral positronium atom, one would expect to find ortho- ($^3\text{S}_1$) and para-Ps ($^1\text{S}_0$) with a probability given by the respective multiplicity of these spin states: this means that 1/4 of the positronium should be in the singlet state and 3/4 in the triplet state.

There is also the theoretical possibility of looking for resonances in the e^- -Ps scattering cross section, but most of the calculated widths are too narrow (of the order of $10^{-5} - 10^{-3}$ eV) to be resolved with an experimentally available electron beam. Laser spectroscopy, on the other hand, is able to provide the necessary resolution. One has to keep in mind, though, that there are rather strict selection rules for optical transitions; from the $^1\text{S}^e$ ground state only resonances of $^1\text{P}^o$ symmetry are accessible by one-photon transitions. Others might be excited by two-photon absorption (as in the Doppler-free two-photon spectroscopy of the hydrogen $1\text{S} - 2\text{S}$ transition), but this requires high intensities and is not easy to realize. For this reason, the main focus in this section is on the $^1\text{P}^o$ resonances with their relevance to the photodetachment cross section. Looking at the energy scale, the most interesting of these are the resonances around the $n = 2$ threshold. Even they would require rather short wavelengths (~ 230 nm for a positronium ion at rest).

Concerning the possible experimental observation of the doubly excited states of Ps^- , there remains one important aspect to discuss: what happens to an excited positronium negative ion? In principle, there are three decay channels: annihilation, autoionization and deexcitation in a radiative cascade to the ground state. Ho [Ho85] has investigated this problem, and he found the autoionization to dominate over the direct annihilation channel. In fact, autoionization rates are several orders of magnitude larger than direct annihilation rates. This means that the doubly excited states should be observable in

the photodetachment cross section. Ho also concluded that the deexcitation by photon emission should be far less probable than the autoionization process. For the decay rate measurements to be discussed later (see chapter 4), this means that feeding effects are negligible as a source of systematic errors: even if a significant fraction of the positronium ions was formed in one of the excited states, they would rather decay by autoionization than by radiative transitions to the ground state.

A number of publications can be found on the subject of Ps^- resonances; most of them concern the calculation of resonance parameters (positions and widths) for a specific symmetry. Different techniques have been employed in the theoretical study of the Ps^- resonances: among them are the complex rotation method, the more qualitative discussion of adiabatic potential curves in hyperspherical coordinates and the (hyperspherical) close-coupling method. The first of these, the so-called complex rotation method, is a mathematical procedure to compute the resonance parameters by finding the complex singularities of the Hamiltonian [Ho83a]. Their complex coordinates provide information about position and width of the individual resonances: $E' = E_{\text{res}} - i\Gamma/2$, where E' is the (complex) singularity, E_{res} and Γ are the resonance position and width, respectively. By using this method, Ho and Bhatia have calculated the parameters for a large number of resonances up to the Ps ($n = 6$) threshold, thereby covering several symmetries: $^1S^e$ [Ho79, Ho84], $^3S^e$ [Ho84], $^{1,3}P^o$ [BH90, HB91, HB93], $^3P^e$ [HB92], $^{1,3}D^e$ [BH93], $^{1,3}D^o$ [HB94].

The adiabatic studies of the positronium ion in hyperspherical coordinates follow a completely different approach: after transforming the Hamiltonian to hyperspherical coordinates (R, Ω) , where R is the hyperradius and Ω represents the hyperangles, solutions of the Schrödinger equation for fixed R are sought for. This leads to the adiabatic wavefunctions $\Phi_\mu(R, \Omega)$ and, from the corresponding eigenvalues, the hyperspherical potential curves $U_\mu(R)$. Now, the full wavefunction $\Psi(R, \Omega)$ can be expanded as

$$\Psi(R, \Omega) = \sum_{\mu} F_{\mu}(R)\Phi_{\mu}(R, \Omega). \quad (2.17)$$

In this way, a system of coupled equations for the radial functions $F_{\mu}(R)$ is obtained. The adiabatic approximation neglects the coupling between the different ‘channels’ $\Phi_{\mu}(R, \Omega)$. As R measures the overall size of the system, this is somewhat similar to the adiabatic approximation in molecular physics: in the Born-Oppenheimer approximation changes in the internuclear distance are assumed to be decoupled from the electronic motion. For an expansion of the adiabatic wavefunctions $\Phi_{\mu}(R, \Omega)$, different basis sets can be employed. In [Bot87], for example, hyperspherical harmonics are used (together with

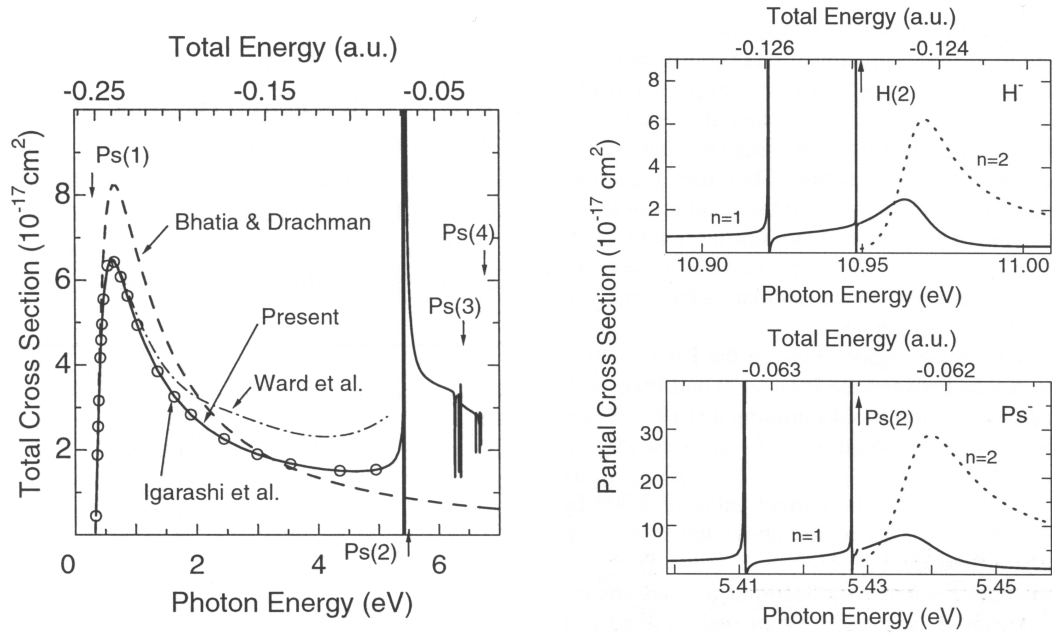


Figure 2.3: The photodetachment cross section of the positronium negative ion. The left panel shows the results of a hyperspherical close-coupling calculation by Igarashi et al. for the total cross section. The right panel shows partial cross sections for the production of $\text{Ps}(n = 1)$ (continuous curve) and $\text{Ps}(n = 2)$ (dotted curve). Only the first two resonances of the series below the $n = 2$ threshold of the neutral atom are shown. For further resonances, the distance to the threshold decreases exponentially. From [IST00] (for a discussion of the discrepancies between the different calculations, see there).

a special selection scheme of relevant contributions for faster convergence) to compute hyperspherical potential curves for several symmetries. As it turns out, the coupling terms are no longer negligible in those regions of R where two adiabatic curves are trying to cross. There they even become leading contributions; in [Bot87] the consequences are discussed on a case-by-case basis. Igarashi et al. [IST00] have chosen atomic orbitals (with standard spherical harmonics) as a basis for a variational calculation of the adiabatic wavefunctions; this leads to what they call the ‘hyperspherical close-coupling method’. With the ground-state and continuum wavefunctions obtained in this way, they computed the photodetachment cross section from Fermi’s golden rule:

$$\sigma \propto |\langle \Psi_f | D | \Psi_i \rangle|^2, \quad (2.18)$$

where Ψ_i and Ψ_f are the initial and final-state wavefunctions, respectively, and D is the dipole operator. Fig. 2.3 shows a part of their results. In the left panel, also the cross sections calculated by other authors are drawn for comparison. All of these earlier

Reference	Feshbach resonances				shape resonance	
	E	Γ	E	Γ	E	Γ
	[10^{-2} a.u.]	[10^{-6} a.u.]	[10^{-2} a.u.]	[10^{-6} a.u.]	[10^{-2} a.u.]	[10^{-4} a.u.]
[BG86] ^a	-6.2587		-6.2506		-6.21	4
[BH90] ^b	-6.31558(2)	1.0(3)				
[HB93] ^b					-6.217(2)	4.5(3)
[IST00] ^c	-6.3155	0.92	-6.2543	0.25	-6.2158	6.4

^a Estimates from an adiabatic calculation in hyperspherical coordinates.

^b Computed using the complex rotation method.

^c Results of a hyperspherical close-coupling calculation. The energies are estimated to be reliable to four digits, the widths to $\pm 20\%$.

Table 2.3: Theoretical positions and widths for the calculated $^1P^o$ resonances around the $Ps(n=2)$ threshold of $-6.25 \cdot 10^{-2}$ a.u. as predicted in different publications.

publications, however, are limited to the off-resonant energy region up to the $Ps(n=2)$ threshold [BD85, WHM87, INO00]. The obvious deviations between the different results are discussed in [IST00]. Despite the title ‘Resonant photodetachment of the positronium negative ion’, Botero and Greene [BG86] have also determined only resonance parameters, but not the resonant cross sections.

For every $Ps(n)$ threshold in the energy range considered (in [IST00], up to $n=6$), there is a series of Feshbach resonances just below threshold. These resonances can be interpreted as a consequence of the attractive dipole potential which results from the degeneracy of the excited states in positronium. Further, there is a shape resonance above the $n=2$ threshold. As already discussed at the beginning of this section, only resonances of $^1P^o$ symmetry contribute to the photodetachment cross section in the dipole approximation. For this reason, these are the only resonances showing up in this calculation.

In this context, it should be mentioned that the equivalent of the $^3P^e$ metastable state existing in the case of H^- lies above the $Ps(n=2)$ threshold. Therefore, it also leads to a shape resonance, which is, however, not accessible by one-photon absorption [Bot87].

From an experimental point of view, the doubly excited resonances below the $Ps(n=2)$ threshold can provide a way of measuring the ground state binding energy of Ps^- in a photodetachment experiment: the photon energies at the Feshbach resonances correspond to the energy differences between the ground state and the respective resonances; these in turn rapidly converge to the known $n=2$ threshold of neutral positronium. Another, though not very precise, possibility to measure the binding energy is given by an experi-

mental determination of the threshold photon energy for off-resonant photodetachment.

A summary of the theoretical results on the $^1P^o$ resonances around the $n = 2$ threshold, which are the most interesting ones for photodetachment experiments, can be found in table 2.3. Up to now, no experimental test of these predictions has been reported.

2.4 Ps^- : Atom or molecule?

In addition to the aspects discussed in the preceding sections, the positronium negative ion has attracted attention also as a very special Coulombic three-body system. When studying three-body systems, usually very different methods are used, depending on the type of system: on the one hand there is the molecular physics approach of the Born-Oppenheimer approximation, on the other hand the independent particle model of atomic physics. The former is used, e.g., to describe the H_2^+ molecule, where an electron moves in the field of two heavy particles while the vibrations and rotations of these are assumed to be decoupled from the electronic motion. In the latter, to describe H^- , two light electrons in the central potential of a heavy nucleus are considered. These two regimes also give rise to different sets of approximate quantum numbers. Nevertheless, the equations governing both systems are mathematically identical. The only difference is given by the particle mass ratios. Furthermore, there are examples where the traditional, usually well-justified approximations fail: in two-electron atoms, for example, the independent-electron model cannot account for some highly correlated doubly excited states. An interesting question is the transition from the regime of the atomic models to the regime of the molecular Born-Oppenheimer approximation. In this respect, the positronium negative ion is an intermediate system between the limiting cases of ${}^\infty\text{H}^-$ and ${}^\infty\text{H}_2^+$. Several authors investigated this transition by calculating the properties of Coulombic three-body systems with arbitrary mass ratios (see, for example, [BD87, LL88, CL90, FB92]). Moreover, Rost and Wintgen [RW92] tried to apply the molecular approach to Ps^- by using the line joining the two electrons as a molecular axis. As it turned out, several resonances of the positronium negative ion can be described in this way (in [RW92], only S states were studied), and it is possible to assign molecular quantum numbers to them. This probably means that Ps^- does not simply consist of three particles “tumbling about their centre of mass” [BG86], rather there is a highly correlated and structured motion.

2.5 Conclusion

Quite a few properties of the positronium negative ion have been investigated theoretically, but experimental data is largely unavailable; so far only the decay rate has been measured [Mil83]. The experimental value of the decay rate ($\Gamma_{\text{exp}} = 2.09(9) \text{ ns}^{-1}$) has an error of 4.3%, which is an order of magnitude larger than the corrections due to the three-gamma decay and the radiative corrections. Therefore, the error is still too large to present a critical test of the theory. An order-of-magnitude increase in experimental precision would bring the uncertainty down to the level of the current calculations ($\Gamma_{\text{theo}} = 2.086(6) \text{ ns}^{-1}$). The binding energy of the positronium ion is calculated to be $E = -0.012008(5) \text{ a.u.} = -0.32675(14) \text{ eV}$. Experimentally, this value could be tested — together with a search for the predicted doubly excited resonances — by a photodetachment experiment. To reach a precision of the same order of magnitude as the theoretical uncertainty of $\sim 1.5 \cdot 10^{-4} \text{ eV}$, a measurement to an accuracy of about 3.5 GHz would be necessary.

Another parameter which could be measured is the $3\gamma/2\gamma$ branching ratio. This would directly probe the three-gamma decay rate of Ps^- .

Chapter 3

The Heidelberg Ps^- set-up

This chapter describes the set-up used for producing negative positronium ions. As the formation of Ps^- requires low-energy positrons, the available positron sources in general and the specific source of the Heidelberg set-up are briefly discussed (sec. 3.1). Section 3.2 gives a short account of positron moderation. A discussion of the magnetic transport and energy-selection system follows in section 3.3, and the production of positronium ions, together with the experimental formation set-up, is explained in sec. 3.4. More detailed information on the design and construction of the set-up can be found in the diploma theses of F. Plenge [Pl00], K. Degreif [Deg01] and F. Fleischer [Fle01].

3.1 The positron source

For producing positrons, several methods are available. Generally speaking, they can be divided in two groups: on the one hand, radioactive β^+ -sources can be employed, on the other hand it is possible to make use of the pair-creation process. An example for the latter group is given by the LINAC-based positron sources, where a high-energy electron beam is sent onto a fixed high- Z target. The electrons lose part of their energy by bremsstrahlung processes, and the so-produced γ -rays in turn lead to electron-positron pair creation in the field of the target nuclei. Also the NEPOMUC positron source, which is discussed in detail in sec. 5.1, is based on this process. These techniques can provide very high intensities, but they require large facilities. On the contrary, radioactive sources are simple; however, due to practical problems of handling and radiation shielding, their maximum positron flux is limited.

For designing and setting up the Heidelberg Ps^- experiment, a table-top sized source independent from beam-time schedules was desirable. Therefore the present set-up contains a radioactive ^{22}Na positron source. As for other proton-rich nuclei, ^{22}Na decays either by β^+ decay ($\sim 91\%$ branching ratio) or by electron capture ($\sim 9\%$). A level scheme is shown

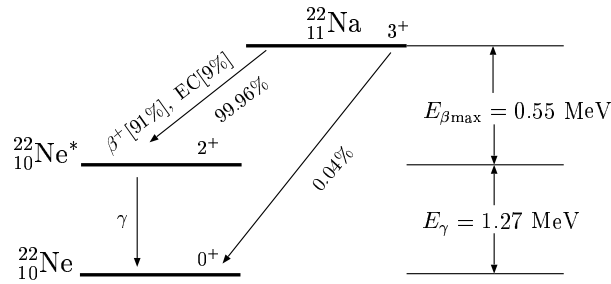


Figure 3.1: Level scheme of ^{22}Na .

in fig. 3.1. The beta decay does not lead to the ground state of the daughter nucleus, rather it populates an excited state, which in turns decays via emission of a 1273 keV γ -ray. In some experiments using positrons, especially in positron annihilation lifetime spectroscopy, this prompt gamma ray turns out to be useful as a start signal. Here it only contributes to the gamma background, and it is the main concern in terms of radiation shielding.

For protection from this γ -radiation, most experiments using such sources surround the vacuum chamber containing the source by a lead housing. In the Heidelberg Ps⁻ set-up, part of the necessary shielding is mounted inside the vacuum vessel. This not only reduces the amount of shielding material, it also allows for a simpler access to the outer parts of the source set-up. To keep the inner shielding as compact as possible, a special tungsten alloy (DENSIMET¹) with a density of 19 g/cm³ is used instead of lead. The source is mounted in the central 20 mm diameter bore of a massive DENSIMET cylinder of 170 mm diameter. In backward direction the bore is blocked by the source holder (also made of DENSIMET), in forward direction it provides the exit channel for the positrons. A sketch of the source chamber is shown in fig 3.2, including the moderator arrangement to be discussed in the next section.

^{22}Na has a half-life of about 2.6 years. For the γ -measurement described in section 4.2, a source of originally 10 mCi activity was used, which at the time of the measurement (11/2002) had decayed already to ~ 4 mCi. For the stripping experiment (section 4.3), the source has been replaced by a new one from iThemba Labs, South Africa. It was delivered with a nominal activity of 40 mCi (11/2003), corresponding to about $1.5 \cdot 10^9$ β^+ decays per second.

¹ DENSIMET, available from the PLANSEE GmbH (<http://www.plansee.com/>), is an alloy made of tungsten and a smaller fraction of other metals. The advantage in comparison to pure tungsten is its greatly improved machineability.

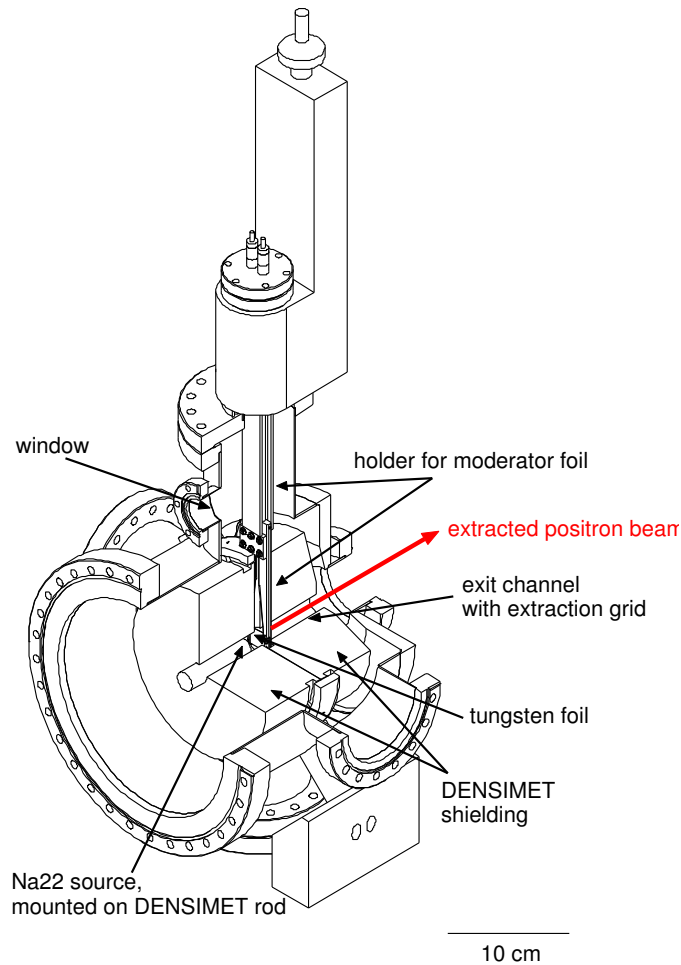


Figure 3.2: Sketch of the source chamber of the Heidelberg Ps^- set-up.

3.2 Creating slow positrons by moderation

Largely independent of the type of positron source used (cf. section 3.1), additional effort is necessary to obtain a monoenergetic low-energy beam of positrons. The positrons coming from a source usually have rather high energies and a broad energy distribution. In the case of a ^{22}Na β^+ -source, for example, the emitted positrons have kinetic energies of up to about 550 keV. As only a definite energy class of positrons seems to contribute to the formation process of Ps^- [Fle01], these are clearly not directly usable.

Low-energy positrons are also used in many solid-state physics applications, therefore moderation techniques have been developed to slow down the positrons to eV energies. Though greatly varying in the details of their realization, they all share the same basic mechanism: the particles lose their kinetic energy by inelastic collisions in a solid. The

collision partners involved are mainly electrons, at lower energies (~ 10 eV) also plasmons and finally even phonons can contribute. With the positron lifetime in a solid ($\sim 10^{-10}$ s) being about two orders of magnitude longer than the thermalization time, a fraction of the thermalized positrons can diffuse to the surface. If a material with a negative positron work function is used, there is a certain probability for reemission of these particles, the kinetic energy being defined by the value of the work function². The seemingly odd feature of a negative positron work function is displayed by a number of substances. Examples are tungsten ($\Phi_+ = -2.9$ eV) and platinum ($\Phi_+ = -1.8$ eV). A schematic overview of the processes occurring in the interaction of positrons with a moderator foil in transmission geometry is given in fig. 3.3. Over the past decades, much work has been dedicated to the optimization of such moderators (for a review, see e.g. [Col00]). Also solid rare gases have been explored as moderators [MVA94, JLF⁺97]. They reach significantly higher efficiencies, but they also require very special conditions like a cryogenic environment and ultra-high vacuum. Altogether, the design of positron moderators is a specialized field, and a lot of empirical facts can be found in the literature. For example, elaborate annealing and cleaning procedures have been tried to minimise the effects of impurities and defects, where positrons can be trapped. These questions are beyond the scope of this text; for more details refer to the literature.

In any case, the design of the positronium ion set-up required a robust moderator with a reliable long-term stability. This is especially true because of the long measurement times needed to obtain the desired statistics (see chapter 4). For this reason, highly efficient but unstable moderators like solid neon are not applicable. In the end, a simple transmission-geometry moderator made of a $4\ \mu\text{m}$ polycrystalline tungsten foil was chosen. The foil, mounted on a retractable holder, is placed directly in front of the sodium source inside the 20 mm bore. For annealing purposes, it can be pulled out of the DENSIMET shielding (see fig. 3.2). To extract the moderated positrons, the foil is biased to a positive voltage (+30 V) with respect to a grounded grid mounted on its downstream side at the entrance to the extraction channel.

2 Strictly speaking, this is true only for completely thermalized positrons. In all moderators there is also a fraction of particles which leave the solid before complete thermalization is reached. These so-called epithermal positrons still have kinetic energies of a few eV. In the highly efficient rare-gas moderators only epithermal positrons are produced: complete thermalization is prevented by the large band gap of these materials.

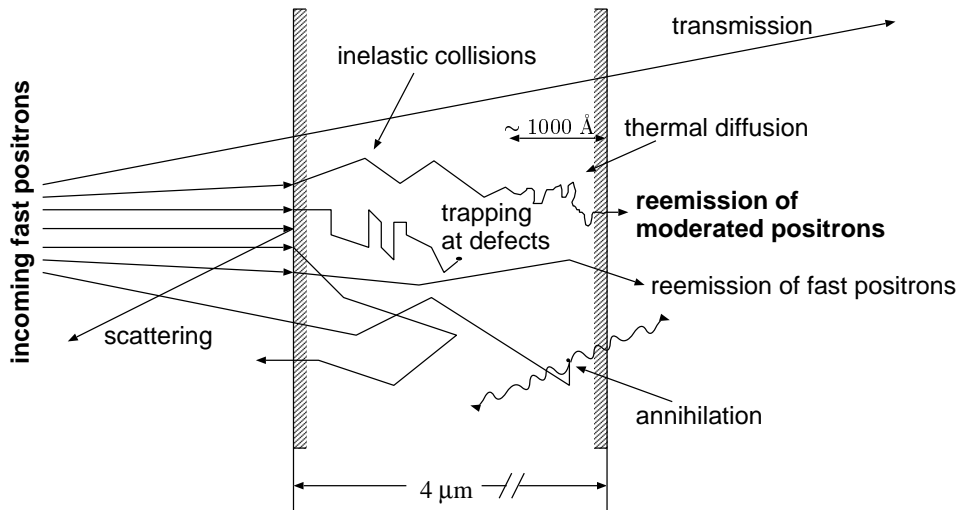


Figure 3.3: Schematic drawing showing the different processes occurring in the interaction of positrons with the tungsten moderator foil. From [Ple00].

3.3 Magnetic transport and energy selection

To avoid losing the positrons by scattering and annihilation, the beam has to be lead through an evacuated beamline to the experiment chamber. The whole set-up is pumped by two turbo pumps, one attached to the source chamber, the other one to the experiment chamber. Typical pressures reached in the apparatus are in the $10^{-7} - 10^{-8}$ mbar range. For guiding and collimation of the beam, a longitudinal magnetic field is employed. For the greater part, this field is created by copper coils wound directly onto the beamline tubes. Where this is not possible, e.g. in the chambers, Helmholtz coils are used. The positrons spiral along the magnetic field lines, thereby eliminating the divergence of the beam. With the radius of a charged particle's cyclotron motion being

$$a = \frac{mv_{\perp}}{qB}, \quad (3.1)$$

the effective beam diameter is influenced by two parameters: the transversal velocity v_{\perp} and the magnetic field B . In order to keep the transversal component of the velocity small, special care was taken to maintain the homogeneity of the magnetic field and the parallelism of the E - and B -fields in the region of the electric extraction field. The choice of the magnetic field strength B has been considered in detail in [Ple00] and [Deg01]. In the adiabatic regime, which is applicable here, the beam diameter r changes as $r \propto 1/\sqrt{B}$. Therefore, a compression of the beam is possible by increasing the magnetic field from the source to the point of use. On the other hand, the transmission through the 20 mm

bore in the shielding improves with a higher field strength already in the source region. The optimization of these parameters has been done in [Deg01]: around the source a field of $B = 25 \text{ G}$ is applied, rising to about 120 G at the Ps^- production foil (see ch. 3.4).

The positron beam, as coming from the source chamber, is not yet monoenergetic, but there is a large contribution of unmoderated or only partially moderated positrons. Additionally, a strong background of gamma radiation from the source is present. For this reason, the magnetically guided beam of low-energy positrons (having an energy of $\sim 33 \text{ eV}$, as defined by the reemission energy and the extraction voltage) is lead through an S-shaped beamline of two 45° toroid sections, thereby effectively removing the higher-energy components and the γ -rays. The energy selection is based on the transversal drift which a charged-particle beam experiences in a toroidally bent magnetic field [Jac81]. The drift is perpendicular to the bending plane, and it increases with the square-root of the energy:

$$\Delta y[\text{mm}] = 0.58 \frac{\alpha[^\circ] \sqrt{E[\text{eV}]}}{B[\text{Gauss}]}, \quad (3.2)$$

where a toroidal sector of angle α is used [Ley97]. Thus, the higher-energy positrons can be removed by an adjustable slit system located at the point of maximum displacement from the axis between the two 45° toroid sections. After passing through the two toroids of opposite curvature, the remaining beam leaves this section again on the beamline axis. Residual shifts due to asymmetries in the overall coil configuration and the effects of the external magnetic field are compensated by a pair of correction coils sitting on the beamline. Fig. 3.4 gives a schematic illustration of the complete set-up with positron source, moderator and transport system.

For more details on the requirements of adiabaticity, the choice of parameters for optimum transmission etc., refer to [Deg01], where the characteristics of the magnetic transport system have been studied. There also the overall moderation efficiency ϵ of the set-up has been determined, defined (following [CM82]) as the number of low-energy positrons transmitted along the beamline and up to the grounded grid in the experiment chamber, normalized to the number of β^+ decays, i.e.

$$\epsilon = \frac{\text{number of slow positrons per second}}{\beta^+ \text{ activity of the source}}. \quad (3.3)$$

As a result, an overall efficiency of $\epsilon = 1.2(2) \cdot 10^{-4}$ has been observed. Compared to the values reported in the literature for high-efficiency moderators, this is rather low. As stated above, robustness and stability was given priority over the maximum moderation efficiency. In [Fle01] it was demonstrated that the positron flux does not show any short-time fluctuations. Concerning slow variations, the relative change was shown to be smaller

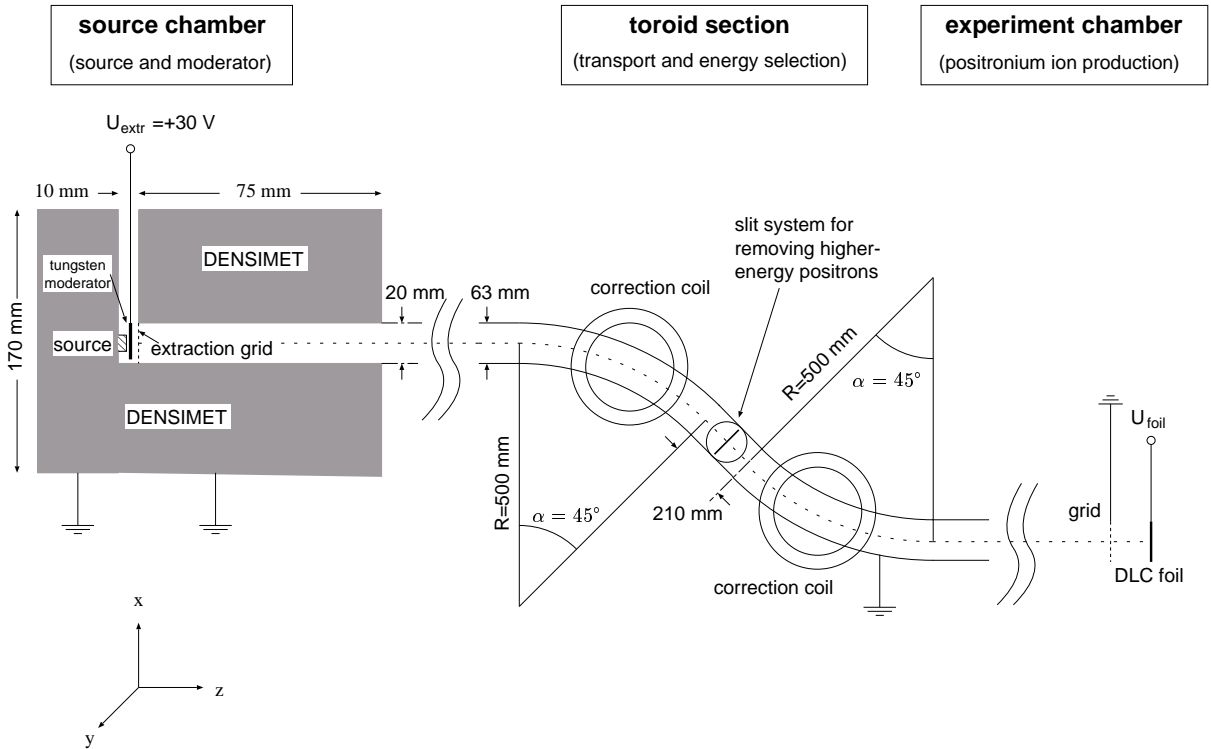


Figure 3.4: Schematic illustration of the set-up including source, moderator and transport/energy-selection section.

than $2 \cdot 10^{-3} \text{ h}^{-1}$, and it was most probably due to an instable operation of the old detector used for the measurement — this detector was not used for the decay rate experiment. In any case, small drifts of the moderation efficiency at time scales \geq a few days do not matter as they are averaged out by the measurement procedure used in the decay rate measurements (see sec. 4.2.1). [Fle01] also contains a determination of the beam diameter in the experiment chamber (see next section). Its measured size is about 7 mm.

3.4 Production of positronium negative ions

Once a low-energy positron beam is available, a simple beam-foil arrangement can be used for producing positronium negative ions. This method was first employed by Mills [Mil81a]. A schematic drawing of our set-up is shown in fig. 3.5(a): the positron beam of ~ 7 mm diameter enters through the grounded grid (copper, 35 mm diameter, 88% transmission) on the left, and it is accelerated towards a very thin DLC³ foil with a nominal

3 DLC (Diamond-Like-Carbon) foils are special carbon foils with a very low pinhole density, made by

thickness of ~ 5 nm. The foil has a usable diameter of 12 mm, and it is supported by a copper grid of 86% transmission. To ensure a very high degree of flatness, these grids are mounted in special frames (see fig. 3.5(b)). The energy of the impinging particles can be adjusted by changing the potential of the foil. As Mills found out, a small fraction — about 10^{-4} — of the positrons forms Ps^- when emerging from the back side of the foil. Here a second electric field accelerates the negatively charged ions, while the transmitted positrons are repelled towards the foil. In [Fle01] a systematic investigation of different carbon foils, especially varying in thickness, has been performed in order to study the influence on the Ps^- formation probability: the optimum incident positron energy increases with increasing thickness, the achieved maximum formation efficiency was found to decrease. There was no evidence for a significantly different behaviour of DLC foils and standard carbon foils with respect to the production of positronium ions. In total the probability of Ps^- formation varied between $1 - 3 \cdot 10^{-4}$ for the different foils we had at our disposal. During the experiments discussed in chapter 4, two DLC foils of somewhat different thickness have been used. Accordingly, the maximum Ps^- rate was reached for different foil potentials: in the γ -measurements, using a DLC foil of ~ 5 nm, the optimum value was $U_e = -500$ V, while the DLC foil used for the stripping measurements of ~ 8.5 nm thickness performed best at a potential of -800 V.

An important aspect of the Ps^- formation process is the question of the typical kinetic energy of a positronium ion as it leaves the foil. If the two electrons are picked up sequentially — which seems to be a sensible assumption —, Ps^- could be formed by charge exchange in a collision of a neutral positronium with a carbon atom. One can expect this to happen especially for collisions in which the kinetic energy is not sufficient to lift the electron into a continuum state, but only to the bound state of Ps^- . As the second electron in the positronium ion is bound by 0.3 eV, this leads to an expected average kinetic energy of the newly formed Ps^- of less than 0.3 eV. In [Mil83] Mills measured the average longitudinal kinetic energy of the positronium ions on formation to be $T_0 = 13_{-10}^{+19}$ eV. Nevertheless, he also expected a substantially smaller value for T_0 , and, considering the large error, he sees his experimental result to be in accordance with the estimate $T_0 < 0.3$ eV [Mil05]. In sec. 4.3.2 we will give an experimental determination of T_0 .

Taking the probability for Ps^- formation of about 10^{-4} and the moderation efficiency $\epsilon \simeq 10^{-4}$ into account, the set-up is expected to generate positronium ions with a total rate of $\sim 1.5 \text{ s}^{-1}$ and $\sim 15 \text{ s}^{-1}$ for the two ^{22}Na sources of 4 and 40 mCi activity used in

V. Liechtenstein [LIO⁺97].

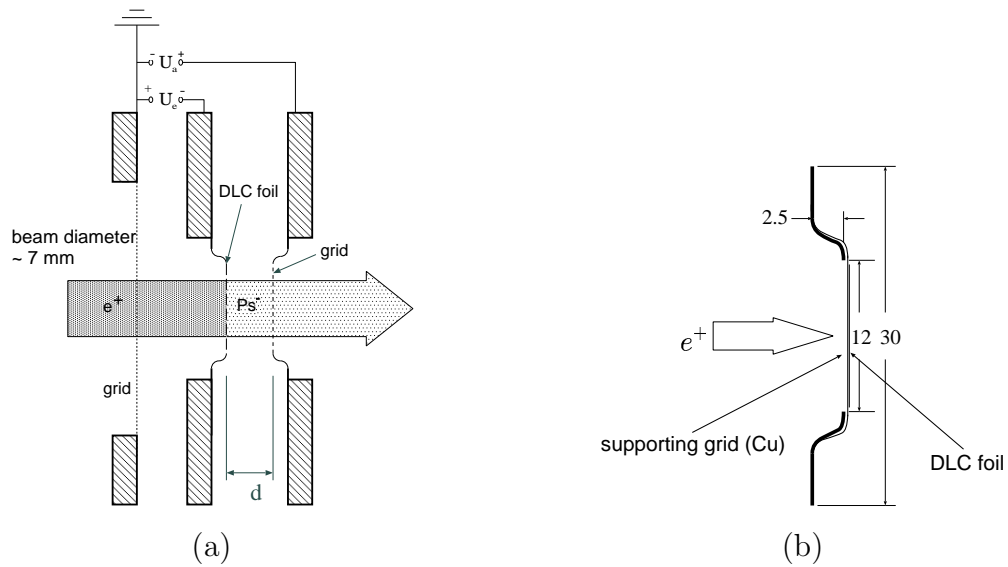


Figure 3.5: (a) Schematic drawing of the arrangement for Ps^- production. (b) Sketch of the mounting frame of a DLC foil.

the following experiments, respectively.

The just described source of positronium ions is well suited for experimental investigations of this system. The main topic of this work is the measurement of the total decay rate of Ps^- , and it will be discussed in the next chapter. All relevant parameters used in operating the set-up are listed in Appendix A.

Chapter 4

Measurement of the decay rate

In this chapter a new measurement of the total decay rate of the positronium negative ion is reported. After explaining the principle of the decay rate experiment and some general features of the corresponding set-up in sec. 4.1, a short discussion of an experimental realization based on the detection of the Doppler-shifted annihilation radiation of accelerated Ps^- ions with a Ge photon detector is given. Together with an analysis of the results this can be found in sec. 4.2. For a detailed description of the set-up used for this measurement refer to [Les03], which also contains a preliminary analysis. Sec. 4.3 introduces an improved method of detecting the positronium ions. It is based on an acceleration and stripping scheme similar to that of a tandem accelerator, and it counts the stripped positrons instead of the annihilation photons. In this way, a significantly improved signal-to-background ratio is reached. Besides the principle of the method, a detailed discussion of the experimental set-up and the results of a precise decay rate measurement using this approach are presented. The chapter concludes with an investigation of the different sources of error in the decay rate experiment in sec. 4.4 and a summary of the results in sec. 4.5.

4.1 Principle of the decay rate experiment and set-up

Because of its small mass, voltages of a few kV are sufficient to accelerate a positronium ion to velocities of a few percent the speed of light. With such velocities and an expected lifetime of about half a nanosecond, a particle travels a few millimetres before it decays. Therefore, a time-of-flight-based approach to the decay rate measurement seems to be the most natural possibility: a flight distance d between the production foil and the acceleration grid is varied, and the number of ions surviving the flight across d is recorded. Fig. 4.1 shows a schematic illustration of the measuring principle.

When the relation between d , the width of the acceleration gap, and the respective time

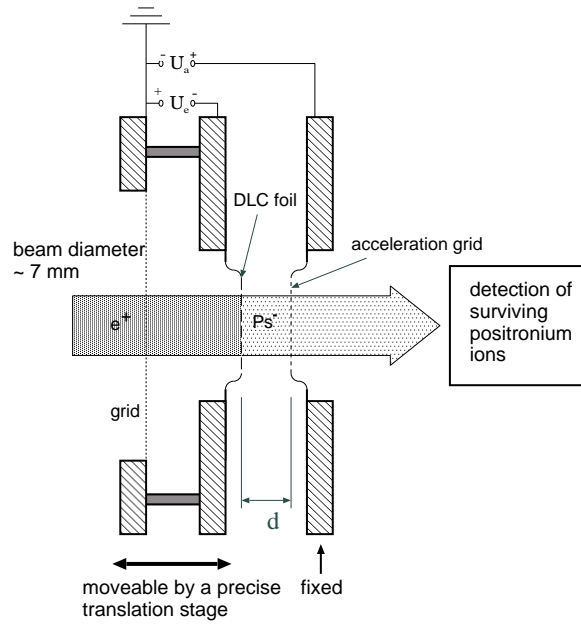


Figure 4.1: Schematic illustration showing the principle of the decay rate measurements: the Ps^- ions are accelerated across a gap of variable width d , and the number of surviving ions is recorded as a function of d .

of flight t' is known, the decay rate Γ of the positronium negative ion can be determined. The time of flight has to be calculated for the reference frame in which the ion is at rest; in other words, t' measures the proper time for crossing the gap d . A simple relativistic calculation [Fle01] yields

$$\begin{aligned}
 t' &= \frac{d}{\Lambda c} \left[\ln \left(1 + \Lambda + \Lambda_0 + \sqrt{(\Lambda + \Lambda_0 + 1)^2 - 1} \right) - \ln \left(1 + \Lambda_0 + \sqrt{(\Lambda_0 + 1)^2 - 1} \right) \right] \\
 &\simeq \frac{d}{\Lambda c} \ln \left[1 + \Lambda + \sqrt{\Lambda^2 + 2\Lambda} \right] \left(1 - \sqrt{\frac{\Lambda_0}{\Lambda}} \right), \quad (4.1)
 \end{aligned}$$

where we have set $\Lambda_0 = T_0/(3m_e c^2)$ (with T_0 being the average longitudinal kinetic energy of the positronium ion when leaving the formation foil) and $\Lambda = eU/(3m_e c^2)$. $U = U_a - U_e$ is the acceleration voltage across the gap (see fig. 4.1). In the approximation leading to the second line it is assumed that $\Lambda_0/\Lambda \ll 1$. As a result, the proper time needed for crossing the gap is strictly proportional to its width d . Therefore, the measured rate of the positronium ions surviving the acceleration across the gap d , $n(d)$, decreases exponentially with increasing d : $n(d) = n_0 \exp(-\mu \cdot d)$. Comparing with the law of exponential decay $\propto \exp(-\Gamma t'(d))$, the relation between the decay rate Γ and the experimentally determined value of μ is found to be

$$\mu \cdot \Lambda c / \ln [1 + \Lambda + \sqrt{\Lambda^2 + 2\Lambda}] = \Gamma \cdot \left(1 - \sqrt{\frac{\Lambda_0}{\Lambda}}\right). \quad (4.2)$$

The conversion factor depends on the acceleration voltage U and on the initial kinetic energy T_0 of the Ps^- ions (cf. sec. 3.4). A possible way of taking T_0 into account consists of performing several measurements at different values of Λ (i.e. different acceleration voltages U); by plotting the uncorrected decay rate $\Gamma^* = \Gamma(1 - \sqrt{\Lambda_0/\Lambda}) = \mu[\Lambda c / \ln(1 + \Lambda + \sqrt{\Lambda^2 + 2\Lambda})]$ against $\Lambda^{-1/2}$, a non-negligible value of $T_0 > 0$ should be reflected by a Γ^* value decreasing with $\Lambda^{-1/2}$. The decay constant Γ can then be determined by extrapolating Γ^* for $\Lambda \rightarrow \infty$, while T_0 is given by the slope of Γ^* with $\Lambda^{-1/2}$.

In order to realize a decay rate experiment of this type, three main requirements have to be fulfilled: first, a directed, monoenergetic beam of Ps^- ions is needed; this is exactly what the Ps^- set-up presented in chapter 3 supplies. Second, the number of positronium ions surviving the acceleration over the gap d has to be determined; for this purpose, two methods have been employed, which will be described in more detail in the next sections. And thirdly, the gap width d has to be varied precisely. The latter requirement could be satisfied by mounting the Ps^- formation foil and the grounded entrance grid on top of a precise linear translation stage, which was in turn mounted inside the vacuum chamber. Apart from the required mechanical precision necessary to set the foil position with a high accuracy and reproducibility, a further requirement was that the stage should not disturb the guiding magnetic field, which excluded conventional stepper motors as they usually incorporate ferromagnetic parts. An additional complication is given by the necessary vacuum-compatibility of the stage, but as no ultra-high vacuum is needed in this experiment, this fortunately did not impose a very strict limitation. Nevertheless, it turned out to be difficult to find a device which meets all these specifications. Finally, an inchworm-driven linear translation stage, the vacuum-compatible, antimagnetic version of the LT-105-50-LM from Feinmess Dresden GmbH¹ was chosen. Consisting only of antimagnetic parts and having a position reproducibility of $\pm 1 \mu\text{m}$, it fulfils the criteria mentioned above. It incorporates an optical position encoder and can therefore be used in closed-loop operation. The position encoder features an index mark for finding the zero position of the translation stage. In the decay rate experiments, this index mark is used to frequently recalibrate the position measurement. Such a reset of the stage is done in the beginning of a run and at regular intervals during the experiment (after 50 measurement cycles, see sec. 4.2.1). An additional advantage is the possibility of controlling the device via a standard serial RS232 connection. The stage has an adjustable range of ca. 50 mm,

¹ <http://www.feinmess-dresden.de/>

but due to obstructions by the other parts of the set-up (e.g. the bronze gaze screening, see below), only slightly more than 25 mm of this range are usable at present. The minimum value used for d is 2.7 mm, the maximum 28.0 mm. For controlling the stage, the C program `motor` is used. It is documented in [Les03], where also some tests of the translation stage are reported. As the absolute values of d also depend on the mounting position of the translation stage in the vacuum chamber, these absolute values are known only to ~ 0.5 mm. The $\pm 1 \mu\text{m}$ positioning accuracy refers only to relative positions, i.e. differences Δd .

The grounded entrance grid and the DLC foil have been described already in sec. 3.4. For the acceleration grid an empty DLC foil support has been used. As the different high voltage cables connecting the grids to the respective electrical feedthroughs inevitably generate stray fields, the immediate surroundings of the beam are screened by a grounded cylinder of bronze gaze. This cylinder is centred on the chamber axis, and it stretches from the beam entrance to the first grid of the experiment set-up.

4.2 The γ -method

In order to perform a decay rate measurement as described in sec. 4.1, the positronium ions surviving the flight across the acceleration gap d have to be detected. In the following, a method for detection and identification of the accelerated positronium ions via their annihilation radiation is described, which we used in a first exploratory decay rate measurement.

As discussed in sec. 2.2, Ps^- predominantly decays into two photons of 511 keV each, which is also the main decay channel for annihilation of free electron-positron pairs and of the neutral positronium atom. For this reason, it is of crucial importance to be able to distinguish between these different sources of annihilation radiation. Here a simple trick can be used: when accelerating the Ps^- ions to velocities of a few percent the speed of light, the annihilation gammas which are detected in forward direction show an appreciable Doppler-shift. According to the Doppler formula, the laboratory-frame energy of a photon emitted with an energy of $E_{\gamma 0}$ (in the rest frame of the particle) is given by

$$E' = \frac{E_{\gamma 0} \sqrt{1 - \beta^2}}{1 - \beta \cos \theta'}, \quad (4.3)$$

where $\beta = v/c$ is the particle velocity and θ' is the lab-frame emission angle. For a positronium ion accelerated to 3.9 keV, for example, the maximum Doppler-shift ($\theta' = 0^\circ$)

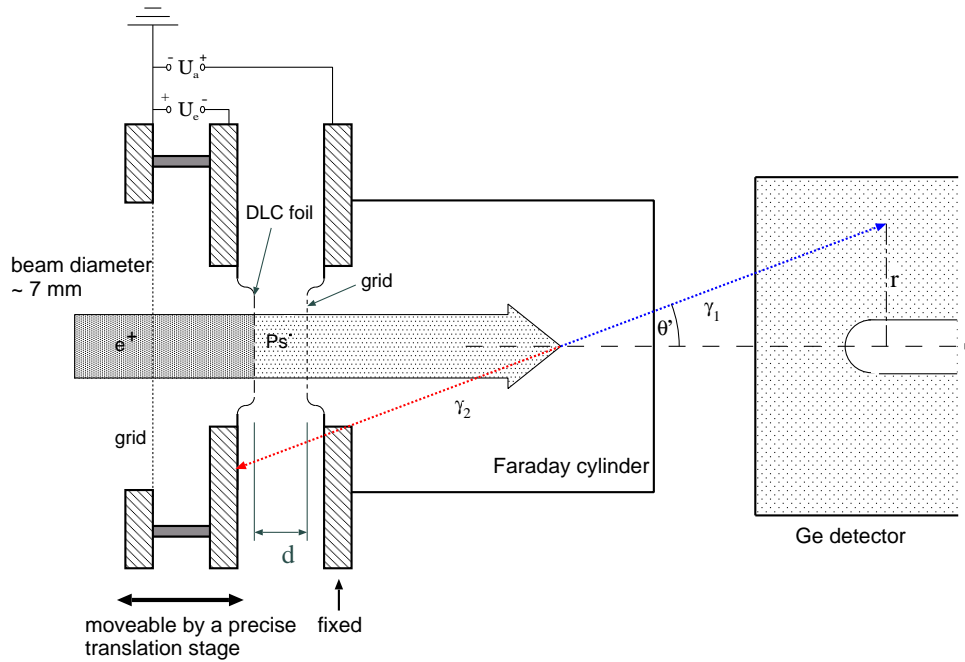


Figure 4.2: Schematic illustration showing the principle of the decay rate measurement using the gamma method. The positronium ions are identified by their Doppler-shifted annihilation radiation. As the fully accelerated Ps^- ions have a velocity of a few percent the speed of light, the Doppler-shift is large enough to distinguish these γ -rays from the 511 keV background caused by other positron annihilations.

amounts to 37.8 keV. This shift is much larger than the typical energy resolution of a germanium gamma-detector of a few keV; thus, it becomes possible to separate the decays of the fully accelerated Ps^- from the large background of positron annihilations in the production foil, which result in unshifted 511 keV γ -rays. This method was first employed in [Mil81a] to confirm the existence of the positronium ion. Later on, it was also used by Mills [Mil83] for the first experimental determination of the decay rate of Ps^- .

Fig. 4.2 shows a schematic illustration of the experimental set-up. The positronium ions are accelerated towards a grid, and after passing through it, they enter the field-free region of a Faraday cage. Inside this cage, the Ps^- ions decay in flight, and the annihilation radiation is recorded by a Ge detector in forward direction. As discussed in sec. 4.1, the necessary variation of the flight gap d is realized by moving the Ps^- formation foil, so the spatial relation between the Faraday cage and the detector does not change — which means that the solid angle subtended by the detector and thus the detection efficiency remains constant.

The decay rate measurement is performed by varying the distance d and measuring the

count rate of the fully Doppler-shifted annihilation radiation as a function of d . Positronium ions decaying inside the acceleration gap do not have a definite energy; they contribute to the background between the 511 keV line and the fully shifted peak.

4.2.1 The set-up for the γ -method

Due to the small count rate of Ps^- annihilations (at the time of the γ -measurement the ^{22}Na source used had an activity of ~ 4 mCi), the detector had to be placed as close as possible to the decaying positronium ions to optimize the detection efficiency. Moreover, a careful shielding of the detector from the room background was necessary. For this reason, the detector was surrounded by a lead housing with an inner lining of copper sheets wrapped around the detector capsule to reduce the contribution of X-ray fluorescence from the lead bricks. Of course these X-rays do not contribute directly to the energy region we are interested in ($\sim 511 - 550$ keV), but they may influence this spectral region via pile-up with one of the numerous 511 keV photons from the annihilation processes in the foil. These annihilation quanta by far dominate the overall count rate. This can be seen in fig. 4.3, where a typical gamma spectrum in the energy range from 0 to 2000 keV is shown. It has been obtained using the full set-up with an acceleration voltage $U = U_a - U_e = 3900$ V and a distance $d = 2.77$ mm. The figure caption additionally lists a few of the more prominent lines of the spectrum.

In order to minimize uncertainties due to possible drifts in the positron flux and to account for the decaying source activity, the measurements at different acceleration gap widths d were not done sequentially but in many short cycles. The order of the single measurements at a given set of distances within one cycle was chosen randomly. To reach approximately the same number of Ps^- counts at every individual distance, the respective data-taking time is scaled by a factor of $\exp(d/d_{\text{Ps}^-})$, where d_{Ps^-} is the length travelled within one Ps^- lifetime:

$$\Delta t(d) = \Delta t_0 \cdot \exp((d - d_{\text{closest}})/d_{\text{Ps}^-}). \quad (4.4)$$

The time interval Δt_0 for the shortest distance d_{closest} was set to 30 min. In this way a decay rate measurement at $U = 3900$ V and distances $d \in \{2.77 \text{ mm}, 5.27 \text{ mm}, 7.77 \text{ mm}, 10.27 \text{ mm}, 12.27 \text{ mm}\}$ has been performed. During the experiment, the data was recorded event-wise and saved. The average count rate of the Ge detector was $\sim 1000 \text{ s}^{-1}$, about a factor of ten below the limiting rate of the DAQ system. The integrated measuring time was ca. 25 days, at the smallest distance an additional run of nine days was used to collect statistics on the line shape. More details on the decay rate measurement using

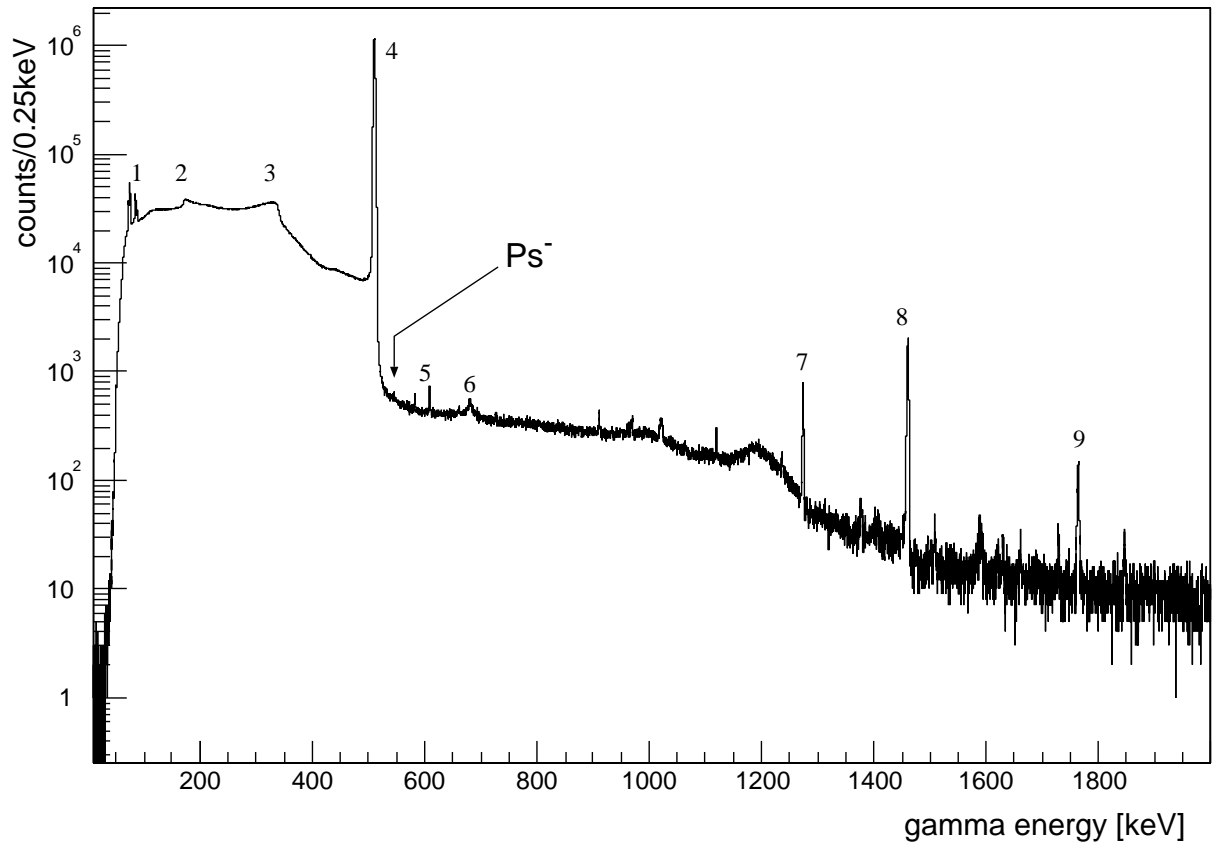


Figure 4.3: Gamma spectrum observed at an acceleration voltage $U = U_a - U_e = 3900$ V and a gap width of $d = 2.77$ mm. A few of the more prominent lines are marked: (1) X-ray fluorescence lines from the lead shielding, (2) backscatter peak of the 511 keV line, (3) Compton edge, (4) 511 keV from electron-positron annihilation, (5) several natural radioactivity background lines, (6) pile-up of (2) and (4), (7) 1273 keV γ from the daughter nucleus of ^{22}Na , (8) ^{40}K background line at 1461 keV, (9) ^{214}Bi . The γ -line from the Ps^- annihilations is barely visible. From [Les03].

the γ -method can be found in [Les03].

A second experiment at $U = 1000$ V has been tried; a serious analysis turned out to be impossible because of the bad signal-to-background ratio. This is due to the smaller Doppler shift of $\Delta E_\gamma = 18.4$ keV, which brings the signal considerably closer to the 511 keV background peak.

4.2.2 Results

A preliminary analysis of the measurement has been made within the framework of a diploma thesis [Les03]. This included an attempt to correct for the Doppler broadening of the annihilation line with the help of the interaction radius information from an online

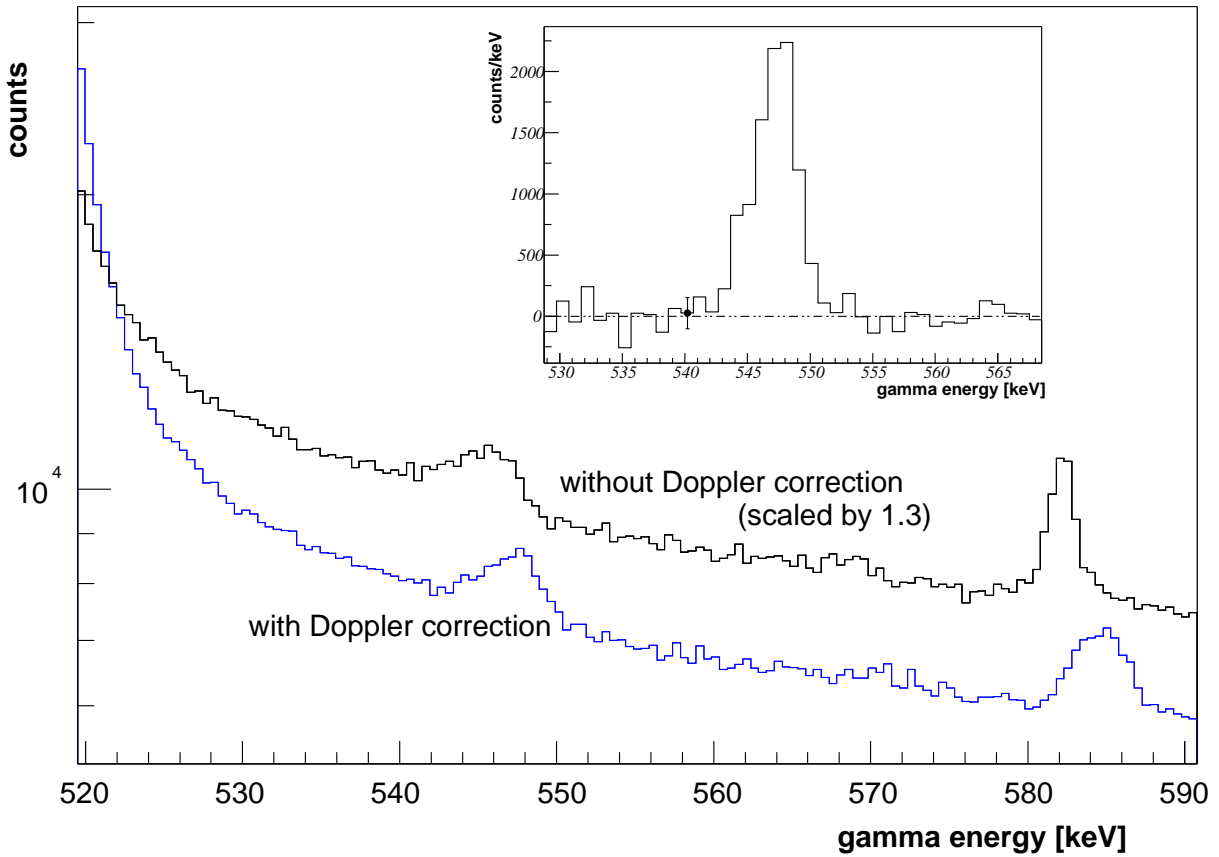


Figure 4.4: Typical gamma spectra (only the relevant energy interval is shown). The black and the blue histograms show the measured gamma spectrum at $U = 3900$ V and $d = 2.77$ mm without and with Doppler correction, respectively. For clarity, the uncorrected spectrum has been scaled by a factor of 1.3. The inset shows the Doppler-corrected spectrum after background subtraction. The exemplary error bar does not account for the uncertainty introduced by the background subtraction, but it shows only the statistical counting error. For more details refer to the text.

pulse-shape analysis of the detector signals [Lau04]. Knowing the approximate radius r of the first interaction of the γ -ray in the detector (see fig. 4.2) and the mean distance between the decay vertex and the point of interaction, one can estimate the emission angle θ' and correct the measured γ -energy using eq. (4.3). The effect of this Doppler correction can be seen in fig. 4.4, where the relevant part of the spectrum obtained at $d = 2.77$ mm is shown. The black histogram indicates the uncorrected spectrum, the blue one the spectrum after applying the Doppler correction, assuming $v/c = 0.7$ and correcting the measured γ -energy with the aid of the measured θ' value for a detection angle of $\theta' = 0^\circ$. As expected, the corrected Ps^- peak is centred around the position of the peak's higher-energy flank in the uncorrected spectrum — this corresponds to

the maximum Doppler shift reached at $\theta' = 0^\circ$. The resulting line shape of the Ps^- signal is now almost symmetric, but its width amounts still to 3.9 keV FWHM. This is significantly larger than the resolution of the detector of 1.95 keV (at 550 keV) [Les03] — which is evident also from the comparison with the background line in the uncorrected spectrum in figure 4.4 —, and the effective improvement in the peak-to-background ratio is marginal. The poor quality of the Doppler-shift correction is due to the relatively large diameter of about 7 mm of the Ps^- beam (see fig. 4.2) and the limited accuracy of the θ' determination caused by the close-up geometry. Therefore we did not use the Doppler correction in the final analysis of the data.

In order to determine the Ps^- peak area $N(d)$, an empirical background function is fitted in the energy interval [527, 565] keV (the region of the peak itself excluded), and the peak area after subtraction of this function is summed up numerically. To describe the background as a function of the γ -energy E , we use

$$B(E) = a_0 + a_1 \exp((E - E_0)^{a_2}) + a_3 \exp\left(-\frac{\Gamma d}{\Lambda c} \ln \frac{E}{E_{\gamma_0}}\right) \left(\frac{\Gamma d \Theta(E_{\max} - E)}{\Lambda c E}\right). \quad (4.5)$$

Here the a_i are fit parameters, E_0 is set to 546 keV, $E_{\gamma_0} = 511$ keV is the rest-frame photon energy, $E_{\max} = 548.8$ keV is the fully Doppler-shifted energy, and $\Lambda = eU/(3mc^2)$. In this expression, the a_3 -term accounts for the contribution of those positronium ions which decay during the acceleration [Les03].

As an example, the inset of fig. 4.4 shows the peak measured at $d = 2.77$ mm after subtraction of the fitted background. For each distance, the peak area N (without background) has been integrated over the interval [543, 548] keV. The results are listed in tab. 4.1, together with the errors σ_{count} and σ_{bg} , the respective measuring times and the final count rates N/t . The results of two measurements were combined for the data point at $d = 2.77$ mm: one was obtained from the decay rate experiment, the other one was deduced from a separate run at $d = 2.77$ mm performed 51 days after the other measurements. For the latter, the decay of the positron source ($t_{1/2} = 2.603(2)$ a [LS78]) was taken into account by multiplying the total Ps^- count rate by a factor of 1.038. Of the errors listed, the error σ_{stat} is determined by the counting error of the peak area before background subtraction, i.e. it is the square root of the number of counts in the interval [543, 548] keV. The second error, σ_{bg} , takes into account the error of the background subtraction. Additionally, a systematic error due to the lacking knowledge of the real physical background function has to be assumed. From the χ^2 of the exponential fit, this

d [mm]	t [s]	N	σ_{stat}	σ_{bg}	N/t [s^{-1}]
2.77	838622	13021	391	165	0.01553(51)
5.27	137078	1043	155	67	0.0076(12)
7.77	223435	1138	195	84	0.00509(95)
10.27	375414	1958	249	108	0.00519(72)
12.77	580665	1542	306	134	0.00266(57)

Table 4.1: Results of the decay rate measurements using the γ -method (analysis method 1). The acceleration voltage was 3900 V. Listed are the distance d , the measuring time t , integrated number of counts in the Ps^- peak N and its statistical counting error σ_{stat} , the statistical error of the background σ_{bg} and the resulting count rate N/t .

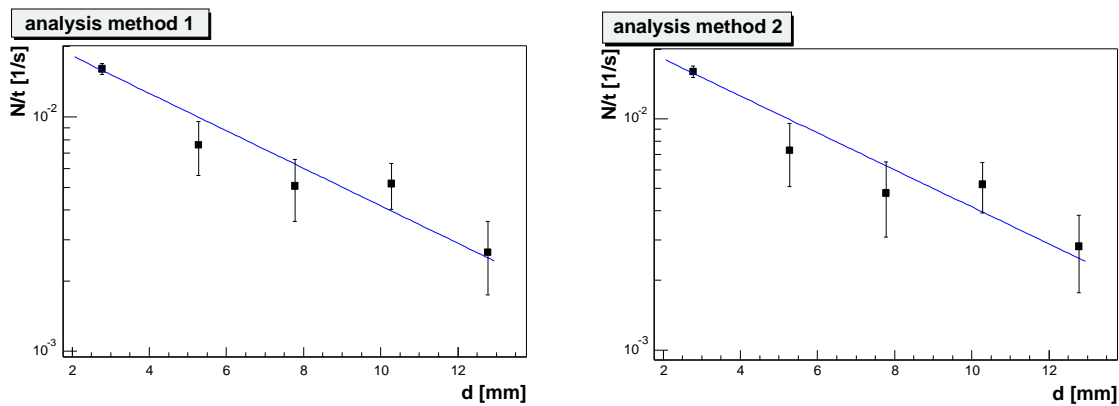


Figure 4.5: The exponential decay as measured with the γ -method (acceleration voltage $U = 3900$ V). The integrated count rate in the fully Doppler-shifted peak (after background subtraction) is plotted as a function of the distance d ; the blue line represents the result of an exponential fit $n_0 \exp(-\mu d)$. The two diagrams are generated by different data analysis methods. Left: a simple fit is used for background subtraction; right: an iterative approach ensures a consistent description of the Ps^- decays (see text).

error is estimated to be about 60% of the total statistical error. This has been included in the total error given for N/t .

In the left panel of figure 4.5 the count rates are plotted as a function of the respective distances d . The blue line represents the result of an exponential fit $n_0 \exp(-\mu d)$. The resulting value for μ is $\mu = 0.184(22) \text{ mm}^{-1}$, and one arrives at

$$\Gamma = 1.97(25) \text{ ns}^{-1}. \quad (4.6)$$

Here the assumption $T_0 = 0$ has been made, i.e. a negligibly small T_0 was assumed.

Using the same technique, Mills [Mil83] performed the measurement at two different

acceleration voltages U and extrapolated the results to $\sqrt{\Lambda_0/\Lambda} \rightarrow 0$. He found a rather strong dependence on U , resulting in an initial energy of $T_0 = 13_{-10}^{+19}$ eV. Assuming this value of T_0 , our measurements would lead to a decay rate of $\Gamma = 2.09(25)$ ns $^{-1}$. Due to the lack of statistics in our own decay rate measurement at $U = 1000$ V, we could not determine T_0 using the γ -method. However, the outcome of the more precise decay rate experiment with the stripping method (cf. section 4.3) strongly suggests that the value of T_0 is indeed negligibly small.

The rate of Ps $^{-}$ ions which survive the acceleration over the gap distance of 2.8 mm at $U = 3900$ V and which are detected in the full energy peak of the Doppler-shifted annihilation radiation amounts to ~ 0.016 s $^{-1}$. Taking into account the estimated rate of Ps $^{-}$ ions produced (~ 1.5 s $^{-1}$), the survival probability of 0.75 for an acceleration gap of 2.8 mm at an acceleration voltage of 3900 V and the estimated full energy peak efficiency of the Ge detector for detecting one of the annihilation γ -rays ($2 \times 0.75\% = 1.5\%$), one arrives at an expected count rate of 0.017 s $^{-1}$, in close agreement with the measured rate. There is one aspect in which the analysis strategy described so far is not very satisfying: the parameter a_3 in (4.5) is an independent fitting parameter. As it accounts for the number of positronium ions decaying during the acceleration, it should be correlated to the number of counts in the Ps $^{-}$ peak. In order to reach a consistent treatment of this contribution, another independent data analysis has been performed. In this second approach the following procedure has been applied: first an accurate theoretical Ps $^{-}$ lineshape — though without Doppler broadening — is constructed. It incorporates the fully shifted peak as well as the contribution of the positronium ions decaying during acceleration, convoluted with a Gaussian detector resolution function. Then, an iterative approach is used to determine $N(d)$, the number of counts in the fully shifted peak. Starting from the values obtained by the method just discussed, the expected contribution from the ions decaying during the acceleration is subtracted from the raw spectra. For these spectra a new background fit using only the first two terms of the background function given by eq. (4.5) is made, and the resulting peak area after background subtraction is determined. This value is in turn used to calculate again the contribution of the positronium ions decaying during acceleration, and so on. Empirically, the method was found to converge; it ensures a consistent ratio of the two Ps $^{-}$ -related spectral features. The result of this analysis is shown in the right panel of fig. 4.5. The differences to the other analysis method are small. Accordingly, the extracted value of $\mu = 0.184(26)$ mm $^{-1}$ is in agreement with the one cited above, and it leads to the same result for the decay rate, $\Gamma = 1.97(28)$ ns $^{-1}$, with a slightly increased error.

Our exploratory measurement of the Ps $^{-}$ decay rate performed with the γ -method there-

fore results in

$$\Gamma = 1.97(28) \text{ ns}^{-1}. \quad (4.7)$$

This value of Γ is in agreement with the theoretical value of 2.0861 ns^{-1} (e.g. [Fro99]), but it is less precise than Mills's result of $2.09(9) \text{ ns}^{-1}$ [Mil83].

4.3 The stripping method

The γ -method described in the preceding section provides an elegant means of detecting the positronium ions which survive the acceleration across the distance d . Nevertheless, there are several problems. Most importantly, it is difficult to determine the area of the rather small peak due to the Ps^- decays in the presence of a gamma background which is by orders of magnitude larger. Furthermore, as the electronics of the Ge detector cannot handle rates higher than ca. 10 kHz without excessive dead-time, the large background count rate limits the maximum usable positron flux. The experiment in section 4.2 was performed with a ^{22}Na source of 4 mCi, corresponding to $\sim 1.5 \cdot 10^4$ slow positrons per second in the experiment chamber, which leads already to a total count rate of about 1 kHz. This means that one cannot perform these experiments with substantially stronger ^{22}Na sources nor it is possible to take advantage of the very high intensities available at the new NEPOMUC positron source (see sec. 5.1), for example. In an attempt to overcome these difficulties, already Mills proposed an alternative approach to detect the surviving Ps^- which is based on stripping the positronium ions and detecting the remaining positrons in an appropriate detector [Mil90]. However, he could not apply this method successfully. The principle of the stripping method as we are employing it is shown in fig. 4.6: after passing the variable-width gap d , the Ps^- ions are post-accelerated towards a second DLC foil. On transmission through the foil they are stripped, and the positively charged positrons again experience an accelerating field. They are then magnetically guided onto a silicon particle detector. This method should be virtually background-free, with no other particles hitting the detector. Also the gamma background is not expected to present a problem because the stripped positrons are stable, and they can be transported a long way from the formation foil before reaching the detector. Additionally, silicon particle detectors are hardly sensitive to gamma rays. Finally, as only the stripped positrons are detected, the method can cope with very high initial positron fluxes.

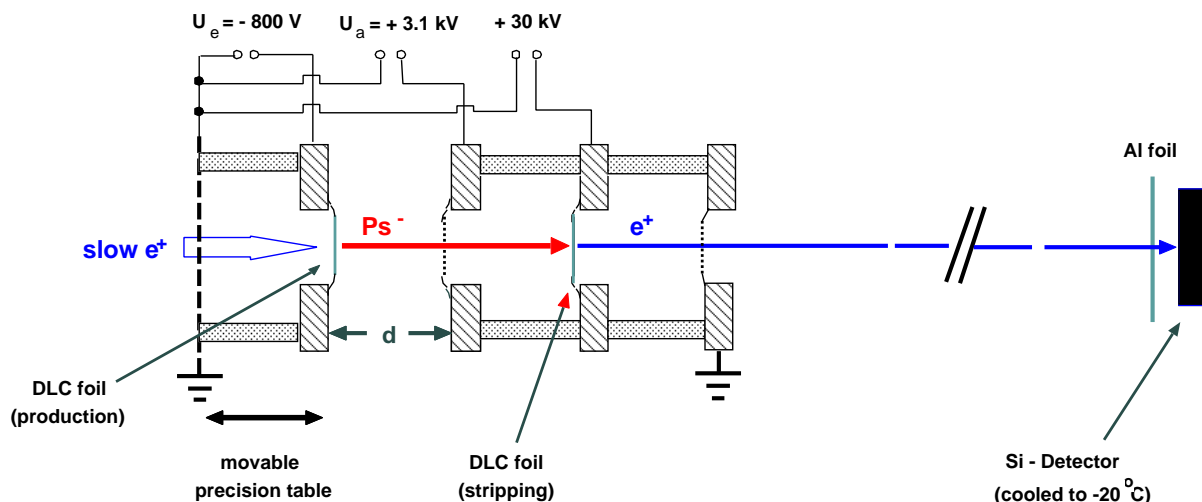


Figure 4.6: The stripping method is based on an acceleration and stripping scheme similar to that of a tandem accelerator: after passing the variable-width gap d , the Ps^- ions are post-accelerated towards a second DLC foil. By traversing the foil they are stripped, and the emerging positively charged positrons experience a further acceleration. The positrons are then magnetically guided onto a silicon particle detector. The voltages given here are typical values.

4.3.1 The stripping set-up

A sketch of the experimental set-up used for the decay rate measurements employing the stripping method is shown in fig. 4.7. Attached to the experiment chamber is a straight beamline of 1.050 m length, the first part of which is made of stainless steel, while the last 0.300 m are formed by an aluminium tube. Although the walls need to be thicker, the lower Z of aluminium leads to a significantly reduced absorption. In this way, it remains possible to detect the annihilation γ -rays in coincidence with the stripped positrons if required. There is no dedicated pump for the new section; rather it is pumped from the experiment chamber.

As it is quite difficult to extract charged particles from a magnetic field without introducing divergences, the guiding field was continued along the whole beamline. As before, this is achieved by means of solenoids wound directly around the beamline tubes — two layers of 2 mm copper wire have been used. At the flange, where the steel and the aluminium tubes meet, the gap is closed by an additional coil of 72 windings on the flange. This configuration ensures a sufficiently homogeneous magnetic field: fig. 4.8 shows the calculated on-axis field around the flange with and without the bridging coil. To keep the beam diameter small, especially in view of the angular spread introduced by scattering processes in the stripper foil, it is desirable to maintain a high magnetic field from the

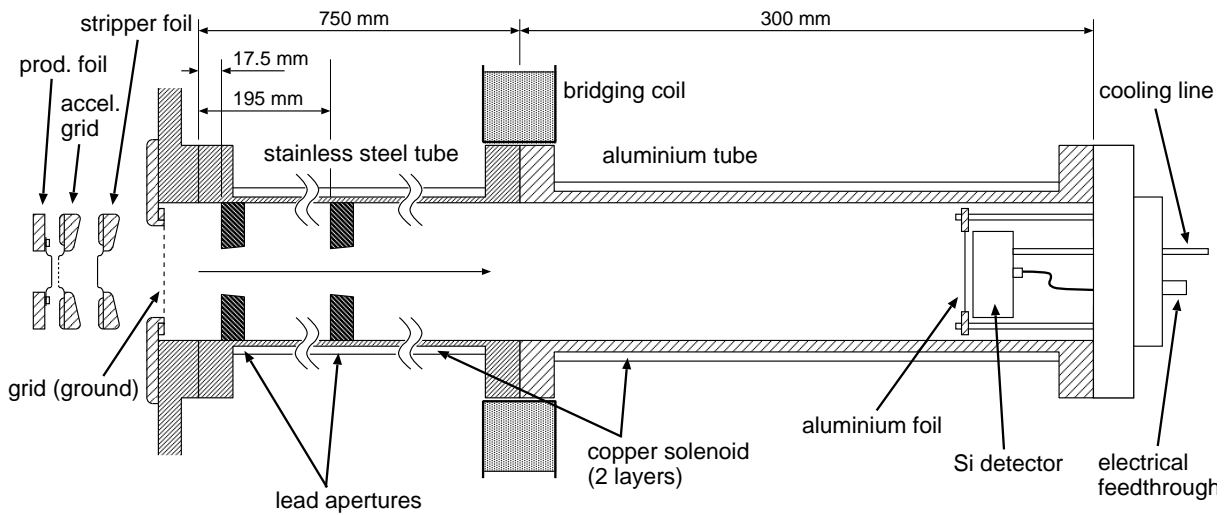


Figure 4.7: The experimental set-up for the decay rate measurements using the stripping method. For further explanations see text.

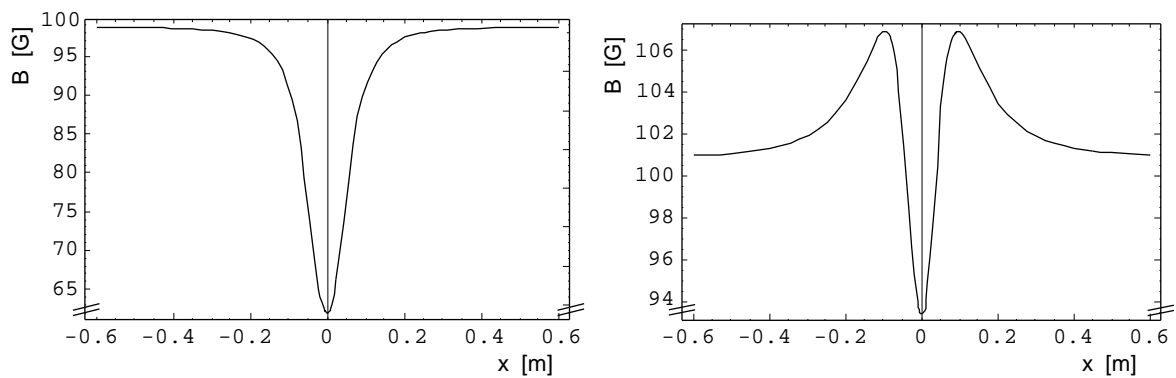


Figure 4.8: Comparison of the magnetic field across the gap caused by the CF flange without the additional bridging coil (left panel) and with the coil (right panel). Both diagrams show the respective calculated field on the axis for a nominal field setting of $B \approx 100$ G.

experiment chamber up to the detector. On the other hand, the usable field strength is limited not only by the power supplies but also by the inevitable heat generation. As a compromise, the current through the three coils is set to 12.5 A, corresponding to a calculated on-axis field of about 160 G. For better heat dissipation, the beamline is air-cooled with fans. With the temperature of the beamline being directly related to the rest-gas pressure inside, this also helps in improving the vacuum.

As far as the type of foils and grids and the mechanism for varying the distance d in the experiment chamber are concerned, the experimental set-up is based on the one for the

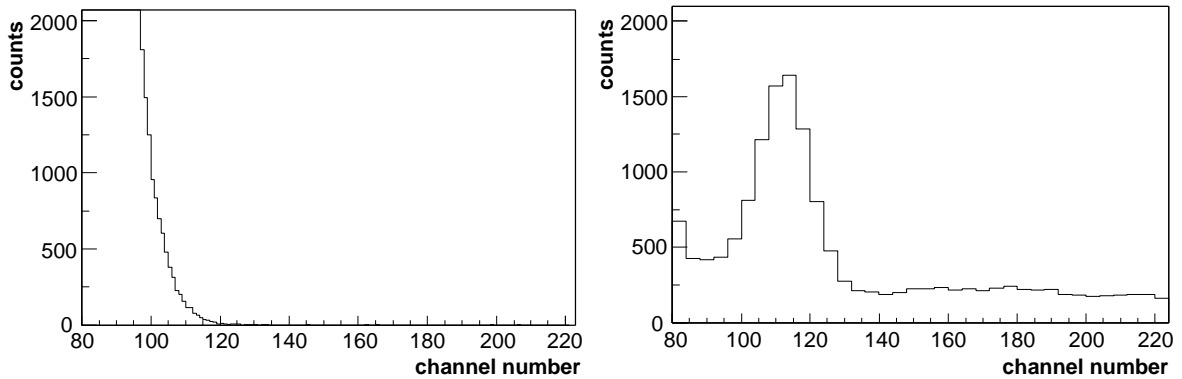


Figure 4.9: *Effect of the cooling of the Si detector: the left panel shows a spectrum recorded with the detector cooling switched off, the right one shows a similar spectrum at a detector temperature of -20°C , which clearly displays the positron peak at $\sim 40\text{keV}$. Note that the measuring time for the two spectra was quite different: while the spectrum on the left was recorded within a few minutes, the one on the right includes more than a day of data-taking.*

gamma measurement. To prepare for the high acceleration voltages at the stripper foil and to prevent high voltage breakdowns, however, the mounts for the first acceleration foil and for the stripper foil were redesigned. Sharp edges have been avoided, and all relevant screws have been countersunk. The high voltages for acceleration are generated by an ISEG NHQ 1010L (acceleration grid, U_a) and an FUG HCN 7E-35000 power supply (stripper foil). The voltage U_e for the production foil is delivered by an Ortec 456 high voltage power supply. The two voltages U_e and U_a , or more precisely their difference $U = U_a - U_e$, are needed in the calculation of the decay rate from the experimentally determined parameter μ (see eq. (4.2)). These voltages have been measured with a precision of $\pm 500\text{ mV}$ using a FLUKE 77 DVM and a recently calibrated (to 10^{-4}) high-voltage probe. However, while the ISEG power supply delivering the voltage U_a is stabilized to within one volt, this is unfortunately not true for the Ortec power supply used for the production foil potential U_e . Repeated measurements over a period of several weeks indicate that one has to assume an error of $\pm 5\text{ V}$ for this voltage. This implies that also the effective acceleration voltage U is known only to this accuracy.

As for the γ -method, only the production foil and the grounded entrance grid are moved by the translation stage. All the other parts are mounted at fixed positions. The distance between the acceleration grid and the stripper foil is 16.8 mm . The last grid of the set-up, the grounded 40 mm diameter grid for positron acceleration (transmission 88%), completely covers the opening between the experiment chamber and the following tube. At the end of the beamline a circular silicon detector of 300 mm^2 area and $100\text{ }\mu\text{m}$ depletion

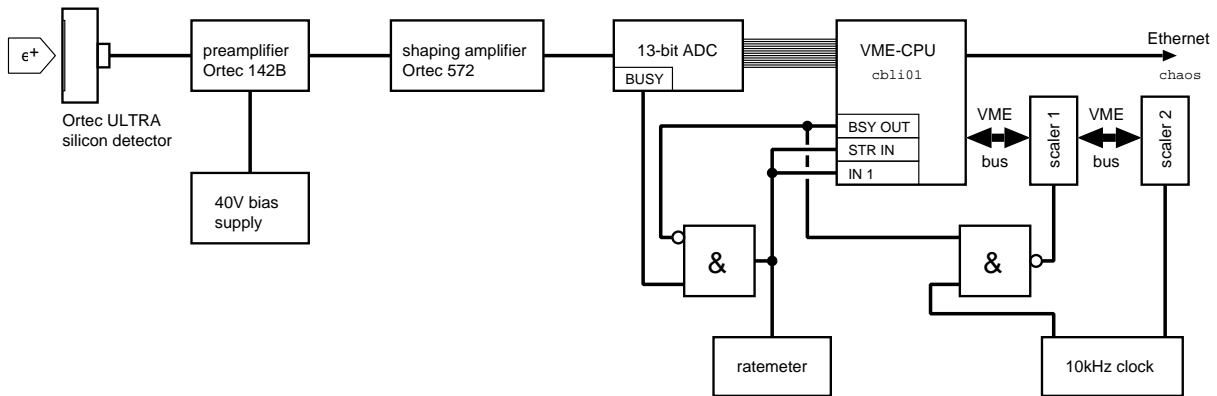


Figure 4.10: Schematic illustration of the data acquisition system for the stripping method. An explanation is given in the text.

depth is mounted (EG&G Ortec model BU-016-300-100), operating at a positive bias voltage of 40 V. The front face of the detector is shielded by a $1.5\ \mu\text{m}$ Al foil to prevent positive ions from hitting the detector (see below). As the positrons to be counted have a kinetic energy of about 40 keV, which is too low to stand out from the electronic noise at room temperature, the detector is cooled to -20°C . To achieve this, the detector is mounted in a hollow copper heat sink, which is soldered to two liquid feedthroughs. A circulating cooler maintains a continuous flow of the cooling agent and controls the temperature. The influence of the detector temperature on the noise contribution in the energy spectrum is illustrated in figure 4.9. Without cooling, the positron peak disappears in the electronic noise, while it is well separated from the noise at a detector temperature of -20°C . A measurement of the energy resolution for alpha particles shows that the resolution deteriorates when the detector has been cold for a while. This is probably due to the condensation of rest-gas components on the detector surface, which seems to cause a visible change in the resolution for alpha particles with their large energy loss dE/dx . Fortunately, the positrons are less affected; in fact, no energy shift of the positron line has been observed during 8 months of continuous operation. From the outside, the detector section is carefully shielded against the environmental background radiation. For this purpose, the aluminium part of the detector beamline is surrounded by a housing made of 5 cm thick lead bricks, and the inner side of the lead housing is lined with 5 mm copper sheets.

Figure 4.10 shows a schematic drawing of the data acquisition system (DAQ): after amplification by a charge-sensitive preamplifier (Ortec 142B) and an Ortec 572 shaping amplifier, the detector signal is processed by a 13-bit ADC ('MPIADC', designed and

built at the Max Planck Institute for Nuclear Physics, Heidelberg). Because of the very small signal amplitude, only the built-in leading edge discriminator of the ADC is used. To avoid any efficiency losses, the ADC is operated in anticoincidence mode with the gate input disconnected. In this mode every signal surpassing the leading-edge discriminator level of the ADC is converted to a 13-bit number. The BUSY output of the ADC triggers the readout, and the energy value is transferred to a VME computer. In case the system is still busy processing the preceding event, the readout is delayed until the CPU is ready again. To achieve this behaviour, the readout trigger is generated as the logical AND of the inverted readout busy signal and the ADC busy. This means that the ADC is read out as soon as the readout busy returns to low; this is of crucial importance because a suppression of the readout would leave the ADC hanging in the busy state. Additionally, two scalers provide information about the total measuring time and the dead time of the DAQ: both are fed by a 10 kHz clock, and one of them is blocked while the ADC is busy. After every event the scalers are read out and reset to zero. All energy and scaler data is collected event-wise and written to a file.

Typical trigger rates in the decay rate experiment are of the order of $\sim 50 \text{ s}^{-1}$, and they are by far dominated by the electronic noise. As one scaler measures the total time, the other one the dead-time-corrected time, the size of the dead-time correction can be calculated: as expected from the low rates, this correction is small (of the order of $2.5 \cdot 10^{-3}$).

First tests of the set-up revealed that there is a large background of ions hitting the detector, which are accelerated in the electric field behind the stripper foil. They show up as a relatively broad, intense peak in the spectrum, moving towards higher energies with increasing stripper foil voltage and being unaffected by changes of the guiding magnetic field. In fact, even when setting the solenoid current to zero, the peak does not vanish. One source of these ions is the cold cathode vacuum gauge in the experiment chamber; therefore, it is switched off during the measurement. As this does not completely remove the ionic background, an aluminium foil of $1.5 \mu\text{m}$ thickness² is placed in front of the Si detector. Even for protons the projected range in aluminium (at 30 keV) is only $\sim 0.3 \mu\text{m}$ [AZ77], so this thickness is more than sufficient to stop the ions, while the energy loss of the positrons (or electrons) is only about 800 eV [LS78]. The set-up including the Al foil has been thoroughly tested, and the irritating peak has vanished from the spectrum. Even with the cold cathode gauge switched on, it does not reappear. A typical spectrum observed with the silicon detector is shown in fig. 4.11. The positron peak at channel 114 is clearly visible, together with a background peak at channel 175 and a relatively broad

² Actually, as no pin-hole-free aluminium foils of this thickness are available, a sandwich of two $0.75 \mu\text{m}$ foils is used.

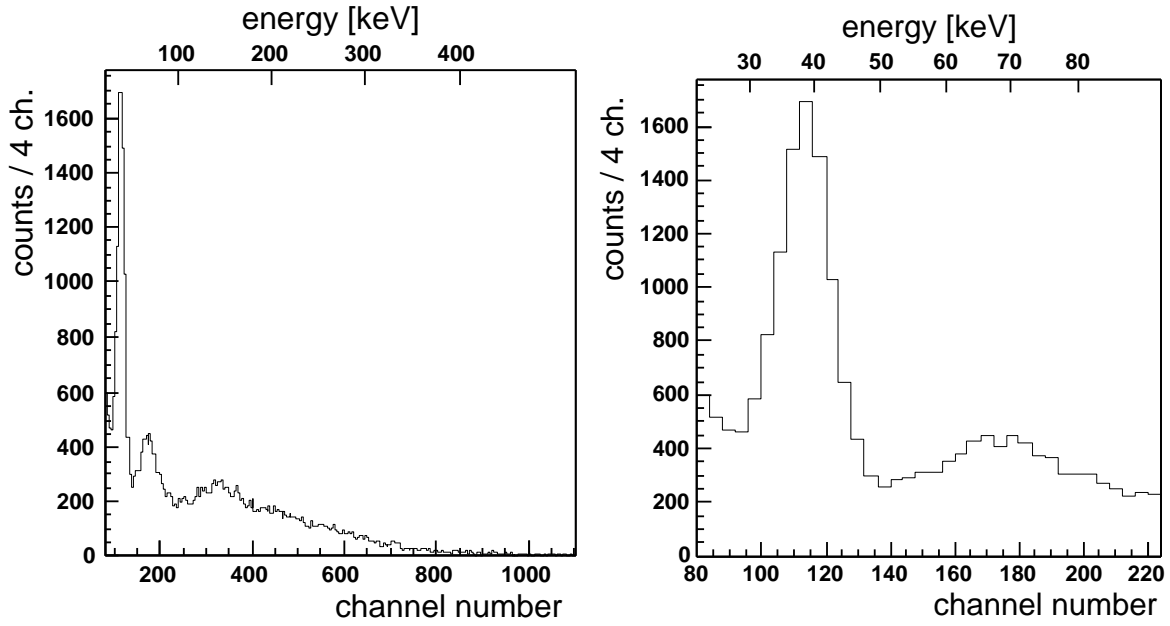


Figure 4.11: Typical example of a spectrum recorded with the Si detector at a gap width $d = 2.7$ mm and $U = 3900$ V. Besides the positron peak around channel 114 the background contribution from Compton electrons, caused by the 511 keV γ -radiation and reaching up to about channel 750, is visible. The right panel shows a close-up of the interesting low-energy part of the spectrum. Note that the spectrum was obtained without the lead apertures shown in fig. 4.7.

structure at even higher energies. Altogether, the background ends roughly at channel 750. Note that this spectrum was obtained without the lead apertures shown in fig. 4.7. Although an energy calibration of the silicon detector spectra is not strictly necessary, it is useful as it allows to check the expectations concerning the position of the positron peak, and it helps in the identification of the processes contributing to the background. Therefore, an energy calibration has been done using an alpha source (mounted in front of the detector instead of the aluminium foil) and a BNC DB-2 pulse generator: after adjusting the pulse generator's amplitude to match the 5486 keV alpha line from ^{241}Am , the pulse amplitude has been attenuated by definite factors of 2, 5, 10, 20 and 50 (see fig. 4.12). Assuming a linear response, the fitted peak positions and the corresponding energies lead to the energy calibration

$$E [\text{keV}] = 0.491(1) \cdot n [\text{channel\#}] - 17.2(29). \quad (4.8)$$

According to this calibration, the position of the positron peak corresponds to an energy of 38.7 ± 2.9 keV. This is in very good agreement with what one would expect from the

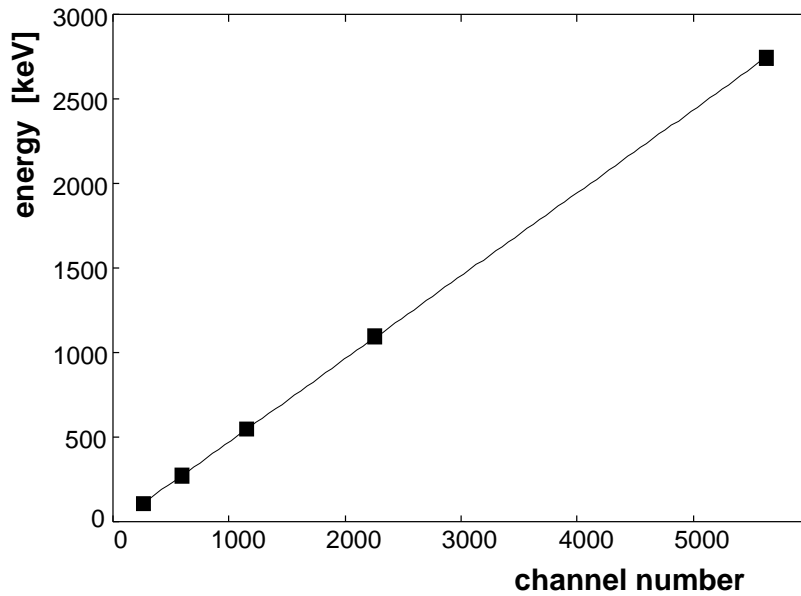


Figure 4.12: Energy calibration of the silicon detector. The error bars are smaller than the point symbols.

acceleration scheme: the positronium ions are accelerated to an energy of 30.8 keV, and after stripping the positrons should have a kinetic energy of $1/3 \cdot 30.8 \text{ keV} = 10.3 \text{ keV}$. In the following electric field the positrons acquire an additional kinetic energy of 30 keV, therefore their final energy — including the energy loss in the foils — is expected to be 39.5 keV.

The second peak at a somewhat higher energy is centred around $68.7 \pm 2.9 \text{ keV}$, and the whole background reaches up to an energy of about 350 keV. Together with the observation that this background component is not stopped by the $1.5 \mu\text{m}$ aluminium foil, this points to Compton electrons as an explanation. The positron annihilations in the production foil form an intense source of 511 keV γ -rays, which in turn interact with the material of the walls, foil holders, etc. The upper limit of the Compton electron energy is given by the Compton formula; for 511 keV photons it is $\sim 341 \text{ keV}$. This is in good agreement with the observed cut-off energy of the background. In contrast to the ionic background, the electrons should be influenced by the magnetic field in the beamline. An experimental test confirms indeed that the shape of the background changes with the magnetic field strength. In fig. 4.13 this is illustrated by plotting the spectrum for different values of the current I_{solenoid} in the solenoids around the beamline between the experiment chamber and the detector. One observes a series of broad peaks, which seem to emerge at the low-energy end of the spectrum and to shift towards higher energies with

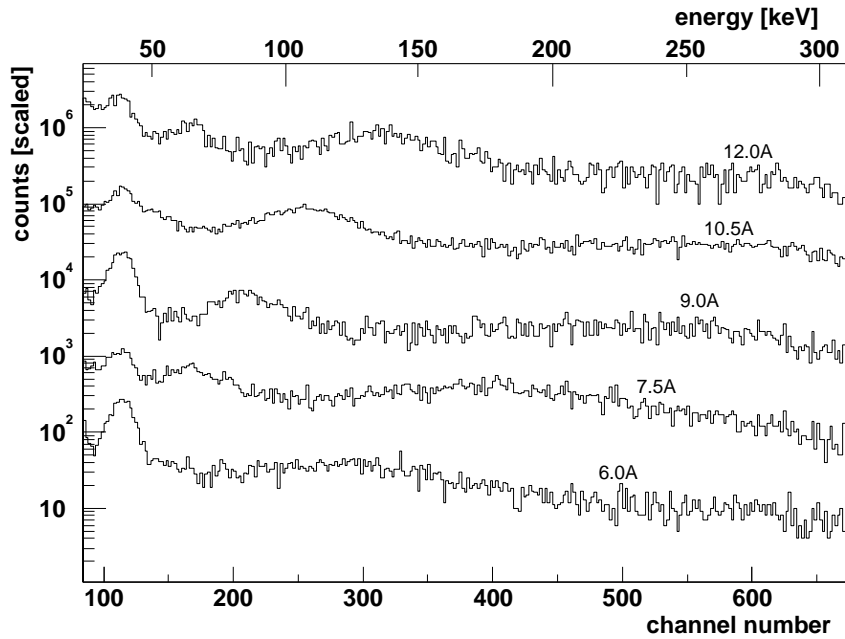


Figure 4.13: Measured silicon particle detector energy spectra for different values of the guiding magnetic field (indicated are the respective solenoid currents). All spectra, which were recorded without the lead apertures, are arbitrarily scaled and are not normalized to the same measuring time. The leftmost peak is the positron signal. The background structures clearly depend on the magnetic field strength.

increasing magnetic field strength. Additionally, a broadening of the peaks occurs as they are shifted towards higher energies.

A simulation³ of the set-up with GEANT4⁴ demonstrates that the magnetic-field dependent transport properties of the beamline can introduce such structures even when starting from a flat energy distribution: in the simulation run leading to the spectrum of fig. 4.14 an isotropic electron source roughly at the position of the stripping foil is used, the energy of each electron is chosen randomly from the interval $[0, 350 \text{ keV}]$. Nevertheless, the simulation, which includes a geometrically idealized model of the whole new detection beamline, also shows field-strength dependent maxima.

This strongly supports the hypothesis that electrons are the source of this background,

³ The source code of the simulation is stored as a tree under the version management software CVS with `$CVSROOT = fleische@lfs1.mpi-hd.mpg.de:/home/cb/psminus/.cvs/`, the module name is `psminus_si`. As it is rather lengthy, the code has not been printed in the appendix. If interested, contact the author.

⁴ GEANT4 is a package for Monte-Carlo simulations of detector systems developed at CERN. For further information refer to <http://www.cern.ch/>.

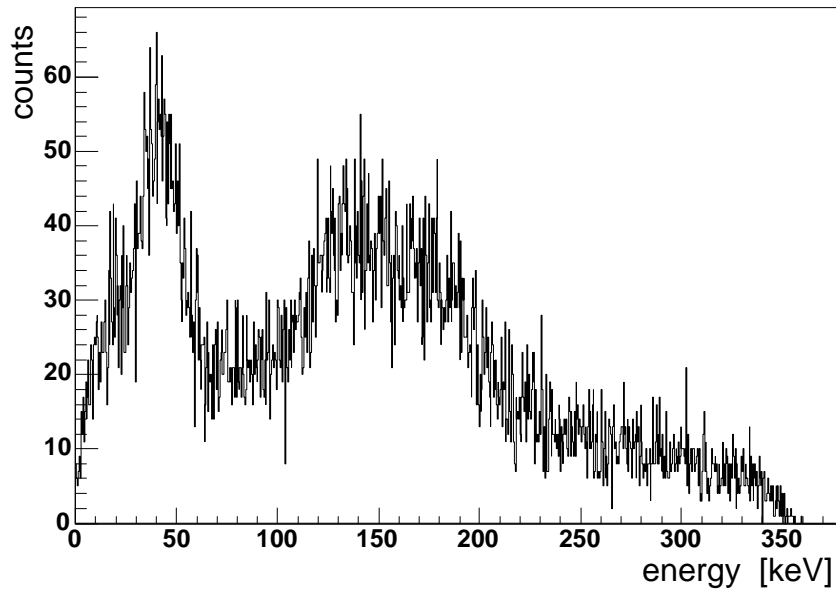


Figure 4.14: Simulated silicon particle detector energy spectra for an isotropic electron source located roughly at the position of the stripper foil. The primary electrons were assumed to have a flat energy distribution reaching up to 350 keV, and the magnetic field was set to $B = 100$ G. Obviously the transport properties of the set-up introduce a magnetic-field dependent structure in the recorded energy spectrum. The simulation has been performed using the GEANT4 package from CERN together with the extension for low-energy electromagnetic processes.

and means of reducing this background contribution have been sought for. As most of the Compton electrons are expected to be produced along the inner side of the beamline walls, it was decided to insert a pair of lead apertures into the tube. These are made of 10 mm lead sheets, and they have an inner diameter of 20 mm on the upstream side, conically widening to 22 mm on the detector side. They shield a large part of the tube walls from irradiation by the annihilation gamma rays coming from the DLC foil, and they help in stopping the already produced Compton electrons. The latter is possible due to the rather large cyclotron radii of these electrons, which are determined by their transversal kinetic energy. The positron beam, on the other hand, should have only small transversal energy components and should therefore be more or less unaffected by the apertures as their inner diameter is chosen a bit larger than that of the sensitive detector area of 19.5 mm. However, due to scattering in the foils also some of the positrons can gain a large transversal energy (see below). As visible in fig. 4.15, the insertion of the apertures causes the positron count rate to drop by 31%⁵, but it indeed leads to a significant reduction

⁵ Comparing the spectra, one observes a total decrease in count rate of 37%. However, to determine the effect of inserting the apertures, a correction for the decay of the ^{22}Na source was applied: as

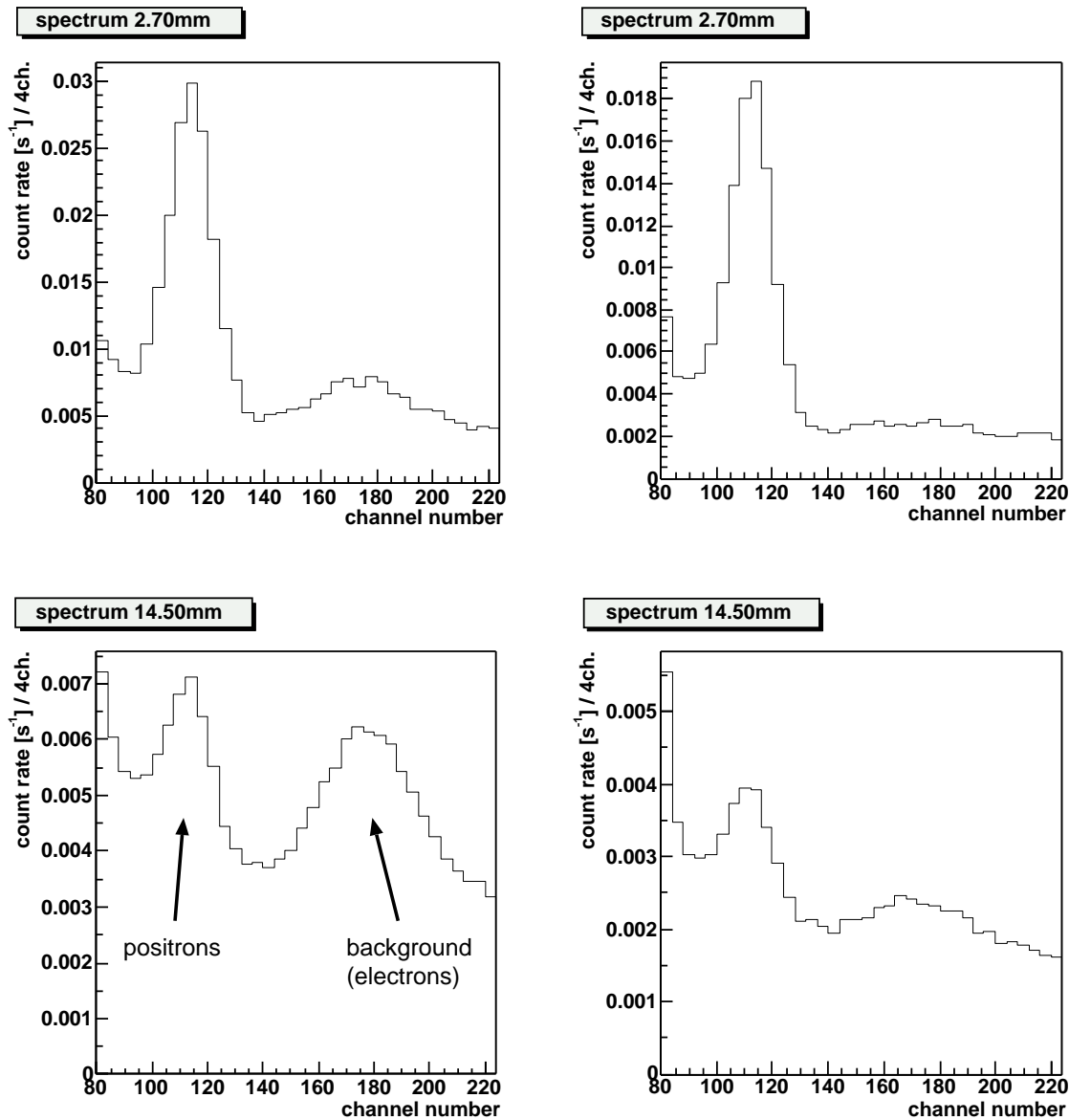


Figure 4.15: Reduction of the Compton-electron background by the lead apertures: In the left column, two spectra taken at $d = 2.7$ mm and $d = 14.5$ mm without the apertures are shown, the right column displays the corresponding spectra with the apertures in place. The spectra have been normalized based on the respective measuring times. The suppression of the background peak around channel 175 is clearly visible. As a side effect, the apertures also lead to a reduced count rate in the positron peak. All spectra were recorded at an acceleration voltage of $U = 3900$ V and with a magnetic field of about 160 G ($I_{\text{solenoid}} = 12.5$ mm) in the detector beamline.

of the background. In this way, a quite favourable signal-to-background ratio has been reached; in comparison to the gamma-method (see sec. 4.2) this is indeed a dramatic improvement.

One would also expect an improved efficiency of the stripping method as compared to the gamma method. This is due to the greater detection efficiency of a silicon particle detector for positrons ($\sim 80\%$) and to the fact that the positrons are guided to the detector in a directed beam, while the germanium detector used in the γ -measurement can observe only a small fraction of the isotropically emitted annihilation radiation. Starting from the expected production rate of positronium ions at the time of the measurement of fig. 4.15 (right column, ca. 8/2004) of $0.8 \times 15 \text{ s}^{-1} \simeq 12 \text{ s}^{-1}$ (cf. sec. 3.4), we can estimate the expected count rate in the Ps^- peak: during the flight from the production foil to the acceleration grid roughly 25% of the ions decay (for $d = 2.7 \text{ mm}$, $U = 3900 \text{ V}$), similarly there is a 54% loss between the acceleration grid and the stripper foil (distance 16.8 mm). Moreover, the beam passes through five grids; for three grids of 86% transmission each (production foil, acceleration grid and stripper foil) and two grids with $T = 88\%$ (the grounded entrance and exit grids), the total transmission is 49%. Taking into account the detector efficiency of 80% and the 31% loss due to the lead apertures, approximately 9% of the produced Ps^- ions, i.e. $\sim 1 \text{ Ps}^-/\text{s}$, should be observed if we assume that all stripped and post-accelerated positrons are transported to the Si detector. Looking at the actual count rate, however, the total rate in the signal peak, amounts only to $\sim 0.08 \text{ s}^{-1}$, about a factor of 12 smaller than expected.

Two effects may be responsible for the smaller rate: (i) the moderation efficiency may have dropped after the exchange of the 4 mCi source by the 40 mCi source. Actually, the moderation foil was not newly annealed after changing the source. However, comparing the Ps^- rates observed with the stripping method before and after the source change, a deteriorated moderation efficiency can at most account for a rate loss by a factor of 1.5, leaving still a factor of 8 unexplained. (ii) The assumption that all stripped and post-accelerated positrons are transported to the silicon detector may be too optimistic. In fact, small scattering angles acquired by the positrons during the stripping process may lead to transversal energies too high to be compensated by the magnetic transport field. Unfortunately, nothing is known about the angular distribution of the resulting positrons in $\sim 5 \text{ nm}$ thick stripping foil, but the observed loss of detection efficiency when inserting the lead apertures into the detection beamline does indicate that the scattering is appreciable and may indeed be responsible for the remaining loss factor. The scattering

the measurement with the apertures has been performed about 3.5 months after the other one, the number of counts in the spectra recorded without the apertures was multiplied by 0.925.

of the positrons in the $1.5\ \mu\text{m}$ thick aluminium foil in front of the silicon detector is expected to be very strong. Inferring from the results discussed in [LBK⁺90], one expects an almost flat angular distribution. Fortunately enough, this foil can be placed very close to the detector surface ($\sim 2\ \text{mm}$) to ensure the detection also of those positrons with larger scattering angles: the loss of efficiency due to the scattering of the positrons in the aluminium foil is therefore expected to be less important.

Even though the detection efficiency of the stripping measurements is not as high as hoped for, the new approach results in a dramatic improvement in the signal-to-background ratio, which should allow for a considerably more precise decay rate measurement than the γ -method.

4.3.2 Results

Using the method described in the preceding section, a new decay rate measurement of the positronium negative ion has been made. To investigate the influence of a possible initial kinetic energy T_0 (cf. sec. 4.1), the measurement was performed for six different nominal values of the acceleration voltage U : $U = 1000, 1300, 1900, 3900, 4000$ and $4800\ \text{V}$. The same scheme of distributing the measuring time to the different flight distances d as in the γ -experiment was used: for every cycle a random order of the distances d is determined, and the duration is chosen according to the expected count rate in order to reach a comparable number of counts for all values of d (see eq. (4.4)). Only the time constant Δt_0 of this process differs from the one used for the γ -experiment, with $\Delta t_0 = 10\ \text{min}$. The whole data was taken over a period of eight months. Therefore, a separate run (#9) at the first acceleration voltage (3900 V) was started near the end of the experiment to be sure of the reproducibility of the results.

As it turned out, a few data files⁶ contained excessive noise. To identify these files, all files have been examined by a script, and after a manual inspection those with an unusually large noise contribution (about 10 files) have been excluded from the final analysis.

Table 4.2 gives an overview of the distances d chosen for each of the runs. In all runs the value of 28.0 mm, close to the present mechanical limit, is included. The spectra recorded at this acceleration gap width are used to determine the background under the positron peak. As the background is caused mainly by Compton electrons, the electronic peak around channel 175 is used for normalization: for each spectrum the integral number of counts in the interval [140, 220] is determined, and the 28.0 mm spectrum is then scaled

⁶ Every measurement cycle produces one data file per value of d . Therefore, depending on d , one data file corresponds to at maximum two hours of data-taking.

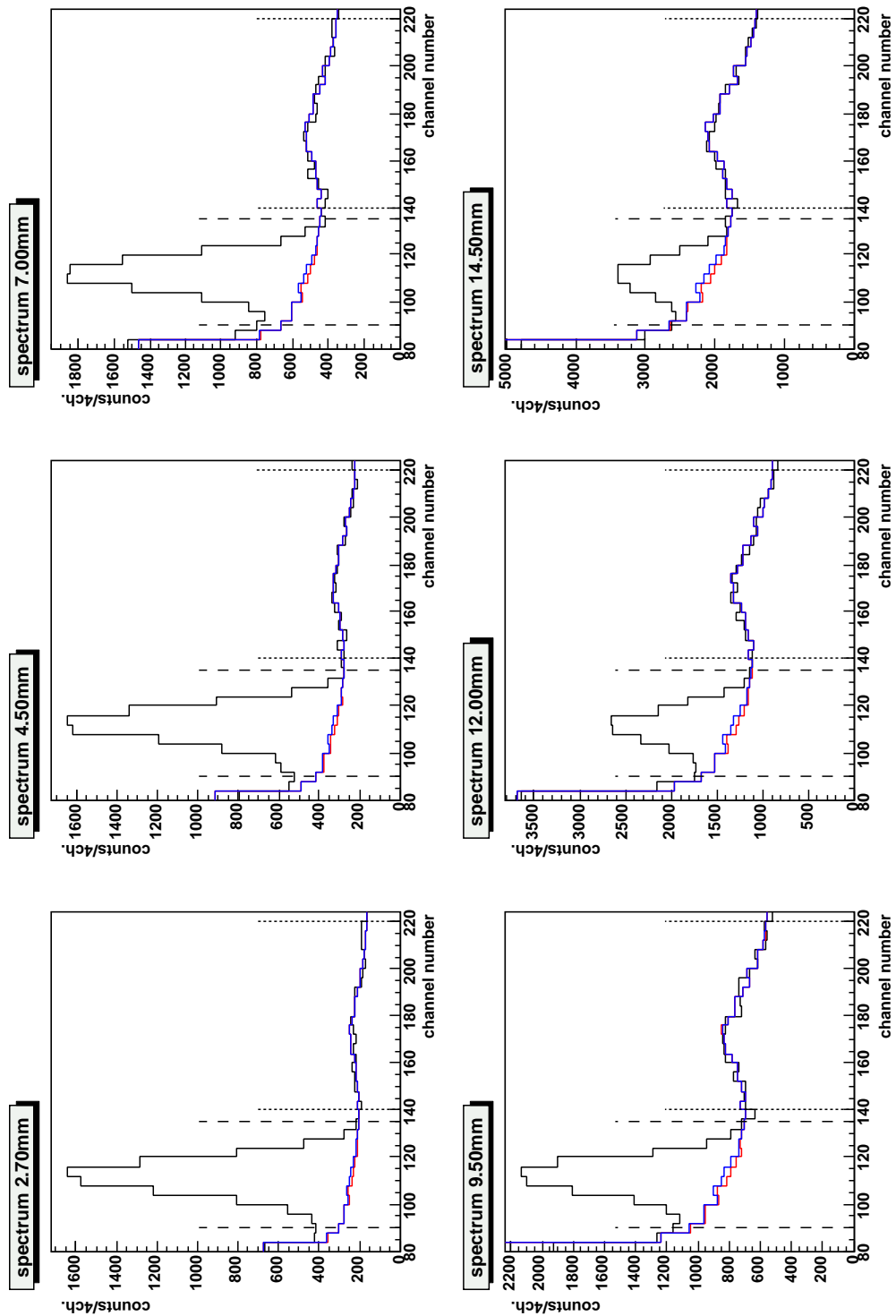


Figure 4.16: The spectra recorded during the decay rate measurement at $U = 3900$ V (sum of runs #1 and #3). The blue histograms show the appropriately scaled approximation to the background, obtained from the spectrum taken at $d = 28$ mm, the red histograms (only visible where different from the blue ones) represent the background after applying a correction for the residual Ps^- contribution in the $d = 28$ mm spectrum (see text). The limits of the region used for peak integration are indicated by the broken lines, the limits of the background region used for scaling of the background spectrum are marked by the dotted lines.

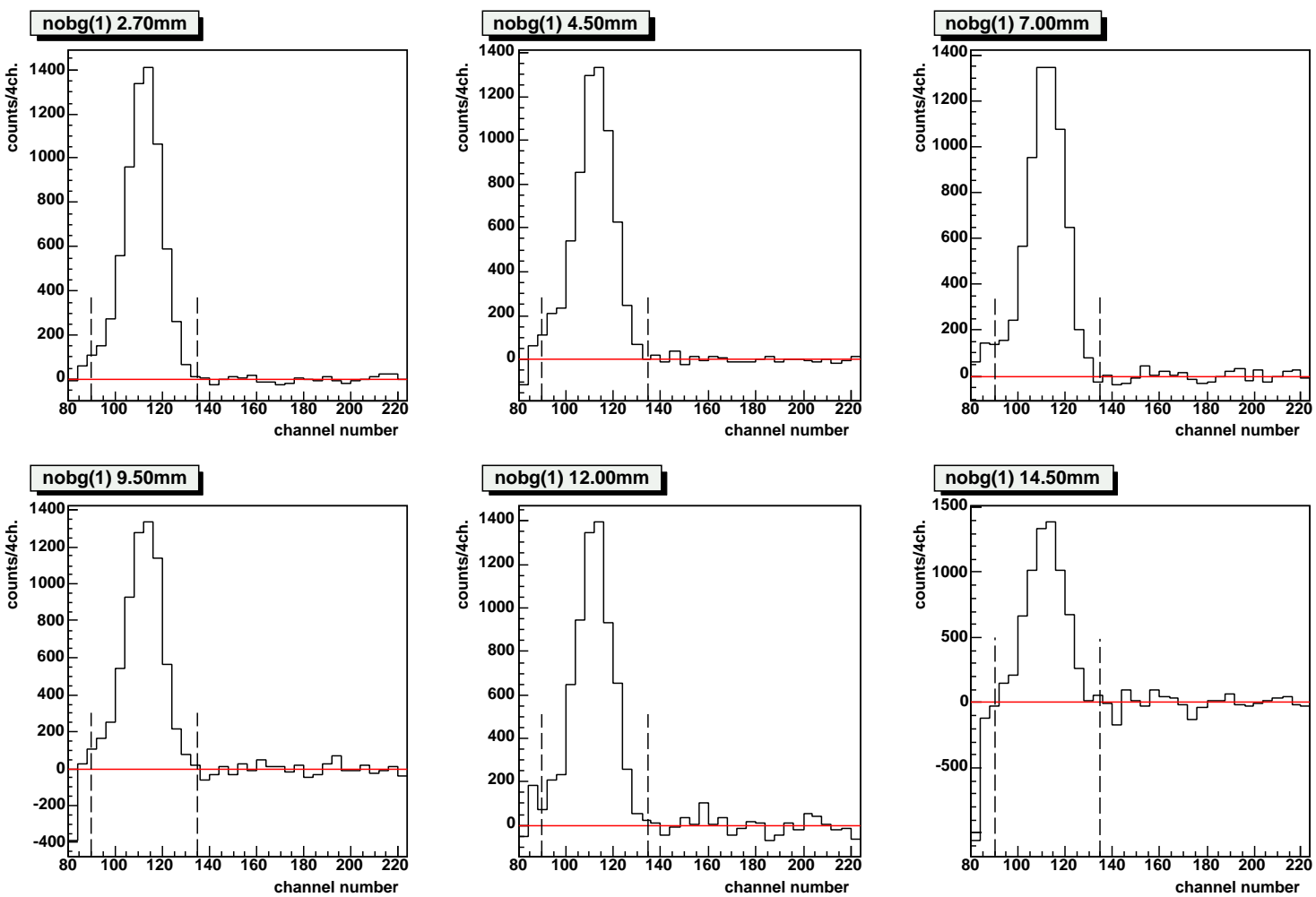


Figure 4.17: The spectra recorded during the decay rate measurement at $U = 3900$ V after subtracting the corrected background. The limits of the region used for peak integration are indicated by the broken lines.

run #	U [V]	used distances d [mm]	time of measurement
1	3900	2.7, 4.5, 7.0, 9.5, 12.0, 14.5, 28.0	2004-06-25 – 2004-07-16
2	1000	2.7, 3.9, 5.1, 6.3, 7.5, 28.0	2004-07-26 – 2004-08-16
3	3900	2.7, 4.5, 7.0, 9.5, 12.0, 14.5, 28.0	2004-08-16 – 2004-09-07
4	1000	2.7, 3.9, 5.1, 6.3, 7.5, 28.0	2004-09-07 – 2004-10-15
5	1900	2.7, 4.4, 6.0, 7.6, 9.4, 10.9, 28.0	2004-10-15 – 2004-11-10
6	4000	2.7, 4.5, 7.0, 9.5, 12.0, 14.5, 28.0	2004-11-10 – 2004-12-13
7	1300	2.7, 4.1, 5.4, 6.8, 8.1, 9.5, 28.0	2004-12-13 – 2005-01-12
8	4800	3.5, 6.1, 8.7, 11.4, 14.0, 16.6, 28.0	2005-01-12 – 2005-02-02
9	3900	2.7, 4.5, 7.0, 9.5, 12.0, 14.5, 28.0	2005-02-02 – 2005-02-14
10	4800	3.5, 6.1, 8.7, 11.4, 14.0, 16.6, 28.0	2005-02-14 – 2005-02-20

Table 4.2: List of the runs for the decay rate measurement with the stripping method, including the acceleration voltages U and distances d used.

to match the corresponding count rate of the other spectra. As an example, fig. 4.16 shows the recorded spectra for $U = 3900$ V (sum of runs #1 and #3). Except for the 28 mm background spectrum, the spectra are drawn in black; along with them the scaled 28 mm spectra are shown in blue. The preliminary ‘background’ spectrum still contains a residual contribution from positronium ions which have survived the flight across the gap of 28.0 mm. Nevertheless, it can be used as a first approximation to the background. After background subtraction, the respective number of positron counts in each spectrum is determined by summing up the bin contents between the channels 90 and 135 (the region indicated by the broken lines in fig. 4.16). In combination with the information about the dead-time-corrected measuring time from the scalers (see sec. 4.3.1), the Ps^- count rates can be calculated. An exponential fit with the function $n_0 \exp(-\mu \cdot d)$ then yields an approximate decay constant μ .

Using this value, the background spectrum measured at 28 mm can be corrected for its residual positron contribution: by multiplying with $\exp[-\mu(28 \text{ mm} - d_{\text{closest}})]$, the background-free positron peak from the spectrum measured at the smallest distance is downscaled according to the difference in flight distance and subtracted from the 28 mm spectrum. The corrected background spectrum is now used to recalculate the Ps^- peak intensities and the decay constant μ , and the procedure is repeated until the peak intensities do not change anymore. The correction caused by the residual Ps^- counts in the $d = 28$ mm spectrum depends on the acceleration voltage U . While it is negligibly small for the runs at 1000 V, increasing the number of Ps^- counts at $d = 2.7$ mm by

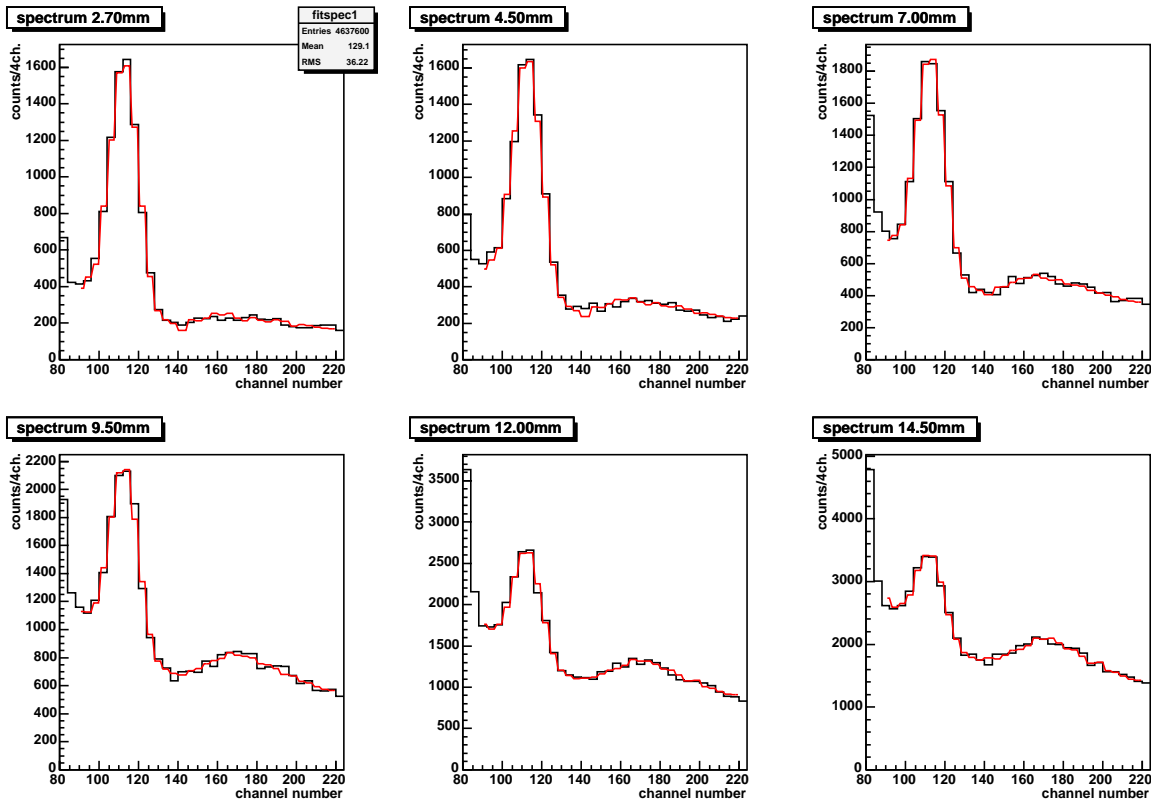


Figure 4.18: Fit to the spectra recorded at $U = 3900$ V, using a linear combination of the corrected 28.0 mm background and the experimental positron line shape. The data is drawn in black, the fit function in red. For details refer to the text.

only $5 \cdot 10^{-3}\%$ and the number of counts at $d = 7.5$ mm by $3 \cdot 10^{-2}\%$, it presents a more significant correction for the 4800 V runs: the Ps^- counts at $d = 3.5$ mm are increased by 1.9%, those at $d = 16.6$ mm by 18.3%. The properly scaled corrected background spectra are shown in fig. 4.16 by the red histograms while the background subtracted spectra are displayed in fig. 4.17.

As the line shape of the positron peak is expected to be independent of d , we can determine an experimental line shape by adding up all background-free peaks. This can then be employed to fit the spectra in the interval $[90, 220]$ using a linear combination of the normalized experimental line shape and the corrected background. Figure 4.18 displays the result of the fits, the corresponding difference spectra (measured spectra - fits) are drawn in fig. 4.19. The comparison of the difference spectra with the 1σ error band shows that the measured spectra are very well accounted for by these fits. They provide us with the final scaling factors for the background spectra. After their subtraction, the

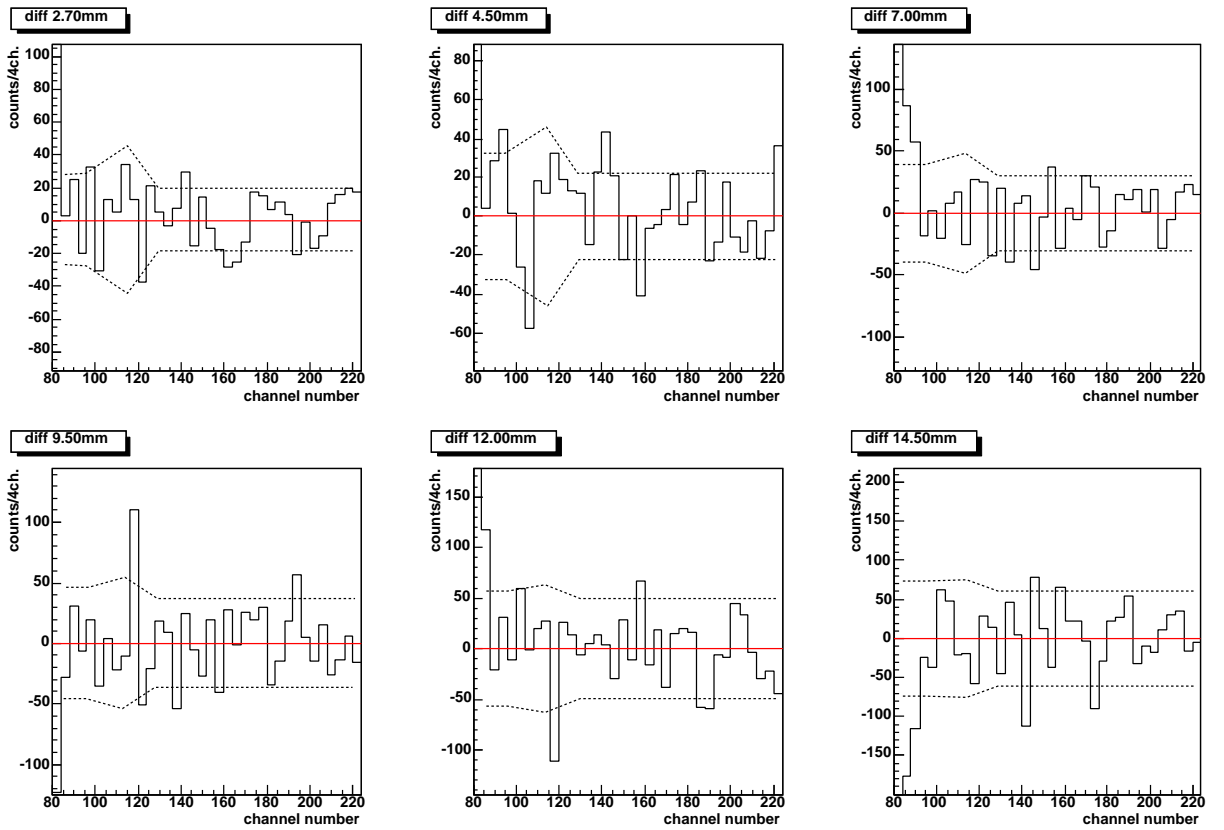


Figure 4.19: Difference (*spectra - fit*) for the spectra recorded at $U = 3900$ V. The dotted lines represent the $\pm 1\sigma$ error band.

number of counts in the Ps^- peaks are finally determined by summing up the peak areas in the interval [90, 135]. The peak areas are then normalized to the respective dead-time corrected measuring times to yield the corresponding rate as a function of the gap width d .

The count rates obtained by this method are plotted as a function of d in fig. 4.20, together with the best fit using the function $n_0 \exp(-\mu \cdot d)$ with n_0 and μ as free parameters. As the errors of the data points are too small to be visible in this graph, fig. 4.21 shows the same data after subtracting the fitted exponential decay.

The indicated errors of the count rates N/t are calculated from the square-root counting errors for the signal and the scaled background. Compared to these errors, the uncertainty in the determination of the measuring times is negligible. A more detailed listing of the numerical results is given in table C.4 in appendix C.

The analysis of the other runs performed at different acceleration voltages was done in the same way (see appendix C). The resulting decay constants μ are given in table 4.3.

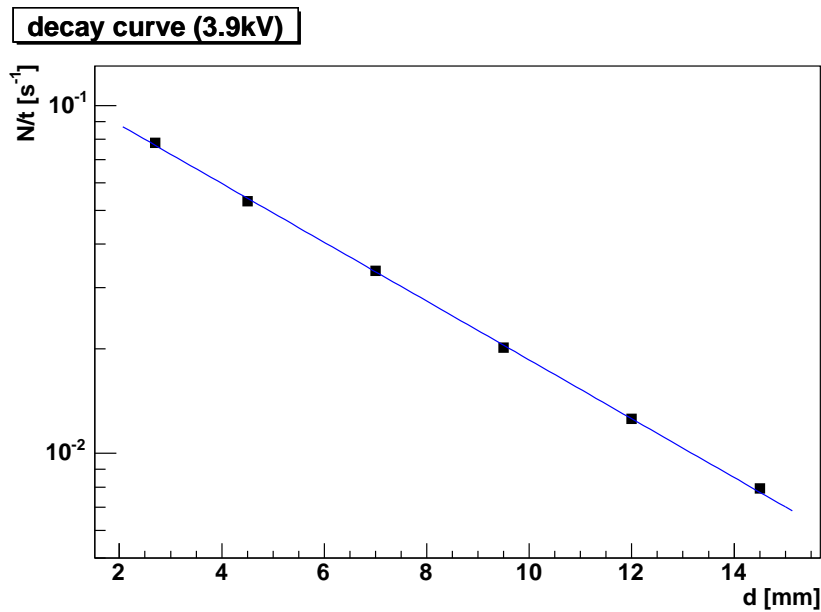


Figure 4.20: Measured decay curve at $U = 3900 \text{ V}$ (sum of runs #1 and #3). Plotted is the count rate (positron peak area after background subtraction, divided by the duration of the measurement) as a function of the distance d between the production foil and the acceleration grid. The error bars are smaller than the symbols. The continuous line represents the best fit to the data using $n_0 \exp(-\mu \cdot d)$ with n_0 and μ as free parameters.

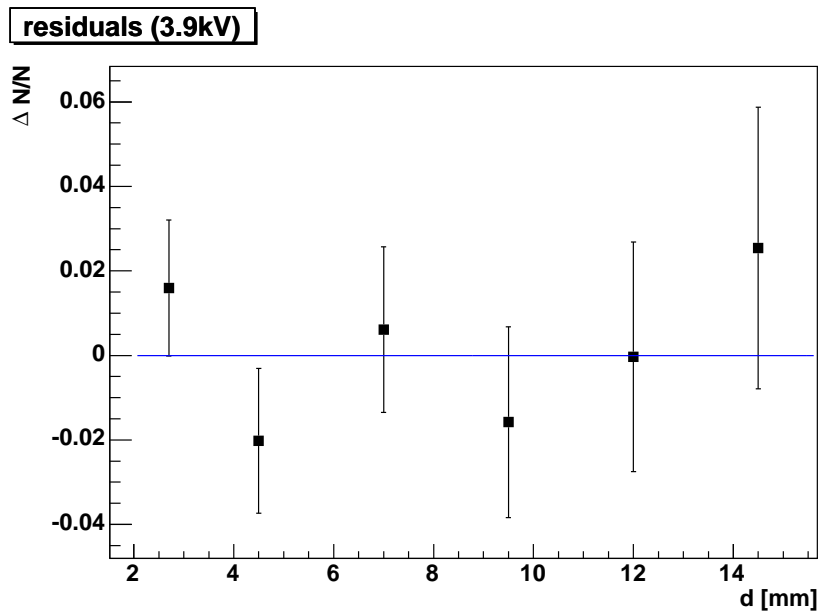


Figure 4.21: Residuals (difference data - fit) divided by the data of the decay curve shown in fig. 4.20.

run #	nominal voltage	U [V]	T [d]	μ [mm ⁻¹]	Γ^* [ns ⁻¹]
2,4	1000	984.5(50)	52.24	0.3956(58)(31)	2.125(35)
7	1300	1284.5(50)	28.54	0.3504(66)(64)	2.150(56)
5	1900	1881.5(50)	18.03	0.2808(53)(59)	2.146(60)
1,3	3900	3874.5(50)	34.73	0.1946(24)(32)	2.074(43)
6	4000	3972.5(50)	32.28	0.1923(21)(13)	2.076(27)
8,10	4800	4765.5(50)	24.78	0.1698(22)(78)	2.007(95)
9	3900	3874.5(50)	11.69	0.1931(34)(34)	2.058(51)

Table 4.3: Results of the stripping measurements: the table lists the nominal acceleration voltage, the measured acceleration voltage U , the measuring time T , the fitted value of μ and the corresponding decay rate Γ^* , respectively. For the μ values two errors are given: the first is the purely statistical error σ_{stat} , the second one is an estimate of σ_{var} (see text).

Several tests were performed in order to check for the consistency of the deduced decay constants μ . It was verified that a change of the peak integration interval, for example from [90, 220] to [100, 220], changes μ only well within the statistical errors. By confining the analysis of the runs to subsets⁷ of the set of distances d , however, more significant changes (i.e. outside of what one would expect on purely statistical grounds) were observed, especially for the runs at $U = 1300, 1900$ and 4800 V. For the runs at lower acceleration voltages, this may be caused by the increasing role of the background in determining the peak intensities and our limited knowledge of it, but in the case of the 4800 V runs it seems that some problems had occurred during the measurement. Similar variations in the resulting μ value at $U = 4800$ V were found by dividing the data in two parts and analysing the first and the second half separately. It might be that due to the higher voltage in this case, sparks between the production foil holder and the bronze gaze screen have occurred and disturbed the experiment. In fact the voltage of 4800 V is only about 100 V below the limit where high-voltage break-downs make the operation of the set-up impossible. Furthermore, unusually high noise contributions were found in the first part of run #8. Note, however, that the result of the control run (#9) shows that the proper functioning of the set-up was not adversely affected. The additional variations in μ reported here are taken into account by adding an additional error σ_{var} to the error budget of μ , which is taken to be the maximum of the variation of μ observed for a given run.

⁷ The following variations have been investigated: leaving out the smallest (largest) distance d , as well as considering only $d \leq 11$ mm or $d \leq 12$ mm.

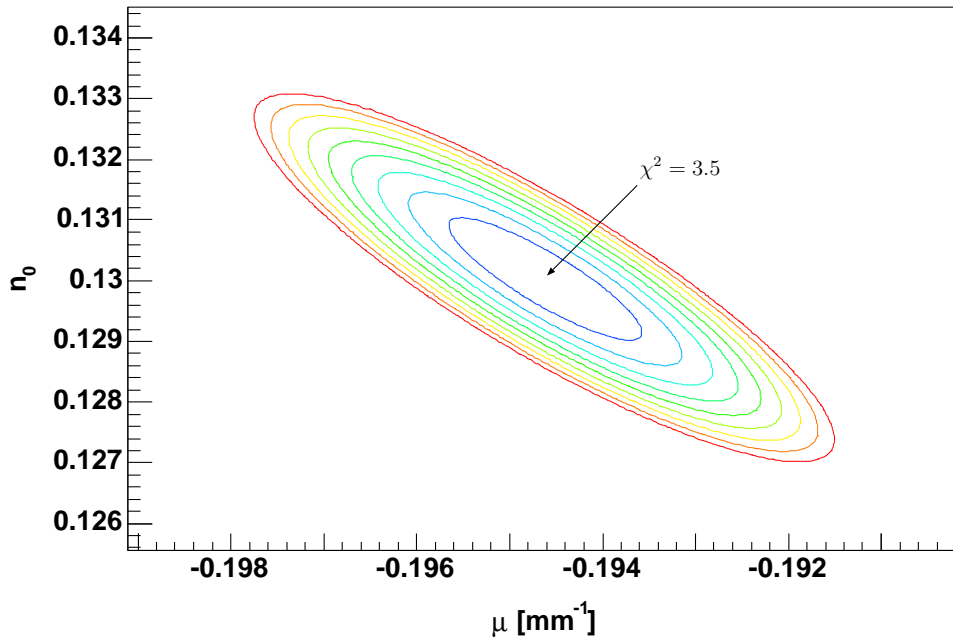


Figure 4.22: Contour plot of χ^2 for the measurement shown in fig. 4.20 as a function of the two fitting parameters n_0 and μ . The equidistance of the contour lines is $\Delta\chi^2 = 0.2$. The minimum in the centre corresponds to the best fit values.

In table 4.3 both errors of μ are given; the first error value refers to the statistical error of the fit, the second one to σ_{var} . The fit error is obtained from the χ^2 plot shown e.g. for the runs #1,3 at $U = 3900$ V in fig. 4.22. The graph shows the contour lines of constant χ^2 in the parameter plane μ vs. n_0 ; the minimum in the centre corresponds to the best fit values, and the contours of constant χ^2 form ellipses around this minimum. The uncertainty in the determination of μ corresponds to the farthest extension of the $\Delta\chi^2 = +1$ ellipse along the μ -axis. The combined error is computed by quadratic addition of the two errors according to $\sigma = \sqrt{\sigma_{\text{stat}}^2 + \sigma_{\text{var}}^2}$.

The calculation of the decay rates Γ^* from the fit results μ is done as explained in sec. 4.1, using the measured values for the acceleration voltages. For the runs #1,3, for example, the value $\mu = 0.1946(40) \text{ mm}^{-1}$ together with $U = 3874.5$ V leads to a decay rate of $\Gamma^* = 2.074(43) \text{ ns}^{-1}$. This and the corresponding results from the other runs are collected in table 4.3. There also the measured values of the acceleration voltages U (cf. sec. 4.3.1) and the total measuring times are listed. For all runs, the error in Γ^* due to the ± 5 V uncertainty of the voltages is more than one order of magnitude smaller than the one caused by the error of μ , and it can safely be neglected (see also sec. 4.4.2).

Having obtained the values of Γ^* for several different acceleration voltages, an investigation

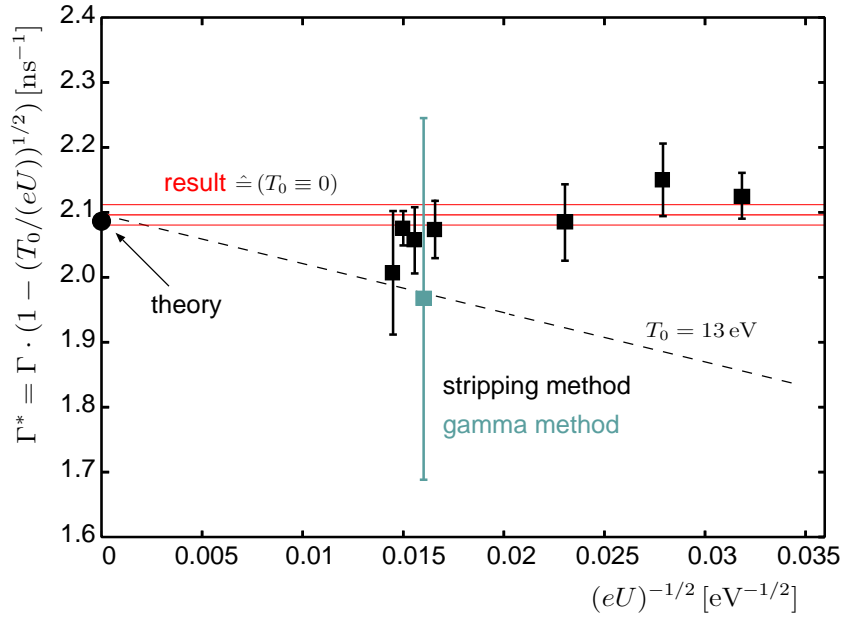


Figure 4.23: Plot of the measured decay rate as a function of $1/\sqrt{U}$. According to eq. (4.1), a non-negligible value of the initial kinetic Ps^- energy T_0 would show up as a negative slope in this plot; the broken line shows the expected dependence for $T_0 = 13 \text{ eV}$ suggested by Mills's result [Mil83] of $T_0 = 13_{-10}^{+19} \text{ eV}$. For comparison, also the result of the γ -experiment is included. The filled circle indicates the value predicted by theory (see sec. 2.2), the continuous line marks the weighted average of the individual results. In order to show the results more clearly, the three data points at $U = 3900 \text{ V}$ and $U = 4000 \text{ V}$ are drawn at slightly shifted positions along the $1/\sqrt{U}$ -axis.

of the initial kinetic energy T_0 of the positronium ions can be performed. Following the procedure described in sec. 4.1, in fig. 4.23 the results for Γ^* are plotted as a function of $1/\sqrt{U}$. If T_0 is significantly greater than zero, Γ^* should decrease linearly with $1/\sqrt{U}$. The only possible value consistent with the data is $T_0 = 0.00_{-0}^{+0.12} \text{ eV}$, corresponding to Γ^* being independent of the voltage U ; the error is determined by the value of T_0 which increases the χ^2 by one compared to the best value at $T_0 = 0 \text{ eV}$. Our result is in accord with the theoretical expectation of $T_0 < 0.3 \text{ eV}$ discussed in sec. 3.4.

As we do not find a dependence of the measured decay rates Γ^* on T_0 , we set $\Gamma = \Gamma^*$ and calculate the final result of our measurement as the weighted average of the individual values Γ^* :

$$\Gamma = 2.093(16) \text{ ns}^{-1}. \quad (4.9)$$

The error follows from usual error propagation, $\Delta\Gamma = \frac{1}{\sum(1/\sigma_i)}$, and amounts to 0.8%. The

error contribution due to our assumption $T_0 = 0$ is negligible.

4.4 Discussion of systematic errors

The achievable accuracy in the decay rate experiment is determined not only by the statistical errors but may be influenced also by systematic errors. In the following an analysis of the possible sources of systematic errors together with estimates of their respective sizes is given. Apart from their relevance in judging the total experimental uncertainty of the present decay rate result, these considerations are also important in view of the planned high-statistics experiment at the NEPOMUC facility (see chapter 5) in order to assess the ultimate limit of accuracy that can be reached.

4.4.1 The low-energy positron beam

The properties of the low-energy positron beam could affect the measurement in three respects: through fluctuations of the number of positrons, by changes in beam energy and by a misalignment between the beam axis and the chamber axis.

In [Fle01] the positron beam has been checked for variations in the particle flux, and no uncontrolled short-term fluctuations were found. Long-term effects, e.g. caused by drifts of the power supplies for the guiding magnetic fields, would be averaged out due to the organization of the measurement process (see also the discussion in sec. 4.2.1). The same argument would apply if there was a drift of the beam energy.

On the other hand, a misalignment of the beam axis with respect to the axis of the translation stage would cause problems: if there is an angle between the two axes, a position dependent fraction of the positron beam may hit the movable Ps^- formation foil, and the number of produced ions would depend on the chosen distance d . As this would lead to measured values of the decay rate which are systematically too high or too low, it is a potentially serious source of systematic errors. For this reason, in [Les03] a careful beam profile measurement was done at production foil positions varying by $\Delta d = 40$ mm. From the results of these measurements, one can derive a limit on the possible transversal shift with respect to the axis of the translational stage of $\Delta x < 0.3$ mm for $\Delta d = 40$ mm. As the maximum change in d used in recording the decay curves is ~ 14 mm, the possible shift reduces to $\Delta x < 0.1$ mm. The beam profile measurements show further [Fle01, Les03] that the positron beam of ~ 7 mm diameter passes well through the centre of the 12 mm diameter foil and that the change of the positron flux is less than 5% when the beam is moved by ± 2 mm. For $\Delta x < 0.1$ mm, this leads to a limit on the relative change in the

number of positrons hitting the foil of $< 2.5 \cdot 10^{-3}$. With the statistical errors of our data points being an order of magnitude larger, this systematic error can be safely neglected at present.

It should be remarked that it is possible to eliminate this source of error completely by modifying the set-up in such a way that the production foil is kept at a fixed position and the acceleration grid and the stripper foil are moved instead.

4.4.2 The acceleration voltages

Altogether, there are three acceleration voltages involved in the decay rate experiment: the voltage U_e , which determines the energy of the positrons hitting the production foil, the grid voltage U_a , which (together with U_e) sets the potential difference across the acceleration gap d and the post-acceleration voltage $U_{\text{strip}} = +30 \text{ kV}$ at the stripper foil (cf. fig. 4.6). A precise knowledge of the absolute value of the latter is not necessary. Of course, the detection efficiency of the stripping set-up depends on it, but it is kept constant and its value does not enter the decay rate result. It may be remarked that a drift of this voltage would be averaged out by our measurement scheme. The other two voltages, however, or more precisely their difference, need to be known in order to calculate the decay rate from the experimentally determined parameter μ . From sec. 4.3.1 the experimental error of the acceleration voltage $U = U_a - U_e$ is known to be $\pm 5 \text{ V}$. By usual error propagation we can derive the relative uncertainty in Γ^* due to this error in the acceleration voltage: starting from eq. (4.2) one obtains

$$\Delta^{(U)}\Gamma^*/\Gamma^* = \left| \frac{\partial\Gamma^*(\Lambda, \mu)}{\partial\Lambda} \right|_{\Lambda=eU/(mc^2)} / \Gamma^*(\Lambda, \mu) \cdot \Delta U. \quad (4.10)$$

As a result, the relative error is $2.5 \cdot 10^{-3}$ in the case of the 1000 V run, decreasing to $5 \cdot 10^{-4}$ at 4800 V. Accordingly, compared to the present statistical uncertainty in the determination of μ , there is room for an order-of-magnitude improvement even with the currently used power supplies, and a further reduction of the error by using a more precise supply for the foil voltage is possible in a straightforward way.

4.4.3 The linear translation stage

As the linear translation stage is used for setting the width d of the acceleration gap, its properties directly influence the achievable level of precision in the decay rate experiment. The parameters of interest in this respect are the position reproducibility and the angular

errors (pitch and yaw). According to the specifications given by the manufacturer (Feinmess Dresden GmbH⁸), the translation stage employed in the decay rate measurements has a position reproducibility of $\pm 1 \mu\text{m}$.

The position reproducibility refers to the uncertainty of reproducing the same absolute setting of the distance d by means of the optical position encoder of the stage. For our application, it determines the precision with which we can measure differences between different values of d . The absolute value of d for a given setting, for example $d = 2.7 \text{ mm}$, depends also on the distance between the fixed acceleration grid and the foil when the translation stage is reset to its zero index mark. This distance is known only to about 0.5 mm , and it amounts to $29.0(5) \text{ mm}$. Fortunately, this value is not needed for the decay rate measurement: as the decay of the positronium ions follows an exponential decay law $\propto \exp(-\mu \cdot d)$, effectively only the differences Δd enter the calculation of the coefficient μ from the experimental count rates. For all data points of the stripping experiment, the error introduced by the uncertainty of $\pm 1 \mu\text{m}$ in setting the production foil position is at least by a factor of 30 smaller than the respective counting error of the data point. Accordingly, this error is negligible in the case of the current measurement. With respect to the planned decay rate experiment with considerably higher statistics, one should note that the relative uncertainty in the determination of μ (and therefore also Γ) due to the $\pm 1 \mu\text{m}$ positioning error of the translation stage will be of the order of $5 \cdot 10^{-4}$.

The pitch and yaw errors of the stage are specified to be smaller than $50 \mu\text{rad}$. These errors affect the parallelism of the production foil and the acceleration grid, the influence of which is discussed in sec. 4.4.4, but as the foil is mounted 55 mm above and 22.5 mm off the centre line of the translation stage, the change in the angle also leads to an error of $\pm 3 \mu\text{m}$ in setting the acceleration gap width.

Being of the order $1.5 \cdot 10^{-3}$, the corresponding uncertainty in the determination of Γ is still by a factor of five smaller than the statistical error of the present decay rate experiment and can therefore safely be neglected.

4.4.4 Field inhomogeneities between the Ps^- foil and the acceleration grid

Another possible source of error in the decay rate measurement may be found in the relative alignment of the Ps^- production foil and the acceleration grid. Ideally, they should be mounted exactly parallel to each other. In practice, this is not easy to guarantee. Fortunately, the decay rate measurement remains at least in first order unaffected by an

⁸ <http://www.feinmess-dresden.de/>

imperfect alignment. If, for example, the foil is mounted at an angle, there are parts of the foil which are closer to the acceleration grid than others. Nevertheless, as long as the foil is shifted parallelly, this does not matter because the change Δd of the acceleration gap width is the same for every point of the foil, and the measurement does not depend on the absolute value of d (see sec. 4.4.3). The same would be true for a slightly deformed foil (for example one that is not exactly flat). The flatness of the foils (and their supporting grids) is specified to be $\leq 10 \mu\text{m}$ [Deg01].

An influence of such misalignments or deformations is only possible due to the deformation of the accelerating electric field. As the field is created by the different potentials of the grid and the foil, any deviations from the ideal geometry lead to inhomogeneities, and the independence of misalignments or deformations stated above is exact only in the case of a homogeneous electric field. To obtain an estimate of the size of such effects, a simple numerical simulation based on classical, nonrelativistic⁹ particle trajectories has been performed, and the time of flight of a positronium ion from the production foil to the stripper foil for different configurations has been calculated.

The electrostatic potential for various 2-dimensional geometries has been computed by numerically solving¹⁰ the Laplace equation with Dirichlet boundary conditions. On two sides the boundary conditions are given by the known potentials of the production foil and the stripper foil, in the other dimension periodicity is assumed. The acceleration grid potential is accounted for by fixing the potential of individual cells in the computational grid. In the z-direction translational symmetry is assumed, i.e. the simulated grid actually consists of a set of parallel wires. Although being a crude approximation, this is certainly on the conservative side with respect to the field inhomogeneities. After solving for the potential and calculating the corresponding electric field, the obtained data (together with a homogeneous magnetic field) is used to compute the time of flight of positronium negative ions for different initial parameters. To this end, the particle trajectories are integrated using a 4th-order Runge-Kutta algorithm [PFTV86]. The parameter of interest is the time of flight from the production foil to the stripper foil; therefore, the integration is stopped when the x-coordinate of the stripper foil is reached. As the algorithm proceeds in discrete steps, one has to be careful to avoid an uncertainty in the results due to a variable ‘overshoot’ across the stripper foil: if the x-coordinate of the particle after an integration step exceeds the x-coordinate of the stripper foil by more than a given tolerance, the

⁹ As we are interested only in the possible error introduced by the field inhomogeneities, a nonrelativistic calculation is sufficient.

¹⁰ The numerical solution was done using a simultaneous over-relaxation algorithm with Chebyshev acceleration [PFTV86].

last step is repeated with a smaller step size. This is done until the overshoot is smaller than the desired tolerance level. The source code of the simulation can be found in the CVS repository `fleische@lfs1.mpi-hd.mpg.de:/home/cb/fleische/.cvs/` as the module `em_simulation`.

To estimate the influence of geometrical imperfections on the achievable precision, the program has been used with a rather fine computational grid of quadratic $1\ \mu\text{m}^2$ cells. This corresponds to the smallest length scale of the problem: the wires of the supporting grids have a diameter of $1\ \mu\text{m}$ (and are $50\ \mu\text{m}$ apart). Also the maximum acceptable overshoot has been set to $1\ \mu\text{m}$. The following configurations have been investigated: an ideally flat foil, a parabolic deformation with $10\ \mu\text{m}$ amplitude over three wire spacings, i.e. $150\ \mu\text{m}$, and a tilt by an angle of 2° . In all cases the deformation has been applied to the production foil, while the acceleration grid was assumed to be ideally flat. Deformations or misalignments of the stripper foil have not been considered because they can only affect the overall detection efficiency, independent of the width d of the acceleration gap. Each configuration has been simulated for two different values of d , $d_1 = 2.7\ \text{mm}$ and $d_2 = 5.0\ \text{mm}$, and two acceleration voltages U , $U = 1000\ \text{V}$ and $U = 3900\ \text{V}$.

In order to assess the error introduced in the rate measurements, the value $\mu_{\text{sim}} := \Gamma(t(d_2) - t(d_1))/(d_2 - d_1)$ has been calculated¹¹, using the time-of-flight results $t(d_1)$ and $t(d_2)$ for Ps^- ions starting at the same position on the foil. The resulting values of μ_{sim} for the different geometries and particle starting points are then compared to the expectation $\mu = \Gamma \cdot \sqrt{6m_e/(eU)}$, which is the nonrelativistic counterpart of eq. (4.2). The observed deviations give an estimate of the uncertainty in the determination of the decay rate due to the imperfect alignment and flatness of the production foil and the acceleration grid. An analysis of the simulation results along these lines shows that the average of μ_{sim} deviates at most by $\sim 3\%$ for the measurement at $U = 1000\ \text{V}$ and by 0.5% for the $U = 3900\ \text{V}$ runs. It has to be taken into account, however, that the range of different acceleration gap widths used in the decay rate measurements was at least a factor of four larger than the value of $d_2 - d_1 = 2.3\ \text{mm}$ in the simulation; as the influence of the field inhomogeneities decreases with d , this error contributes at most on the level of 0.8% for an acceleration voltage of $U = 1000\ \text{V}$ and on the level of 0.2% for the runs at $U = 3900\ \text{V}$. Compared to the statistical errors, this is still negligible at the present level of precision.

¹¹ For Γ , a value of $\Gamma = 2.09\ \text{ns}^{-1}$ was used.

4.5 Conclusion

Summing up the results of the preceding section, several possible sources of systematic errors were considered: a possible change in the number of positrons hitting the production foil when the foil is moved, the precision of the acceleration voltages U , the positioning accuracy in moving the production foil and the effects of possible imperfections in the alignment and flatness of the production foil and the acceleration grid. For our decay rate experiment, we can state that the total error is still dominated by statistics; the above-mentioned errors do not contribute significantly.

The final result of the present decay rate measurement is thus

$$\Gamma = 2.093(16) \text{ ns}^{-1}, \quad (4.11)$$

which is a factor of five more precise than the only previous experimental value of $\Gamma = 2.09(9) \text{ ns}^{-1}$ determined by Mills [Mil83]. Our result is in agreement with the theoretical value of $\Gamma = 2.086(6) \text{ ns}^{-1}$ (see eq. 2.14), but the experimental precision is still a factor of three below that of the theory. It is therefore planned to perform a high statistics decay rate measurement at the considerably more intense positron source NEPOMUC operating at the FRM II in Munich (see sec. 5.1). Judging from the discussion of the systematic errors given above, a further improvement by a factor of 4–5 seems feasible with our present set-up.

Chapter 5

Experiments at the NEPOMUC positron source

In this chapter a number of possible future experiments with the positronium negative ion is discussed. Apart from the first one, which concerns a high-statistics decay rate measurement using the stripping method, these experiments only become possible with the greatly enhanced positron flux of the NEPOMUC source. This new source of positrons is introduced in sec. 5.1. Sec. 5.2 continues with the already mentioned high-statistics decay rate measurement, and in the following sections a photodetachment experiment (sec. 5.3) and a determination of the $3\gamma/2\gamma$ -branching ratio (sec. 5.4) are considered. Sec. 5.5 concludes the chapter with a list of other possible experiments.

5.1 NEPOMUC: principle of operation and status

The NEPOMUC (NEutron induced POSitron source at MUniCh) positron source [HKR⁺04] is an experimental facility located at the FRM II research reactor of the Technical University of Munich. The reactor has been designed as a high-flux neutron source, which is going to be used mainly for applied materials science. In order to produce positrons for the NEPOMUC facility, a beamline ending in a cadmium cap reaches into the moderator tank of the reactor. By means of the thermal neutron-capture reaction $^{113}\text{Cd}(n, \gamma)^{114}\text{Cd}$, cascades of prompt γ -rays are generated. The total deexcitation energy amounts to 9.05 MeV, and on average 2.3 photons of more than 1.5 MeV are emitted. These in turn produce electron-positron pairs in an arrangement of platinum sheets inside the cadmium cap. As already discussed in sec. 3.2, the positrons have rather high energies (with the maximum yield at ~ 800 keV) and a broad energy spectrum. Here the platinum also takes the role of a positron moderator. In the end the particles are extracted by carefully optimized electric fields, accelerated to an energy of a few keV and

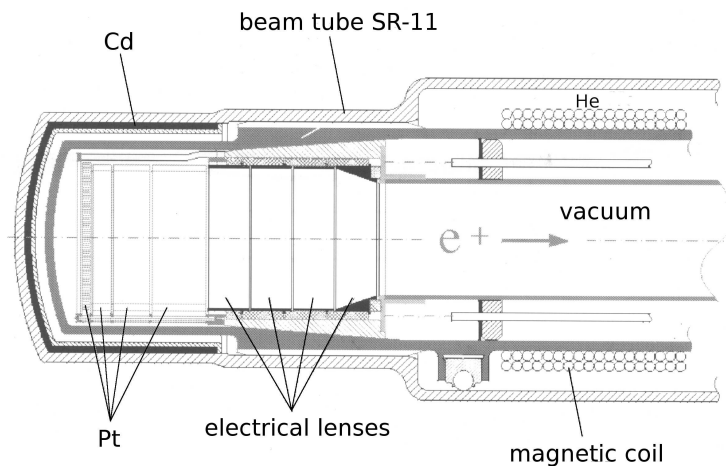


Figure 5.1: Cross section of the in-pile positron source NEPOMUC at the FRM II research reactor. From [HKR⁺02a].

magnetically guided to the experimental hall. Fig. 5.1 shows a cross sectional view of the beamline tip with the positron source. An intensity of about $10^9 - 10^{10}$ moderated positrons per second is expected in the primary beam [HKR⁺02a].

After optimization of the moderator geometry and the extraction potential with the help of simulations [HKR⁺02a], a first test at an external neutron guide of the high flux reactor of the Institute Laue-Langevin in Grenoble was performed. Measurements have been made for different source geometries, and the positron yield was determined depending on the converter mass, the moderator surface and the extraction voltages. Furthermore, an extensive characterization of the source and the positron beam has been done, including studies of the beam profiles, the positron energy distribution and the effects of moderator degradation and annealing [HKR⁺02b]. Using the results of these tests, the final design of the source has been defined. The experiments in Grenoble also back the estimate of the possible positron flux of the complete set-up in Munich. According to [HKR⁺02b], the foreseen intensity of $10^9 - 10^{10}$ moderated positrons per second seems feasible.

In May 2003 the final license for the commissioning of the FRM II reactor was granted. In the meantime the reactor has been put into operation, and the positron source has been shown to work [Hug04]. So far, the design values of $10^9 - 10^{10}$ low-energy positrons per second have not yet been reached; the achieved positron flux is of the order of 10^8 s^{-1} [Hug04], which is already a factor of $\sim 10^3$ higher than available at the Heidelberg set-up with a 40 mCi ^{22}Na source. The first round of user beam times is scheduled for 2005. In a later stage of development, it is planned to introduce a single-crystal tungsten remoderator

outside of the reactor shield in order to improve on the beam quality and diameter.

5.2 A high statistics decay rate measurement

The first and most obvious possibility of an Ps^- -related experiment using the high positron flux of the NEPOMUC source is a repetition of the decay rate measurement with the stripping method. Other than the γ -method, this approach is expected to be able to cope with the high rates in such an experiment. With the existing set-up and the experience gained in Heidelberg, this is rather straightforward to realize, and it is therefore most suitable for learning about the specific problems in connection with the new facility.

The high count rate should allow for a determination of the decay rate which is no longer limited by the statistical errors. In section 4.4 the other sources of experimental uncertainties have been discussed. According to the results of this investigation, a further improvement in precision by a factor of 4–5 seems feasible.

The necessary measuring time at the NEPOMUC source will drop dramatically in comparison to the time needed at our present source. With a moderated positron flux of about 10^8 s^{-1} , the statistics of our decay rate measurement in Heidelberg should be reached within a few hours. Thus, already the present intensity of the positron beam at NEPOMUC of 10^8 s^{-1} is large enough to make a week of beamtime sufficient to reach the precision limits of the current set-up.

At the time of writing, the set-up is being prepared for the transport to Munich, and it is planned to do such a measurement relatively soon.

5.3 Photodetachment experiments

Another option for an experimental study of the positronium ion is a measurement of the photodetachment cross section. Possibly, such an experiment could provide a test of the numerous calculations of the Ps^- resonances (cf. sec. 2.3), and with a measurement of the binding energy, it would allow for a determination of one of the most fundamental properties of this system.

In the following the feasibility of a photodetachment experiment is discussed, and the technical requirements associated with such a project are considered. In order to reach event rates high enough for an experimentally usable signal, a positron source like the ^{22}Na source used so far is clearly not sufficient. Only an intense source like the NEPOMUC facility will bring these measurements into the reach of experiments. The rate of photodetachment processes is not determined by the number of positronium ions alone, but it

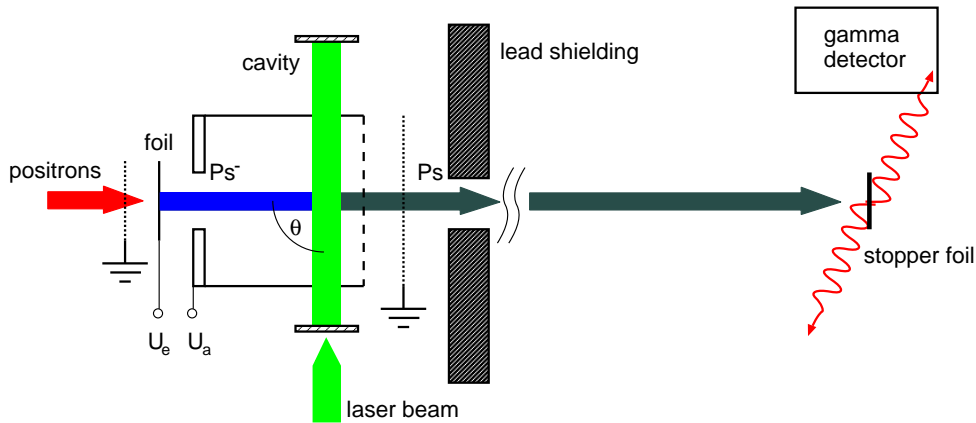


Figure 5.2: Schematic set-up for a photodetachment experiment with Ps^- .

also depends on the available light source. Because of the limited number of positronium ions, laser intensities as high as possible are needed. Although the highest peak power is provided by pulsed lasers, it is obvious that with the DC beam of positronium ions which our set-up delivers and given the low number of particles, only cw lasers are suitable: assuming a primary positron flux of 10^9 s^{-1} and a Ps^- production efficiency of 10^{-4} , a beam of about 10^5 positronium ions per second is produced. For a kinetic energy of 1 keV, this corresponds to a number density of $n \simeq 2 \cdot 10^{-4} \text{ Ps}^-/\text{cm}^3$, and it is easily seen that the probability of hitting any positronium ions with a pulsed laser will be very small.

An investigation of the doubly excited states of Ps^- , in particular around the $\text{Ps}(n=2)$ threshold, will be most interesting. The energy difference between the Ps^- ground state ($E_0 = -0.262008 \text{ a.u.}$) and this threshold ($E_{\text{Ps}(1)} = -0.0625 \text{ a.u.}$) is 5.4 eV, corresponding to a wavelength of about 230 nm. Laser systems providing cw beams in this region of the ultra-violet spectrum (e.g. by second-harmonic generation from an argon-ion laser) exist: in [SPH98], for example, the generation of 750 mW cw laser radiation at 257 nm has been reported.

A measurement of the off-resonant photodetachment cross section, resulting in a positronium atom in its ground state and a free electron, seems to be considerably easier. As visible in fig. 2.3, the maximum of the cross section is predicted to be in the near infrared region of the spectrum, and there is a readily available laser for this purpose: Nd:YAG lasers are sold with output power ratings of up to the order of kilowatts, and the wavelength of 1064 nm is conveniently close to the maximum of the off-resonant photodetachment cross section.

For a laser intensity I , a Ps^- number density n , an interaction volume V and a pho-

photodetachment cross section σ , the rate of photo-produced positronium atoms is given by

$$R_{\text{Ps}} = \frac{I\lambda}{hc} \sigma n V. \quad (5.1)$$

Assuming an overlap region of the laser and the 7 mm diameter Ps^- beam of $\sim 0.4 \text{ cm}^3$ and the number density $n \simeq 2 \cdot 10^{-4} \text{ Ps}^-/\text{cm}^3$ calculated above, 10 W of cw laser power would lead to a rate of photodetachment events of about 0.3 s^{-1} . This estimate is based on the off-resonant photodetachment cross-section of $\sim 4 \cdot 10^{-17} \text{ cm}^2$ (see sec. 2.3). Such a rate of photodetachment events is still quite low but measurable. In order to reach a higher detachment probability, either one has to employ a more powerful laser, or a cavity can be used to increase the laser field intensity in the interaction region. A Q-value of 100 in this cavity would lead to a rate of the order of 30 positronium atoms per second, enough to make a measurement feasible. To give an estimate of the resonant photodetachment rates that can be achieved, the corresponding resonance strengths need to be known. As it seems, they have not been calculated, but we can certainly assume that the resonant cross section is a factor of 10–100 higher than the off-resonant one. Accordingly, the necessary laser intensity is lower in the resonant case, and a laser of 30 – 300 mW should be sufficient to reach a photodetachment rate of $\sim 10 \text{ s}^{-1}$.

To detect the neutral positronium, one could place a stopper foil about a metre from the interaction region in the flight path of the positronium atoms. As discussed in section 2.3, 3/4 of the Ps atoms produced by the photodetachment process are expected to be in the 3S_1 (ortho-Ps) spin state. Other than Ps^- , this state (with a lifetime of 142 ns [VZG03]) is sufficiently long-lived to reach the stopper foil. Interacting with the stopper foil, a large fraction of the positronium atoms is converted to the 1S_0 (para-Ps) state, and the annihilations in the stopper foil can be observed by a carefully shielded gamma detector. Figure 5.2 illustrates the principle of this method.

Of course, it would be desirable to have a possibility of tuning the photon energy; this would allow for an experimental test of the theoretically calculated energy dependence of the cross section. Moreover, a tunable photon energy is necessary to search for the doubly excited resonance states of the positronium ion. For most lasers (except for dye lasers), however, a detuning is only possible within extremely narrow limits. In an photodetachment experiment looking for the resonances of the negative ion of hydrogen (H^-) [BCB⁺83], this problem has been solved in an elegant way using the Doppler effect: by changing the angle between the relativistic ion beam and the laser, a rather large effective detuning can be achieved. Due to its small mass, it is much easier to reach the necessary velocities in the case of Ps^- . A positronium ion accelerated to 50 keV energy, for example,

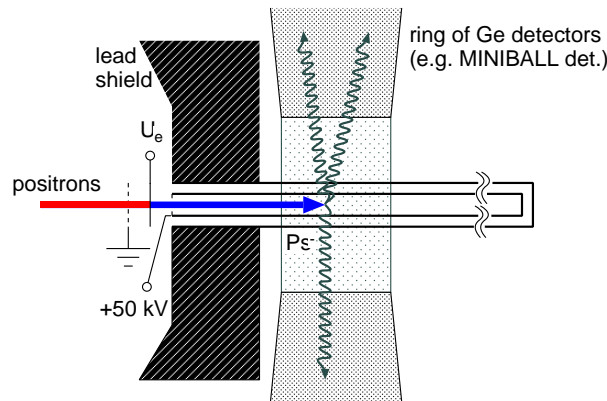


Figure 5.3: Principle of an experiment to measure the $3\gamma/2\gamma$ -branching ratio of Ps^- .

has a velocity of about 25% the speed of light, thus a change in the angle of $\pm 30^\circ$ around the right angle corresponds to a $\pm 12.5\%$ variation in photon energy. The drawback of this technique is the requirement of high particle velocities: at an energy of 50 keV the Ps^- density drops by a factor of seven compared to a 1 keV beam.

To sum up the results, we can state that a photodetachment measurement will become possible with the intense positron source NEPOMUC. With a suitable laser system, such an experiment could search for the predicted resonance states and determine the Ps^- ground-state binding energy.

5.4 The $3\gamma/2\gamma$ -branching ratio

With respect to the decay of the positronium ion, the $3\gamma/2\gamma$ -branching ratio will become accessible to an experimental investigation at NEPOMUC. In order to make a measurement of this ratio, a unambiguous identification of both the 2γ and the 3γ decay channel is necessary. As each of the three photons emitted in the 3γ decay of Ps^- alone does not have a unique energy signature, such an identification is possible only by means of a simultaneous detection of all decay photons. From this consideration it is already clear that a measurement of the branching ratio requires a rather large γ -detector array.

In principle, the experiment can be performed as shown in fig. 5.3: the positronium ions are accelerated to an energy of several tens of keV, then their annihilation radiation is recorded by a ring of germanium detectors. Due to the high kinetic energy of the decaying Ps^- ions, the energies of the annihilation photons sum up to an energy larger than 1022 keV. For 50 keV positronium ions, for example, an energy sum of 1055 keV is expected — one third of the kinetic energy being carried by the remaining electron. Thus, the Ps^- decays

become distinguishable from other positron annihilations. The second reason for the large acceleration voltage is given by the shielding requirements of the germanium detectors: as there is an enormous background of electron-positron annihilations in the region of the Ps^- production foil, the detectors have to be carefully shielded. After acceleration to 50 kV, the positronium ions travel 36 mm during one lifetime, thus it is possible to insert a layer of about 50 mm lead between the production region and the decay/detection region. Starting from an NEPOMUC positron flux of 10^9 s^{-1} , one can estimate the achievable count rates for both 2γ and 3γ events. Setting a distance from the production foil to the start of the decay region seen by the detector ring of 50 mm, positronium ions reach the volume seen by the detectors at a rate of about $2 \cdot 10^4 \text{ s}^{-1}$. With a full-energy peak efficiency of 7%, a rate of detected 2γ events of $\sim 100 \text{ s}^{-1}$ and a rate of 3γ events of $\sim 0.02 \text{ s}^{-1}$ can be expected. In calculating these numbers, a branching ratio of $\Gamma_{3\gamma}/\Gamma_{2\gamma} = 2.6 \cdot 10^{-3}$ (see sec. 2.2) has been assumed.

As these estimates show, a determination of the $3\gamma/2\gamma$ -branching ratio is within reach at the NEPOMUC positron source. It requires, however, an efficient array of germanium detectors as provided e.g. by MINIBALL [EPT⁺01]. The quoted full-energy peak efficiency of 7% could be realized using a ring of four MINIBALL detectors.

5.5 Other possible experiments

Apart from the experiments discussed in the previous sections, there is another project that could be realized at the NEPOMUC positron source. This experiment concerns the production of a directed, pure beam of (3S_1) ortho-positronium atoms at a well-defined energy. Such a beam could be obtained from a beam of positronium ions by photodetachment. The number of ortho-Ps atoms which could be produced in this way has already been estimated to $\sim 30 \text{ s}^{-1}$ in sec. 5.3. This is based on a laser power of 10 W and a Q-value of 100 for the cavity; if one can reach larger values, the rate of positronium atoms increases proportionally.

Having such a beam of ortho-Ps in vacuum at hand, new precision experiments with positronium might become possible: a new measurement of the decay rate of the triplet (3S_1) state of positronium with a kind of recoil-distance method, for example, or Ramsey-type experiments to determine the positronium hyperfine splitting.

Chapter 6

Conclusion and outlook

In this work a new experimental determination of the decay rate of the positronium ion Ps^- has been presented. As a measurement using the γ -method employed in [Mil83] turned out to be not very promising due to a very unfavourable signal-to-background ratio, an improved detection scheme based on a stripping technique has been applied. In the new set-up the positronium ions are stripped to bare positrons and recorded in a silicon particle detector. As expected, this approach leads to a dramatic improvement in the signal-to-background ratio, and it was used to perform the new decay rate experiment. The resulting decay rate value has an error of about 0.8%, thus the experimental uncertainty could be reduced by more than a factor of five with respect to the earlier measurement [Mil83].

The systematic limitations of the set-up have been investigated: it was demonstrated that they have not yet been reached, but a further improvement by more than a factor of about 4–5 does not seem to be possible without modifications to the current set-up. However, this means that a reduction of the error by more than a full order of magnitude with respect to the value of Mills could be achieved, thus bringing down the experimental uncertainty to the level of the present theoretical calculations. With the commissioning of the FRM II research reactor in Munich, a new high-intensity positron source, the NEPOMUC facility, has started operation. A decay rate measurement with the existing set-up at this facility is planned. Other than the old method based on the detection of the annihilation γ -rays, the stripping method should be able to cope with the large Ps^- rates of the order of 10^4 positronium ions per second expected at the NEPOMUC source. Moreover, the perspectives for further experiments on the properties of the positronium ion have been discussed. Most interesting in this respect would be a study of the binding energy and the autodissociative states of Ps^- by means of a photodetachment experiment. With the large positron flux at NEPOMUC such projects in principle become feasible. However, to access the resonances a powerful cw laser is required at a wavelength of about

230 nm. Furthermore, for the first time a measurement of the off-resonant photodetachment cross section seems to be possible, and the process could be used to produce a directed, monoenergetic and pure beam of (3S_1) ortho-positronium in vacuum. Such a beam would possibly allow for new precision measurements of the properties of the triplet state of neutral positronium, which presents an ideal testing ground for bound-state QED calculations.

Another quantity which is brought in the reach of experiments by the NEPOMUC facility is the $3\gamma/2\gamma$ branching ratio: estimates of the achievable count rates for 2γ and 3γ events show that such a measurement becomes possible provided that NEPOMUC succeeds to finally produce the promised fluxes of $\geq 10^9$ positrons per second.

References

- [ARG94] A. H. Al-Ramadhan and D. W. Gidley, *New precision measurement of the decay rate of single positronium*, Physical Review Letters **72** (1994), 1632.
- [AZ77] H. H. Andersen and J. F. Ziegler, *Hydrogen — stopping powers and ranges in all elements*, Pergamon Press, 1977.
- [BCB⁺83] H. C. Bryant, D. A. Clark, K. B. Butterfield, C. A. Frost, H. Sharifian, H. Tootoonchi, J.B. Donahue, P. A. M. Gram, M. E. Hamm, R. W. Hamm, J. C. Pratt, M. A. Yates, and W. W. Smith, *Effects of strong electric fields on resonant structures in h^- photodetachment*, Physical Review A **27** (1983), no. 6, 2889.
- [BD83] A. K. Bhatia and R. J. Drachman, *New calculation of the properties of the positronium ion*, Physical Review A **28** (1983), 2523.
- [BD85] ———, *Photodetachment of the positronium negative ion*, Physical Review A **32** (1985), 3745.
- [BD87] ———, *Three-body Coulomb bound states*, Physical Review A **35** (1987), 4051.
- [BD98] ———, *Relativistic corrections to the binding energy of Ps^-* , Nuclear Instruments and Methods in Physics Research B **143** (1998), 195.
- [BG86] J. Botero and C. H. Greene, *Resonant photodetachment of the positronium negative ion*, Physical Review Letters **56** (1986), 1366.
- [BH90] A. K. Bhatia and Y. K. Ho, *Complex-coordinate calculation of $^{1,3}P$ resonances in Ps^- using Hylleraas functions*, Physical Review A **42** (1990), 1119.
- [BH93] ———, *Complex-coordinate calculations of doubly excited $^{1,3}D^e$ resonance states of Ps^-* , Physical Review A **48** (1993), 264.

- [Bot87] J. Botero, *Adiabatic study of the positronium negative ion*, Physical Review A **35** (1987), 36.
- [BP80] Stephan Berko and Hugh N. Pendleton, *Positronium*, Ann. Rev. Nucl. Part. Sci. **30** (1980), 543.
- [CL90] Z. Chen and C. D. Lin, *Classification of Coulombic three-body systems in hyperspherical coordinates*, Physical Review A **42** (1990), 18.
- [CM82] K. F. Canter and A. P. Mills, *Slow positron beam design notes*, Canadian Journal of Physics **60** (1982), 551.
- [Col00] P.G. Coleman, *The generation and transport of positron beams*, Positron Beams (P.G. Coleman, ed.), World Scientific, 2000.
- [CP86] M. C. Chu and V. Poenisch, *Calculation of the one-photon decay rate of the polyelectron P^{++-}* , PRC **33** (1986), 2222.
- [Deg01] Kai Degreif, *Aufbau eines Experiments zur Messung der Lebensdauer des negativen Positronium-Ions*, Diplomarbeit, Max-Planck-Institut für Kernphysik, Heidelberg, 2001.
- [EPT⁺01] J. Eberth, G. Pascovici, H. G. Thomas, N. Warr, D. Weisshaar, D. Habs, P. Reiter, P. Thirolf, D. Schwalm, C. Gund, H. Scheit, M. Lauer, P. van Duppen, S. Franchoo, M. Huyse, R. M. Lieder, W. Gast, J. Gerl, K. P. Lieb, et al., *MINIBALL — a Ge detector array for radioactive ion beam facilities*, Progress in Particle and Nuclear Physics **46** (2001), 389.
- [FB92] A. M. Frolov and D. M. Bishop, *Theory of bound states in the Coulomb three-body system with unit charges*, Physical Review A **45** (1992), 6236.
- [Fer68] G. Ferrante, *Annihilation of positrons from positronium negative ion $e^-e^+e^-$* , Physical Review **170** (1968), 76.
- [Fle01] F. Fleischer, *Voruntersuchungen zur Messung der Lebensdauer des negativen Positronium-Ions*, Diplomarbeit, Max-Planck-Institut für Kernphysik, Heidelberg, 2001.
- [Fro93] A. M. Frolov, *Annihilation rate in Ps^- and properties of two-electron ions*, Journal of Physics B **26** (1993), 1031.

-
- [Fro98] ———, *Two-stage strategy for high-precision variational calculations*, Physical Review A **57** (1998), no. 4, 2436.
- [Fro99] ———, *Bound-state properties of the positronium negative ion Ps^-* , Physical Review A **60** (1999), no. 4, 2834.
- [FY89] A. M. Frolov and A. Y. Yeremin, *Ground bound states in two-electron systems with $Z=1$* , Journal of Physics B **22** (1989), 1263.
- [HB57] I. Harris and L. M. Brown, *Radiative corrections to pair annihilation*, Physical Review **105** (1957), 1656.
- [HB91] Y. K. Ho and A. K. Bhatia, *$^{1,3}P^o$ resonance states in positronium ions*, Physical Review A **44** (1991), 2890.
- [HB92] ———, *Doubly excited $^3P^e$ resonant states in Ps^-* , Physical Review A **45** (1992), 6268.
- [HB93] ———, *P -wave shape resonances in positronium ions*, Physical Review A **47** (1993), 1497.
- [HB94] ———, *$^{1,3}D^o$ resonant states in Ps^-* , Physical Review A **50** (1994), 2155.
- [HKR⁺02a] C. Hugenschmidt, G. Kögel, R. Repper, K. Schreckenbach, P. Sperr, B. Straßer, and W. Triftshäuser, *Monoenergetic positron beam at the reactor based positron source at FRM-II*, Nuclear Instruments and Methods in Physics Research B **192** (2002), 97.
- [HKR⁺02b] C. Hugenschmidt, G. Kögel, R. Repper, K. Schreckenbach, P. Sperr, and W. Triftshäuser, *First platinum moderated positron beam based on neutron capture*, Nuclear Instruments and Methods in Physics Research B **220** (2002), 220.
- [HKR⁺04] C. Hugenschmidt, G. Kögel, R. Repper, K. Schreckenbach, P. Sperr, B. Straßer, and W. Triftshäuser, *NEPOMUC - the new positron beam facility at FRM II*, Math. Sci. Forum (in press) (2004).
- [HM89a] M. I. Haftel and V. B. Mandelzweig, *Erratum*, Ann. Phys. (N.Y.) **195** (1989), 420.
- [HM89b] ———, *Fast convergent hyperspherical harmonic expansion for three-body systems*, Ann. Phys. (N.Y.) **189** (1989), 29.

- [HM89c] ———, *Precise nonvariational calculation of the positronium negative ion*, Physical Review A **39** (1989), 2813.
- [Ho79] Y. K. Ho, *Autoionization states of the positronium negative ion*, Physical Review A **19** (1979), 2347.
- [Ho83a] ———, Physics Reports (1983), 1.
- [Ho83b] ———, *Positron annihilation in the positronium negative ion*, Journal of Physics B **16** (1983), 1503.
- [Ho84] ———, *Doubly excited resonances of positronium negative ions*, Physics Letters **102A** (1984), 348.
- [Ho85] ———, *Positron annihilation in the doubly excited states of positronium negative ions*, Physical Review A **32** (1985), 2501.
- [Ho90a] ———, *Positron annihilation in positronium negative ions*, Physics Letters A **144** (1990), no. 4,5, 237.
- [Ho90b] ———, *Positronium ions and molecules*, Annihilation in Gases and Galaxies (Washington DC) (R. J. Drachman, ed.), vol. 3058, NASA, NASA Conf. Publ., 1990, pp. 243–256.
- [Ho93] ———, *Variational calculation of ground-state energy of positronium negative ions*, Physical Review A **48** (1993), no. 6, 4780.
- [Hug04] C. Hugenschmidt, private communication, 2004.
- [Hyl47] E. A. Hylleraas, *Electron affinity of positronium*, Physical Review **71** (1947), no. 8, 491.
- [INO00] A. Igarashi, S. Nakazaki, and A. Ohsaki, *Phase shifts of $e^- + Ps$ scatterings and photodetachment cross section of Ps^-* , Physical Review A **61** (2000), 032710.
- [IST00] A. Igarashi, I. Shimamura, and N. Toshima, *Photodetachment cross sections of the positronium negative ion*, New Journal of Physics **2** (2000), 17.1.
- [Jac81] J. D. Jackson, *Klassische Elektrodynamik*, ch. 12, de Gruyter, 1981.

-
- [JLF⁺97] J. Jaeaeskelainen, T. Laine, K. Fallstroem, K. Saarinen, and P. Hautojaervi, *Optimized growth conditions for solid Ar and Kr moderators in slow positron beam*, Applied Surface Science **116** (1997), 73.
- [JR76] J. M. Jauch and R. Rohrlich, *The theory of photons and electrons*, 2nd ed., ch. 12, p. 263sq., Springer Verlag, 1976.
- [Kar02] S.G. Karshenboim, *Precision study of positronium and precision tests of the bound state quantum electrodynamics*, Appl. Surf. Sci. **194** (2002), 307.
- [Kat57] T. Kato, *On the eigenfunctions of many-particle systems in quantum mechanics*, Communications on Pure and Applied Mathematics **10** (1957), 151.
- [KHM93] R. Krivec, M. I. Haftel, and V. B. Mandelzweig, *Precise nonvariational calculation of the two-photon annihilation rate of the positronium negative ion*, Physical Review A **47** (1993), 911.
- [Kry94] S. I. Kryuchkov, *On the one-photon annihilation of the Ps^- ion*, JPB **27** (1994), L61.
- [Lau04] M. Lauer, *Digital signal processing for segmented hpge detectors — preprocessing algorithms and pulse shape analysis*, Ph.D. thesis, Universität Heidelberg, 2004.
- [LBK⁺90] S. Lencinas, J. Burgdörfer, J. Kemmler, O. Heil, K Kroneberger, N. Keller, H. Rothard, and K. O. Groeneveld, *Transport of fast electrons through thin foils*, Physical Review A (1990), 1435.
- [Lee58] Chang Lee, *Stationary states of electron-positron systems and annihilation transitions*, Soviet Physics JETP **6** (1958), 281.
- [Les03] M. Lestinsky, *Eigenschaften des negativen Positronium-Ions Ps^-* , Diplomarbeit, Max-Planck-Institut für Kernphysik, Heidelberg, 2003.
- [Ley97] R. Ley, *Positron production using accelerators*, Hyperfine Interactions **109** (1997), 167.
- [LIO⁺97] V.K. Liechtenstein, T. M. Ivkova, E. D. Olshanski, I. Feigenbaum, R. DiNardo, and M. Doebeli, *Preperation and evaluation of thin diamond-like carbon films for heavy-ion tandem accelerators and time-of-flight spectrometers*, Nuclear Instruments and Methods A **397** (1997), 140.

- [LL88] C. D. Lin and X.-H. Liu, *Methods of solving Coulombic three-body problems in hyperspherical coordinates*, Physical Review A **37** (1988), 2749.
- [LS78] C. M. Lederer and V. S. Shirley (eds.), *Table of isotopes*, 7th ed., Jon Wiley & Sons, Inc., 1978.
- [Mil81a] A. P. Mills, *Observation of the positronium negative ion*, Physical Review Letters **46** (1981), 717.
- [Mil81b] ———, *Probable nonexistence of a $^3P^e$ metastable excited state of the positronium negative ion*, Physical Review A **24** (1981), 3242.
- [Mil83] ———, *Measurement of the decay rate of the positronium negative ion*, Physical Review Letters **50** (1983), 671.
- [Mil90] ———, *Decay rate and other properties of the positronium negative ion*, Annihilation in Gases and Galaxies (Washington DC) (R. J. Drachman, ed.), vol. 3058, NASA, NASA Conf. Publ., 1990, pp. 213–221.
- [Mil05] ———, private communication, 2005.
- [MVA94] A. P. Mills, S. S. Voris, and T. S. Andrew, *Solid Kr moderator for producing slow positrons*, Journal of Applied Physics **76** (1994), 2556.
- [OP49] A. Ore and J. L. Powell, *Three-photon annihilation of an electron-positron pair*, Physical Review **75** (1949), 1696.
- [PFTV86] W. H. Press, B. P. Flannery, S. A. Teukolsky, and W. T. Vetterling, *Numerical Recipes*, Cambridge University Press, 1986.
- [Ple00] Florian Plenge, *Planung und Aufbau eines Experiments zur Untersuchung des negativen Positronium-Ions*, Diplomarbeit, Max-Planck-Institut für Kernphysik, Heidelberg, 2000.
- [PS87] P. Petelenz and V. H. Smith, *Binding energies of the muonium and positronium negative ions*, Physical Review A **36** (1987), 5125.
- [RW92] J. M. Rost and D. Wintgen, *Positronium negative ion: molecule or atom?*, Physical Review Letters **69** (1992), 2499.
- [Sch98] F. Schwabl, *Quantenmechanik (QM I)*, Springer Verlag, 1998.

- [SPH98] U. Schramm, A. Peters, and D. Habs, *Generation of high power cw laser light at 257 nm for laser cooling of intense $^{24}\text{Mg}^+$ beams at the ESR*, *Hyperfine Interactions* **115** (1998), 57.
- [VZG03] R. S. Vallery, P. W. Zitzewitz, and D. W. Gidley, *Resolution of the orthopositronium-lifetime puzzle*, *Physical Review Letters* **90** (2003), 203402–1.
- [Whe46] J. A. Wheeler, *Polyelectrons*, *Annals of The New York Academy of Science* **XLVIII** (1946), 219.
- [WHM87] S. J. Ward, J. W. Humberston, and M. R. C. McDowell, *Elastic scattering of electrons (or positrons) from positronium and the photodetachment of the positronium negative ion*, *Journal of Physics B* **20** (1987), 127.

Appendix

A Parameters for operating the Ps^- set-up

This appendix gives a comprehensive list of the parameters used for operating the Heidelberg Ps^- set-up.

- **Extraction voltage:**

$$U_{\text{extr}} = +30 \text{ V}$$

- **Guiding magnetic field (currents):**

source chamber Helmholtz coils	}	series connected, $I = 4.00 \text{ A}$
toroid beamline		

experiment chamber coil 1: $I = 7.0 \text{ A}$

experiment chamber coil 2: $I = 6.0 \text{ A}$

experiment chamber coil 3: $I = 5.0 \text{ A}$

correction coil 1: $I = 1.00 \text{ A}$, reversed polarity! (red/black: -/+)

correction coil 2: $I = 0.85 \text{ A}$, reversed polarity!

- **Slit positions:**

upper: 24 mm, lower: 28 mm

- **Production foil voltage:**

$$U_e = (-786 \pm 5) \text{ V} \quad (\text{in the case of the } \gamma\text{-method: } -500 \text{ V})$$

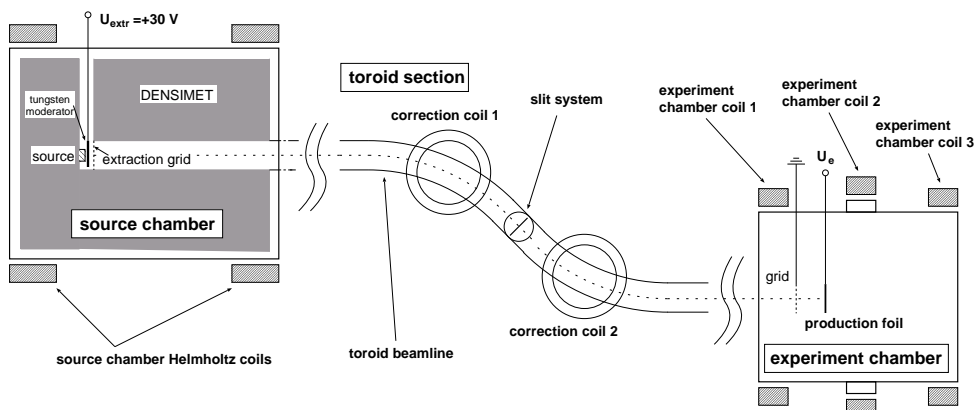


Figure A.1: Overview of the different labels used in the parameter listing.

B Parameters used in the stripping measurement

This appendix lists the additional parameters used in the decay rate measurement with the stripping method.

- **Distance production foil – acceleration grid:**

~ 2.5 mm (minimum, mechanical stop),

29 mm (zero index mark of the translation stage, ~ currently usable maximum)

- **Distance acceleration grid – stripper foil:**

16.8 mm

- **Stripper foil voltage:**

$U_{\text{extr}} = +30 \text{ kV}$ (monitor voltage of the fug power supply: $U_{\text{mon}} = 8.461 \text{ V}$)

- **Guiding magnetic field (currents) in the detector beamline:**

$\left. \begin{array}{l} \text{bridging coil on the flange} \\ \text{detector beamline solenoid} \end{array} \right\} I = 12.5 \text{ A}$

- **Si detector bias voltage:**

$U_{\text{bias}} = +40 \text{ V}$

- **Si detector temperature:**

$T_{\text{det}} = -20^\circ\text{C}$

- **Rest gas pressure (measured in the chambers):**

$p_{\text{vac}} \simeq 10^{-7} \text{ mbar}$

- **lead apertures:**

inner diameter: 20 mm

positions (from the upstream end of the detector beamline): 17.5 mm, ~ 195 mm

C Decay rate measurement data

C.1 Runs #2 and #4 at $U = 1000$ V

d [mm]	time [s]	counts	bg. counts	corr.	N_{e-bg}	N_{bg}^{fit}	N/t [s^{-1}]
2.7	205938	17356 ± 132	7383 ± 86	+0.5	10060	7438	0.04816(73)
3.9	328546	21473 ± 147	11689 ± 108	+0.8	16783	11665	0.02985(52)
5.1	522820	27692 ± 166	18166 ± 135	+1.3	26083	18111	0.01832(38)
6.3	832939	38002 ± 195	28493 ± 169	+2.1	40909	28425	0.01149(29)
7.5	1031924	54002 ± 232	44302 ± 210	+3.2	63608	44344	0.00732(22)
28.0	1304056	37677 ± 194			54096		

Table C.1: Results of the measurement at $U = 1000$ V (sum of runs 2 and 4): for each distance d the measuring time, the integrated number of counts in the positron peak (before background subtraction), the number of counts in the same region of the appropriately scaled 28 mm background spectrum, the correction for the residual Ps contribution in the 28 mm background spectrum, the number of counts in the Compton electron background used for the first normalization N_{e-bg} , the final number of background counts under the peak as obtained from the fit (N_{bg}^{fit}) and the resulting corrected Ps count rate N/t are listed.

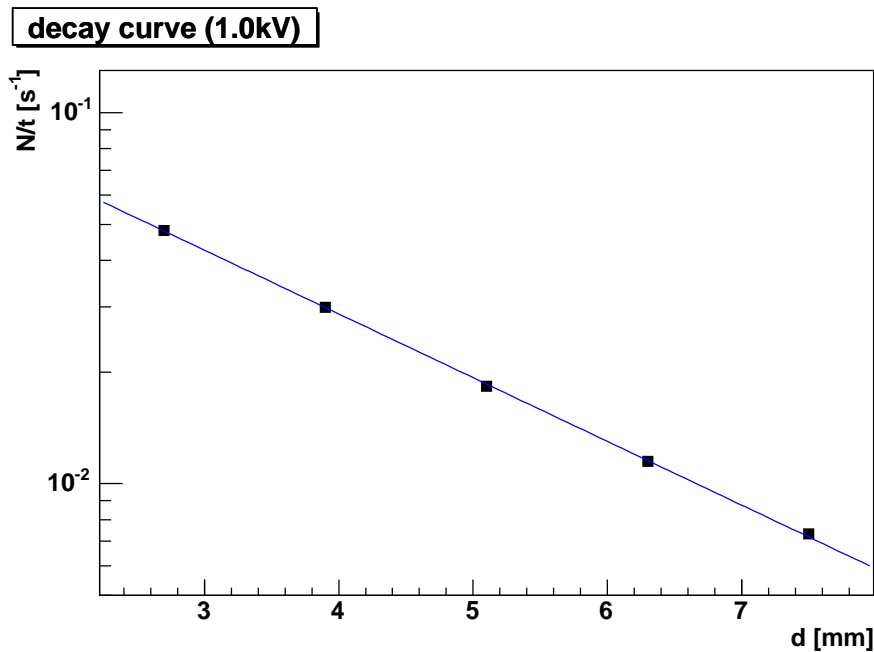


Figure C.1: Measured decay curve at $U = 1000$ V.

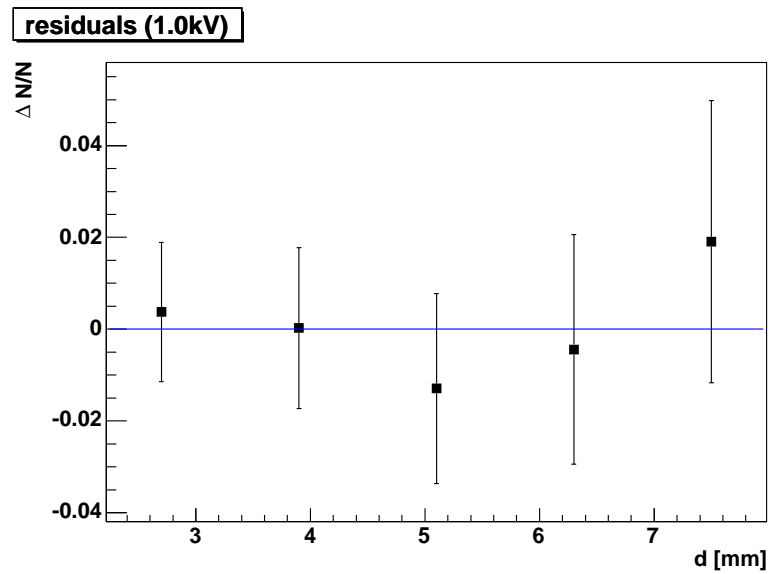


Figure C.2: Residuals (*data - fit*) divided by the data of the decay curve measured at $U = 1000$ V.

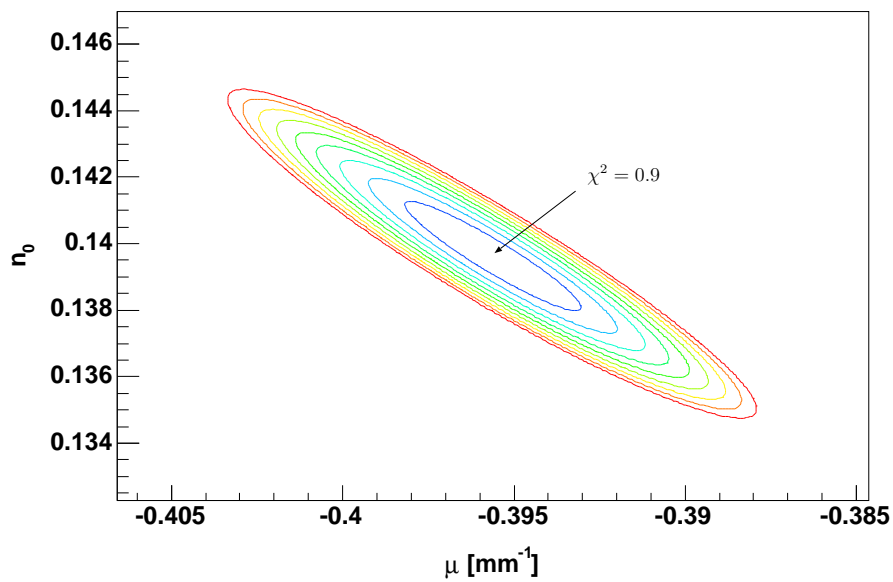


Figure C.3: $U = 1000$ V: Contour plot of χ^2 as a function of the two fitting parameters n_0 and μ . The equidistance of the contour lines is $\Delta\chi^2 = 0.2$.

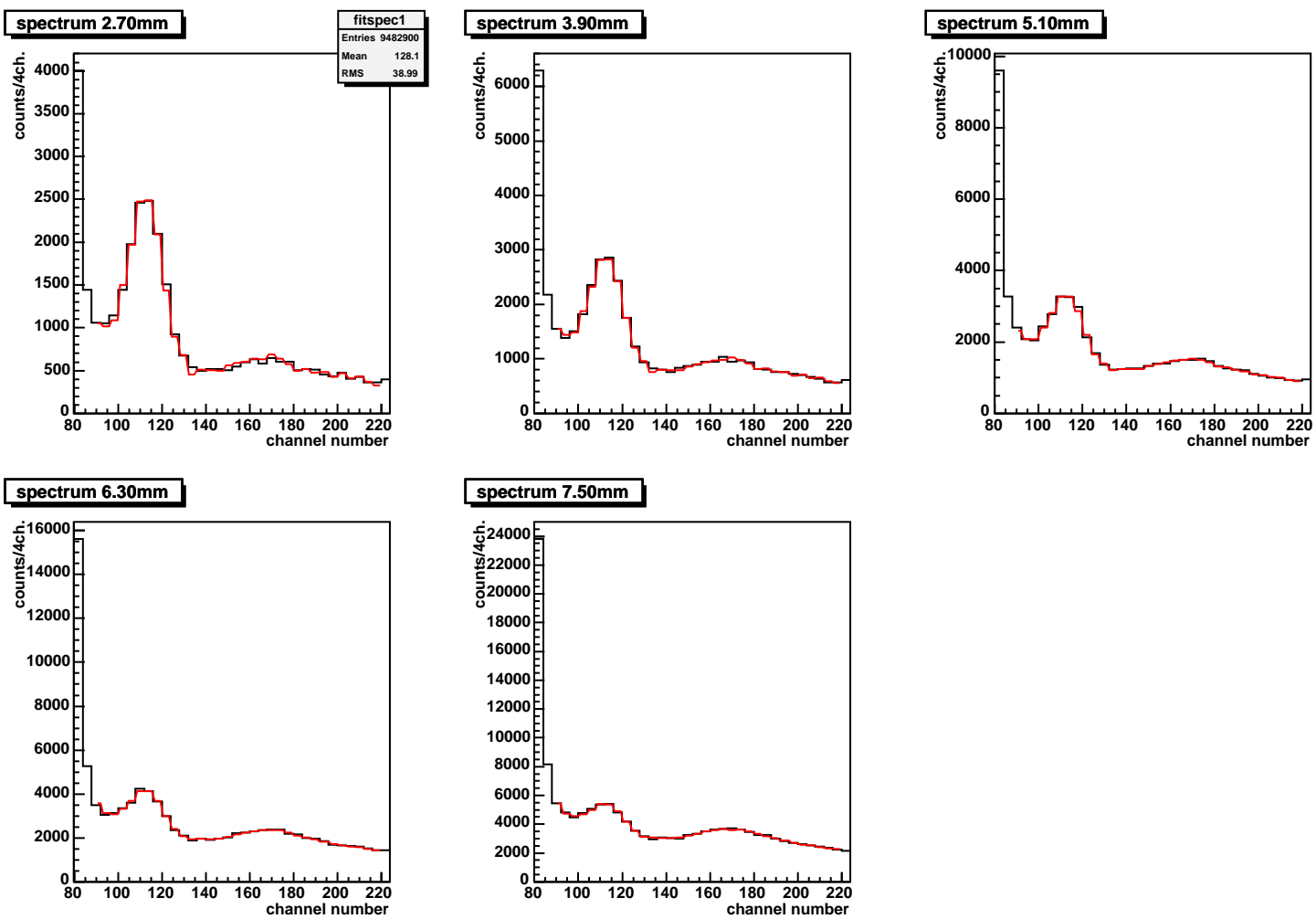


Figure C.4: Fit to the spectra recorded at $U = 1000$ V, using a linear combination of the corrected 28.0 mm background and the experimental positron line shape. The data is drawn in black, the fit function in red.

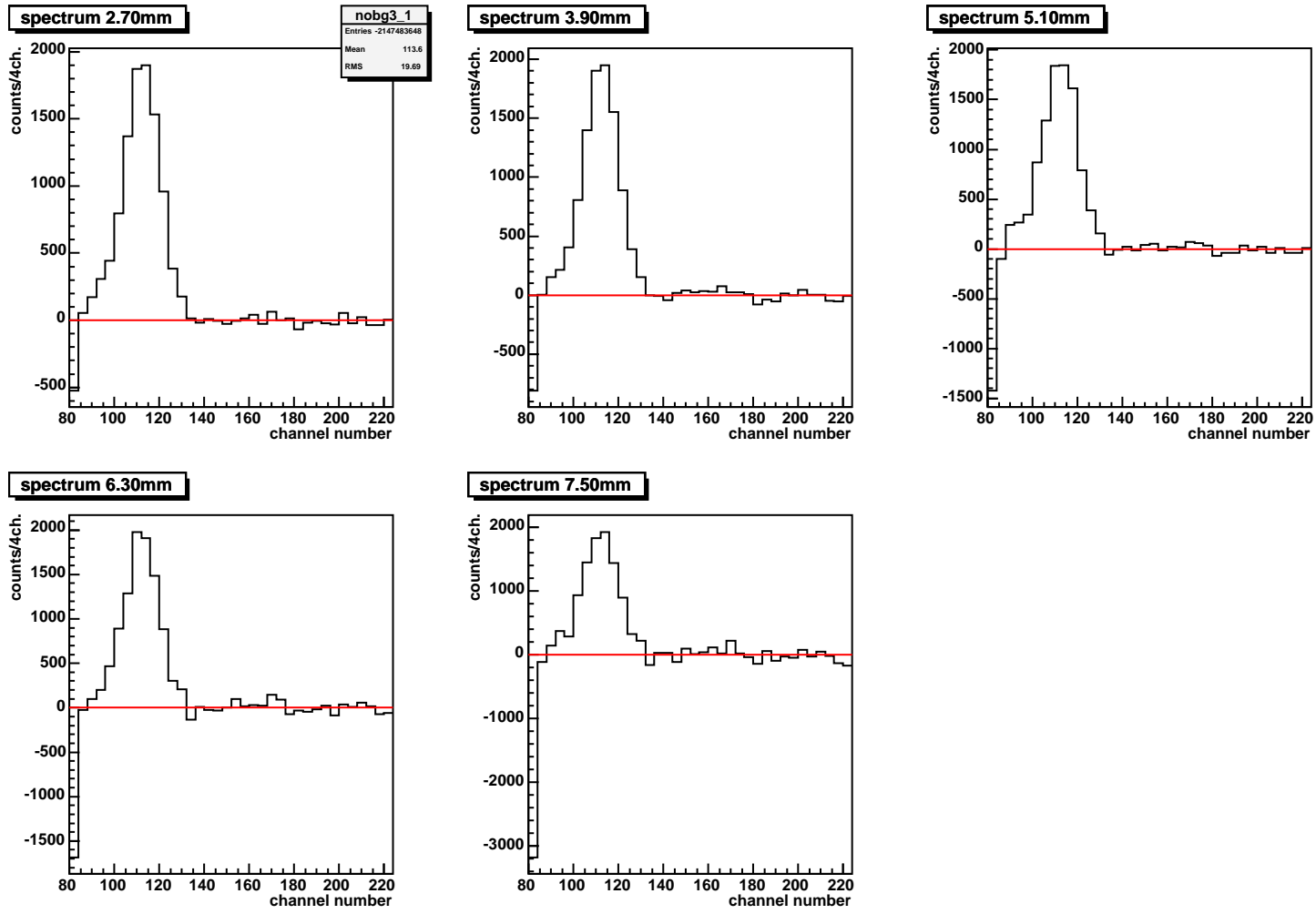


Figure C.5: The spectra recorded at $U = 1000$ V after background subtraction.

C.2 Run #7 at $U = 1300$ V

d [mm]	time [s]	counts	bg. counts	corr.	N_{e-bg}	N_{bg}^{fit}	N/t [s^{-1}]
2.7	70062	6076 ± 78	2318 ± 48	+0.6	3173	2330	0.0535(13)
4.1	112674	7415 ± 86	3676 ± 61	+1.0	5034	3703	0.03294(89)
5.4	175065	9205 ± 96	5593 ± 75	+1.5	7657	5602	0.02058(66)
6.8	281287	12436 ± 112	8886 ± 94	+2.3	12165	8914	0.01252(49)
8.1	436617	17338 ± 132	13684 ± 117	+3.6	18734	13654	0.00844(38)
9.5	695037	25725 ± 157	21505 ± 147	+5.7	29442	21390	0.00480(29)
28.0	695020	18706 ± 137			25610		

Table C.2: Results of the measurement at $U = 1300$ V (run 7): for each distance d the dead-time corrected measuring time, the integrated number of counts in the positron peak (before background subtraction), the number of counts in the same region of the appropriately scaled 28 mm background spectrum, the correction for the residual Ps contribution in the 28 mm background spectrum, the number of counts in the Compton electron background used for the first normalization N_{e-bg} , the final number of background counts under the peak as obtained from the fit (N_{bg}^{fit}) and the resulting Ps count rate N/t are listed.

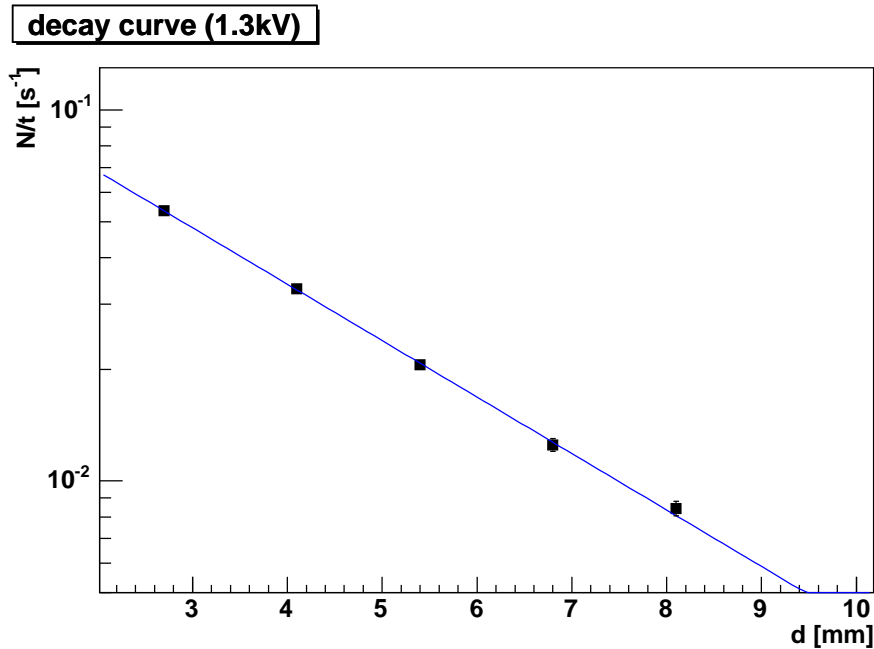


Figure C.6: Measured decay curve at $U = 1300$ V.

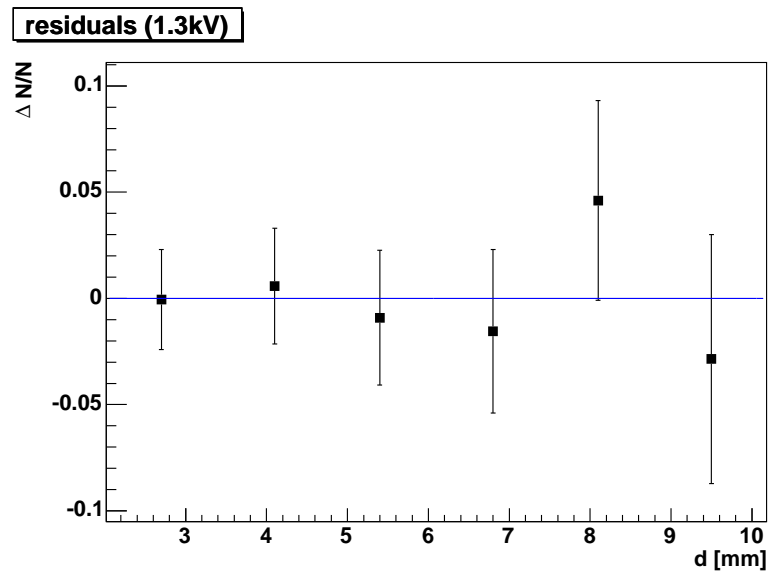


Figure C.7: Residuals ($data - fit$) divided by the data of the decay curve measured at $U = 1300$ V.

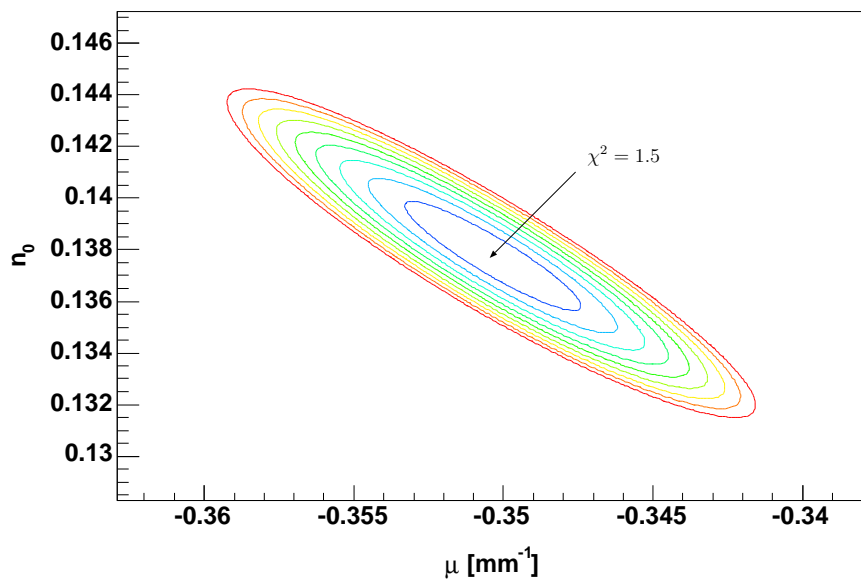


Figure C.8: $U = 1300$ V: Contour plot of χ^2 as a function of the two fitting parameters n_0 and μ . The equidistance of the contour lines is $\Delta\chi^2 = 0.2$.

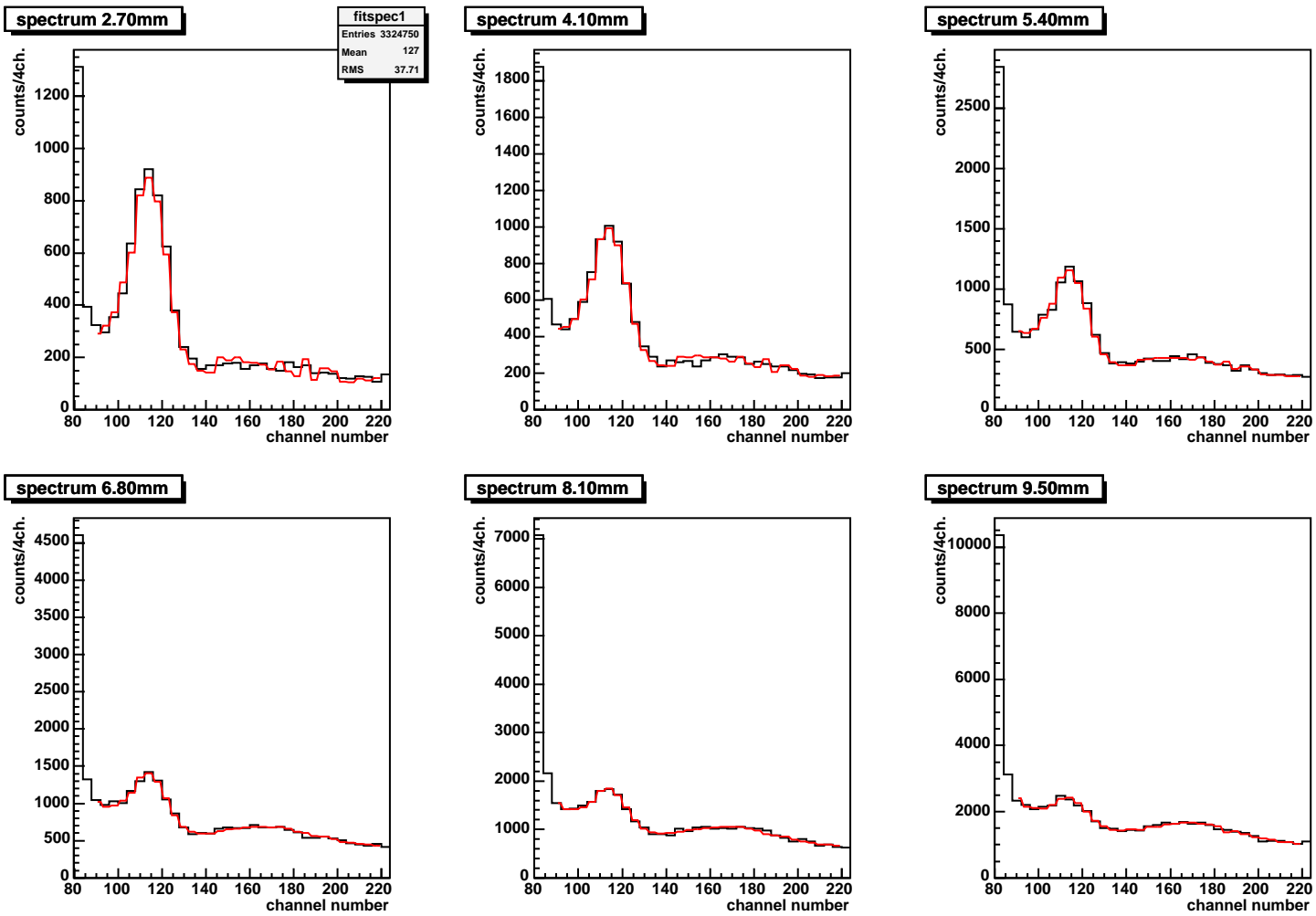


Figure C.9: Fit to the spectra recorded at $U = 1300$ V, using a linear combination of the corrected 28.0 mm background and the experimental positron line shape. The data is drawn in black, the fit function in red.

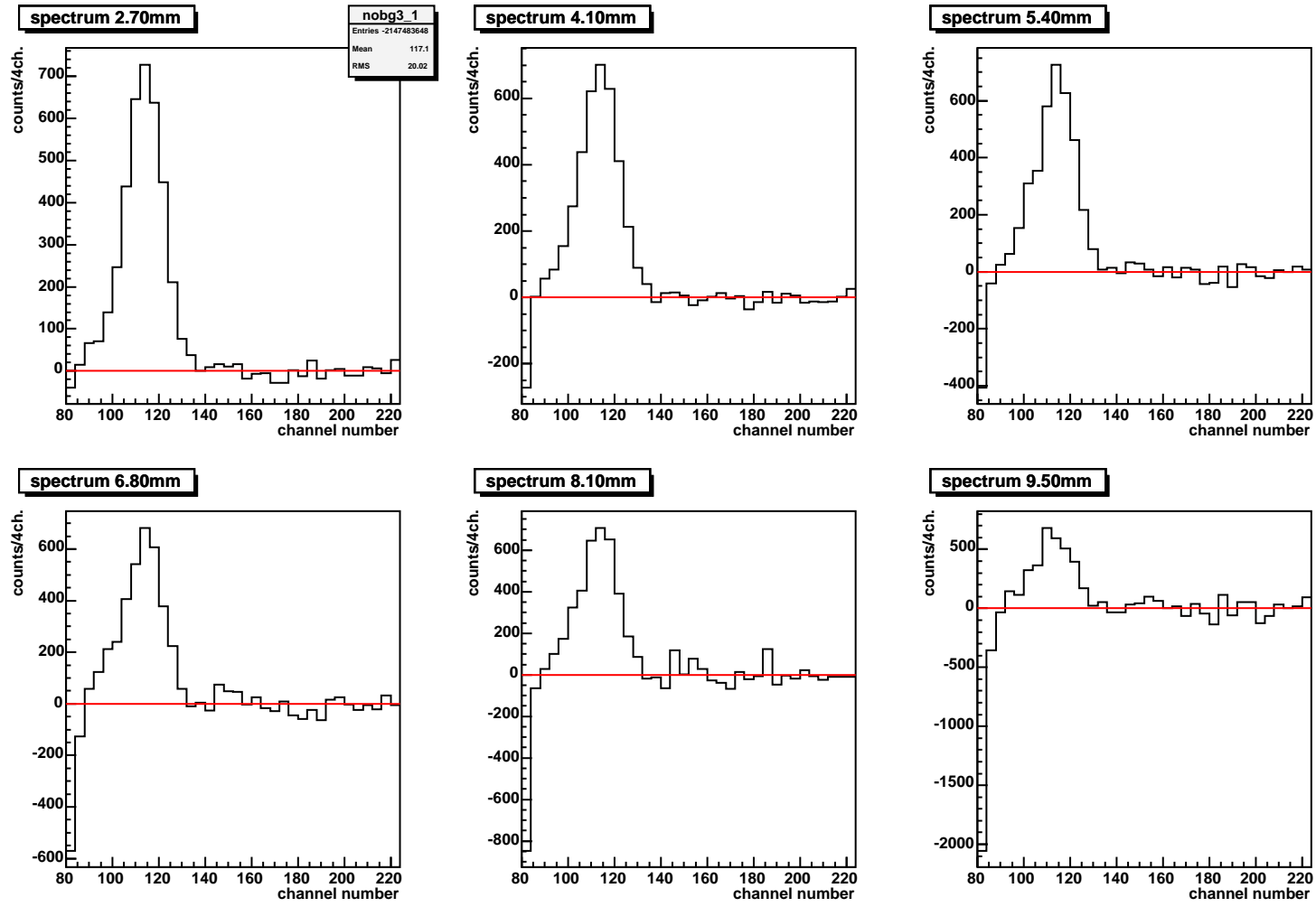


Figure C.10: The spectra recorded at $U = 1300$ V after background subtraction.

C.3 Run #5 at $U = 1900$ V

d [mm]	time [s]	counts	bg. counts	corr.	N_{e-bg}	N_{bg}^{fit}	N/t [s^{-1}]
2.7	44540	4678 ± 68	1525 ± 39	+2.9	2129	1540	0.0704(17)
4.4	71832	5423 ± 74	2451 ± 50	+4.7	3422	2449	0.0414(12)
6.0	111194	6828 ± 83	3670 ± 61	+7.0	5124	3691	0.02821(87)
7.6	174224	8723 ± 93	5710 ± 76	+10.9	7973	5710	0.01729(65)
9.4	288692	12256 ± 111	9297 ± 96	+17.7	12981	9197	0.01060(48)
10.9	439623	17015 ± 130	14041 ± 118	+26.8	19605	13936	0.00700(37)
28.0	427756	11976 ± 109			16722		

Table C.3: Results of the measurement at $U = 1900$ V (run 5): for each distance d the dead-time corrected measuring time, the integrated number of counts in the positron peak (before background subtraction), the number of counts in the same region of the appropriately scaled 28 mm background spectrum, the correction for the residual Ps contribution in the 28 mm background spectrum, the number of counts in the Compton electron background used for the first normalization N_{e-bg} , the final number of background counts under the peak as obtained from the fit (N_{bg}^{fit}) and the resulting Ps count rate N/t are listed.

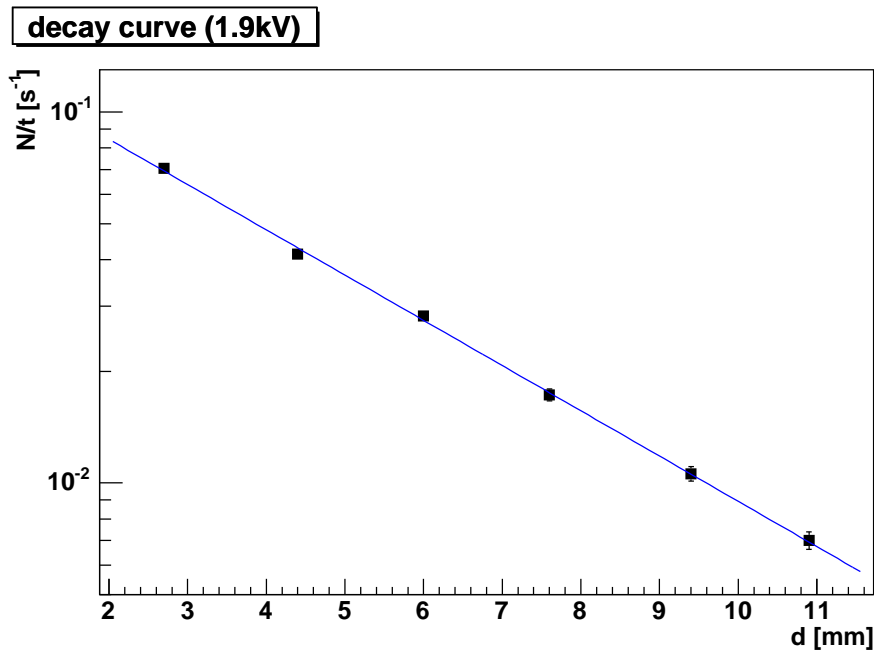


Figure C.11: Measured decay curve at $U = 1900$ V.

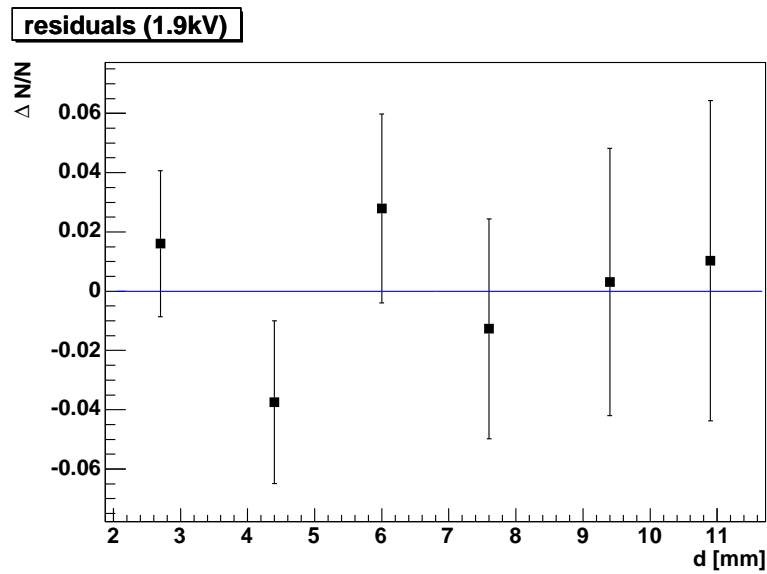


Figure C.12: Residuals (data - fit) divided by the data of the decay curve measured at $U = 1900$ V.

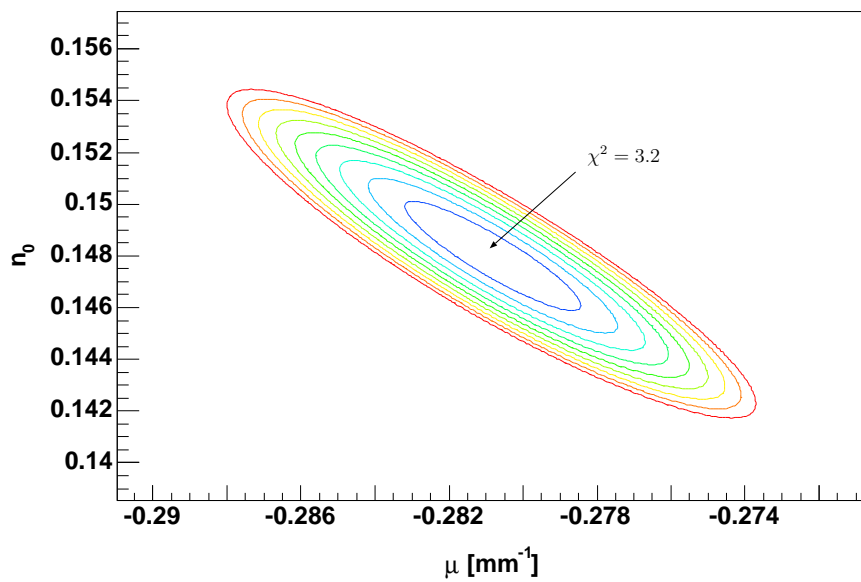


Figure C.13: $U = 1900$ V: Contour plot of χ^2 as a function of the two fitting parameters n_0 and μ . The equidistance of the contour lines is $\Delta\chi^2 = 0.2$.

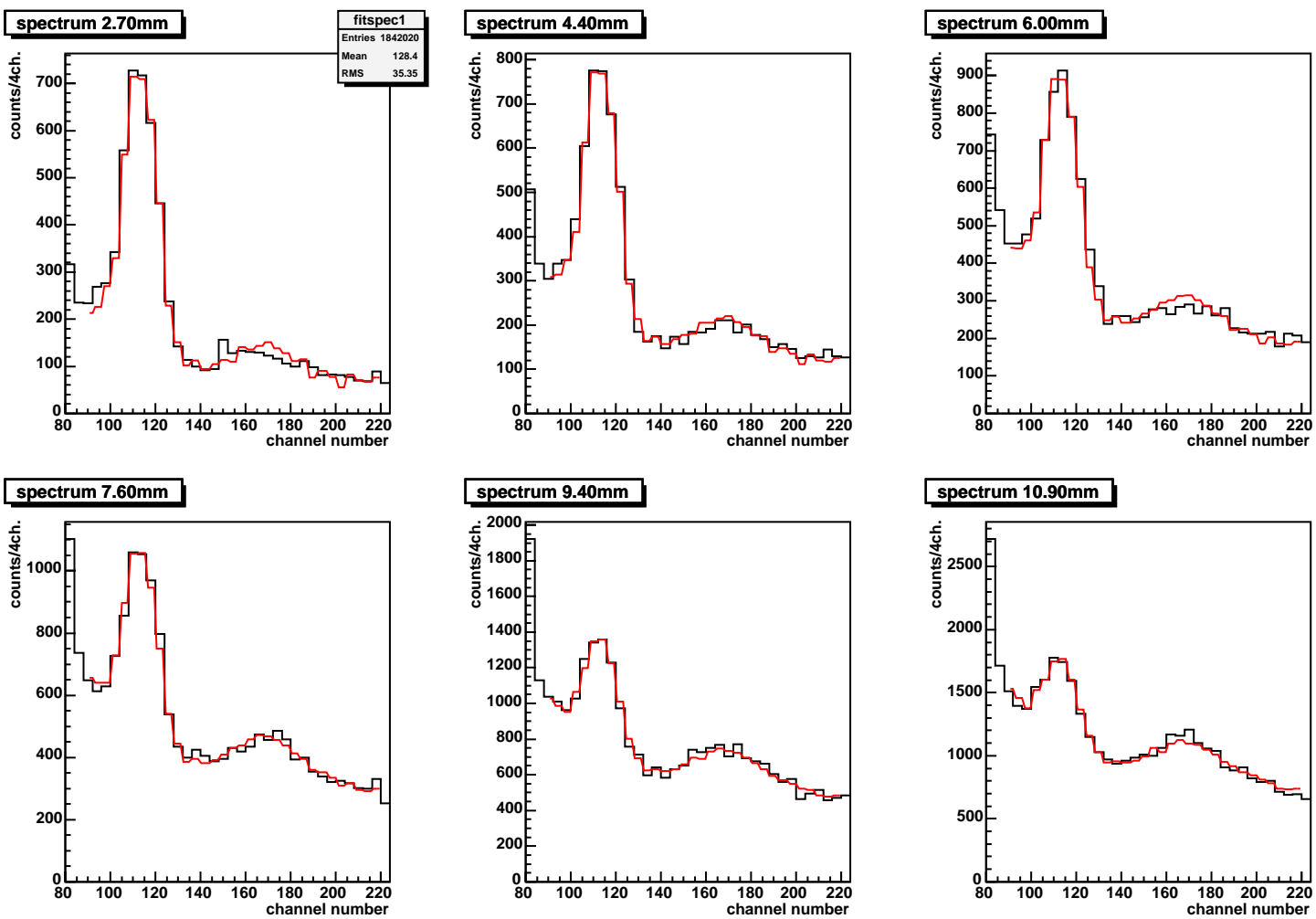


Figure C.14: Fit to the spectra recorded at $U = 1900$ V, using a linear combination of the corrected 28.0 mm background and the experimental positron line shape. The data is drawn in black, the fit function in red.

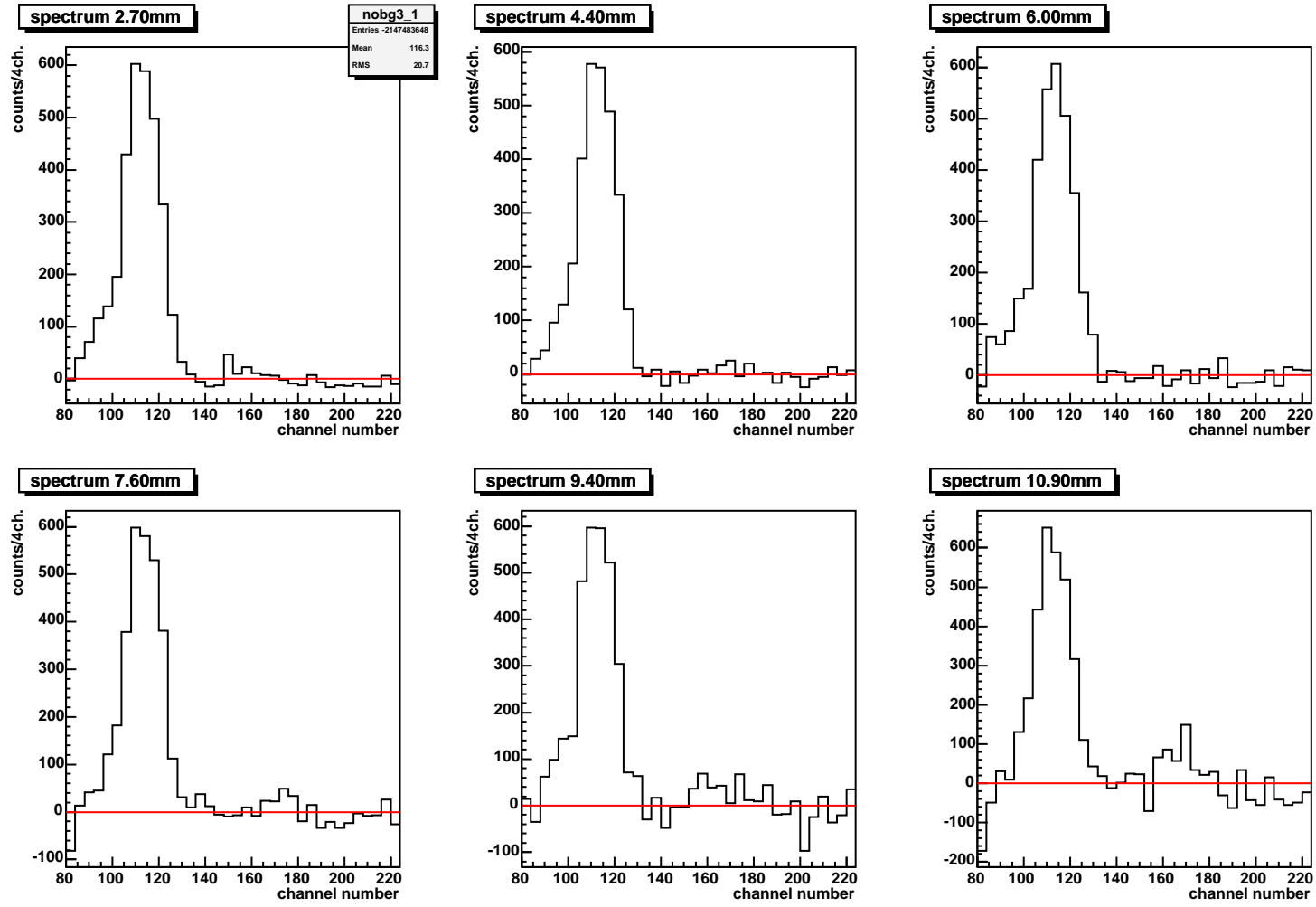


Figure C.15: The spectra recorded at $U = 1900$ V after background subtraction.

C.4 Runs #1 and #3 at $U = 3900$ V

d [mm]	time [s]	counts	bg. counts	corr.	N_{e-bg}	N_{bg}^{fit}	N/t [s^{-1}]
2.7	87336	9702 ± 98	2947 ± 54	+61	4320	2880	0.0781(12)
4.5	123803	10491 ± 102	4001 ± 63	+83	5865	3921	0.05307(93)
7.0	202341	13002 ± 114	6403 ± 80	+132	9385	6224	0.03350(65)
9.5	331977	16576 ± 129	10131 ± 101	+209	14849	9888	0.02015(46)
12.0	536844	22605 ± 150	16124 ± 127	+333	23634	15852	0.01258(34)
14.5	862276	31851 ± 178	25548 ± 160	+527	37448	25011	0.00793(26)
28.0	856278	23432 ± 153			34346		

Table C.4: Results of the measurement at $U = 3900$ V (sum of runs 1 and 3): for each distance d the dead-time corrected measuring time, the integrated number of counts in the positron peak (before background subtraction), the number of counts in the same region of the appropriately scaled 28 mm background spectrum, the correction for the residual Ps contribution in the 28 mm background spectrum, the number of counts in the Compton electron background used for the first normalization N_{e-bg} , the final number of background counts under the peak as obtained from the fit (N_{bg}^{fit}) and the resulting Ps count rate N/t are listed.

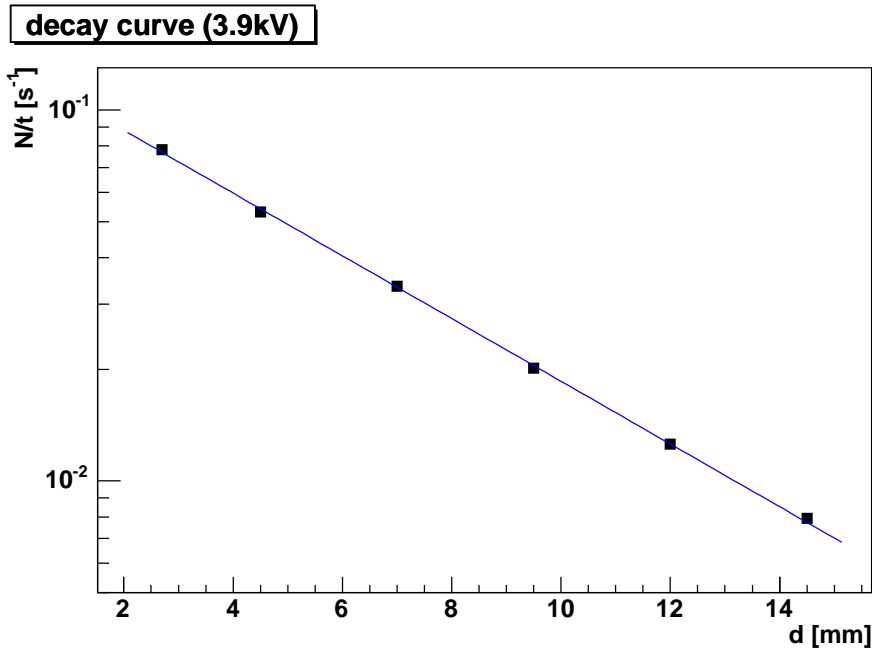


Figure C.16: Measured decay curve at $U = 3900$ V.

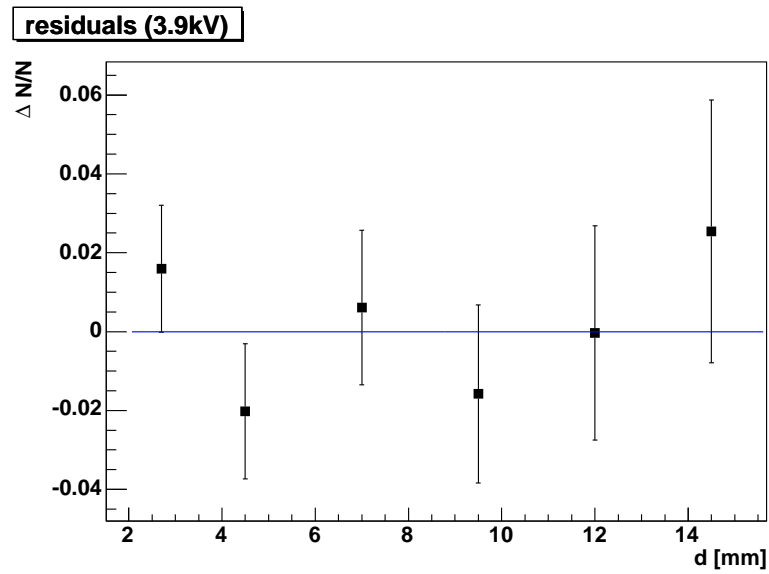


Figure C.17: Residuals (data - fit) divided by the data of the decay curve measured at $U = 3900$ V.

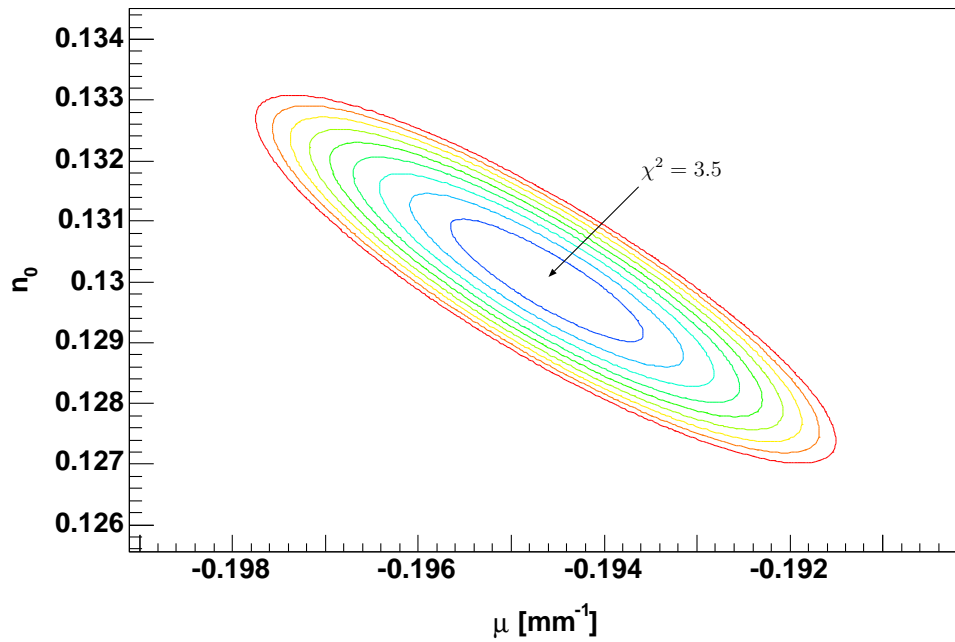


Figure C.18: $U = 3900$ V: Contour plot of χ^2 as a function of the two fitting parameters n_0 and μ . The equidistance of the contour lines is $\Delta\chi^2 = 0.2$.

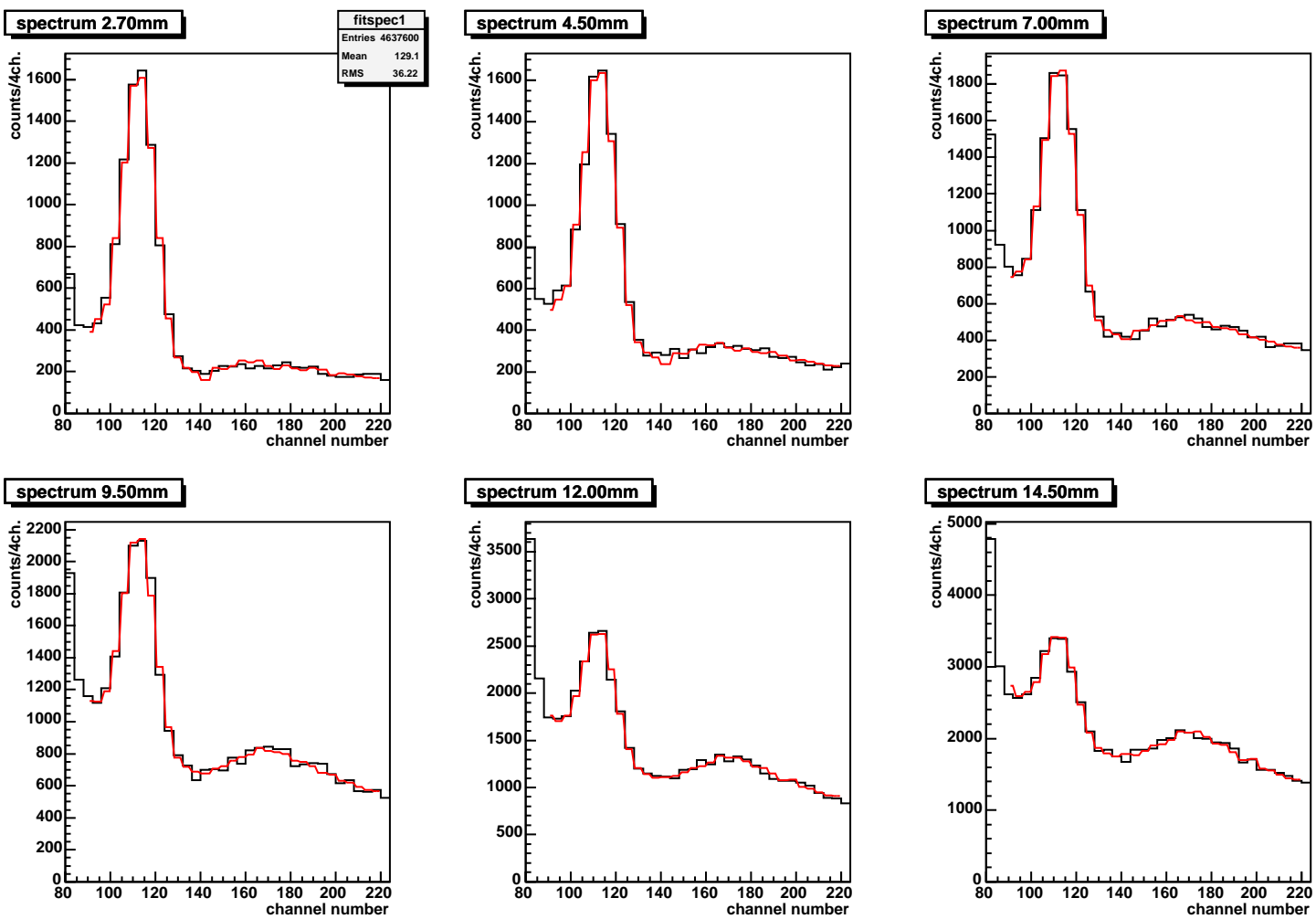


Figure C.19: Fit to the spectra recorded at $U = 3900$ V, using a linear combination of the corrected 28.0 mm background and the experimental positron line shape. The data is drawn in black, the fit function in red.

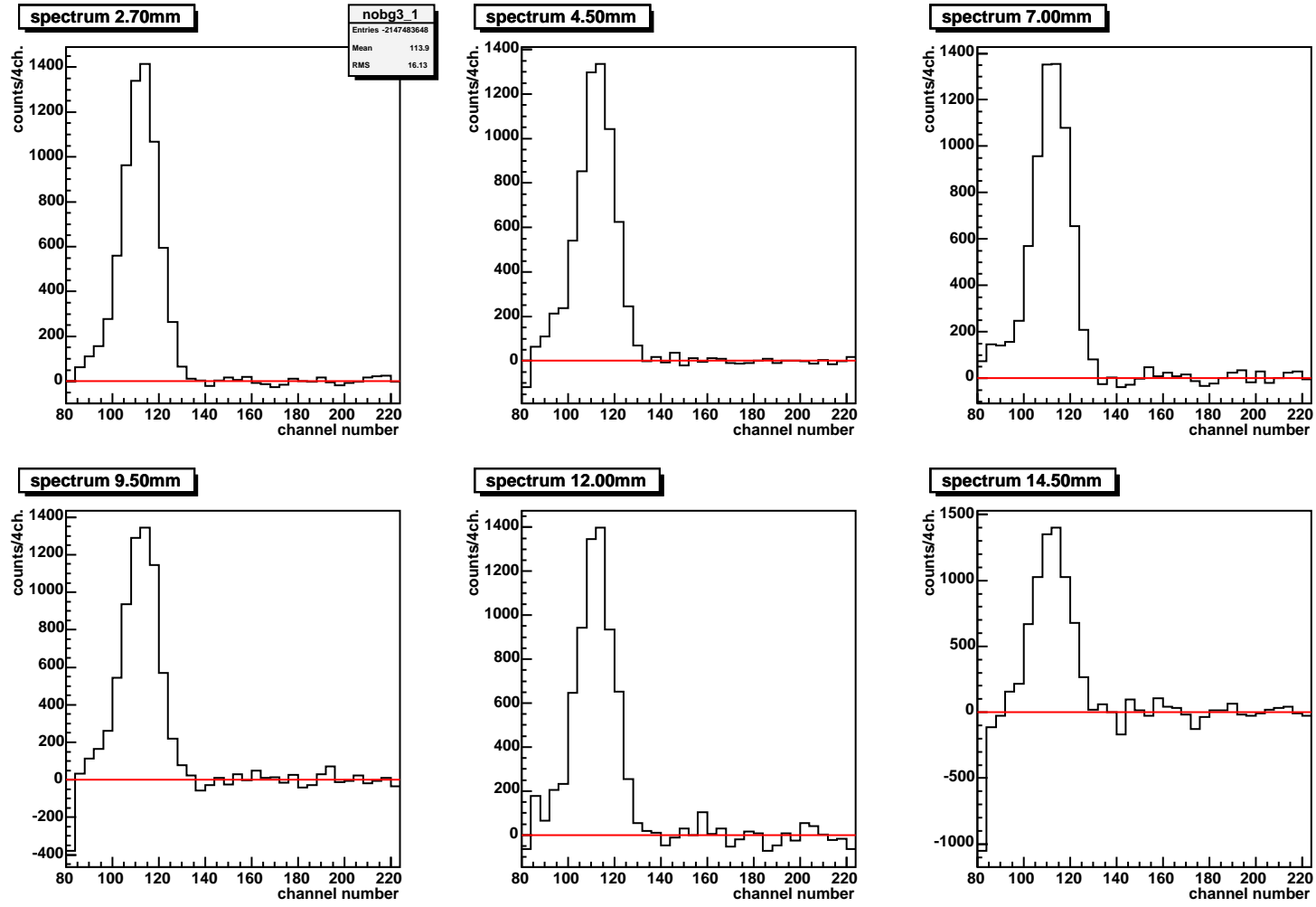


Figure C.20: The spectra recorded at $U = 3900$ V after background subtraction.

C.5 Run #6 at $U = 4000$ V

d [mm]	time [s]	counts	bg. counts	corr.	N_{e-bg}	N_{bg}^{fit}	N/t [s^{-1}]
2.7	64090	8674 ± 93	2280 ± 48	+60	3061	2265	0.1000(16)
4.5	96152	9951 ± 100	3396 ± 58	+89	4559	3300	0.0692(12)
7.0	160751	12323 ± 111	5347 ± 73	+140	7178	5262	0.04392(79)
9.5	281113	16426 ± 128	9084 ± 95	+238	12194	8895	0.02679(54)
12.0	491952	23159 ± 152	15664 ± 125	+410	21027	15190	0.01620(38)
14.5	853244	34722 ± 186	26566 ± 163	+695	35662	25771	0.01049(27)
28.0	841393	24053 ± 155			32289		

Table C.5: Results of the measurement at $U = 4000$ V (run 6): for each distance d the dead-time corrected measuring time, the integrated number of counts in the positron peak (before background subtraction), the number of counts in the same region of the appropriately scaled 28 mm background spectrum, the correction for the residual Ps contribution in the 28 mm background spectrum, the number of counts in the Compton electron background used for the first normalization N_{e-bg} , the final number of background counts under the peak as obtained from the fit (N_{bg}^{fit}) and the resulting Ps count rate N/t are listed.

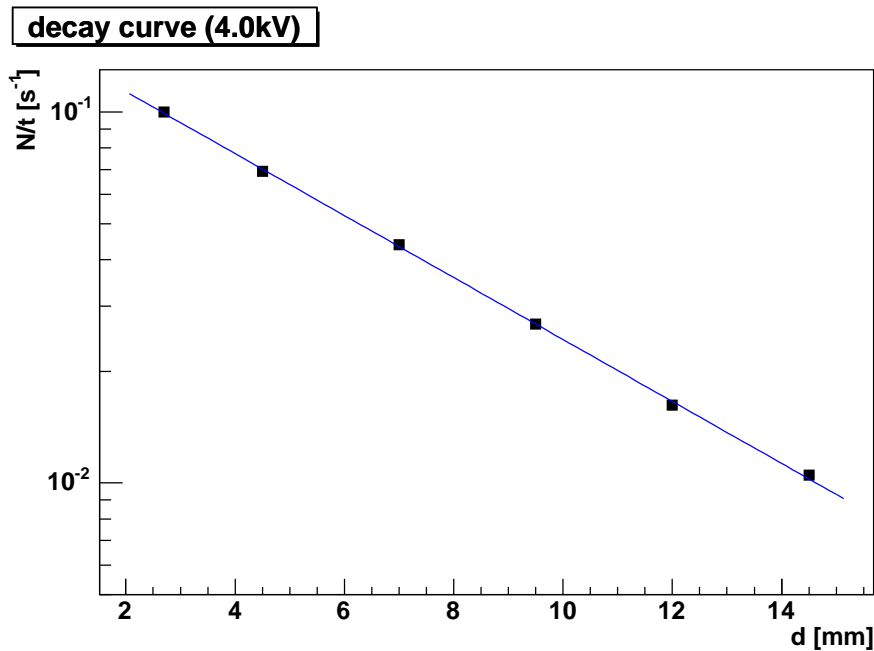


Figure C.21: Measured decay curve at $U = 4000$ V.

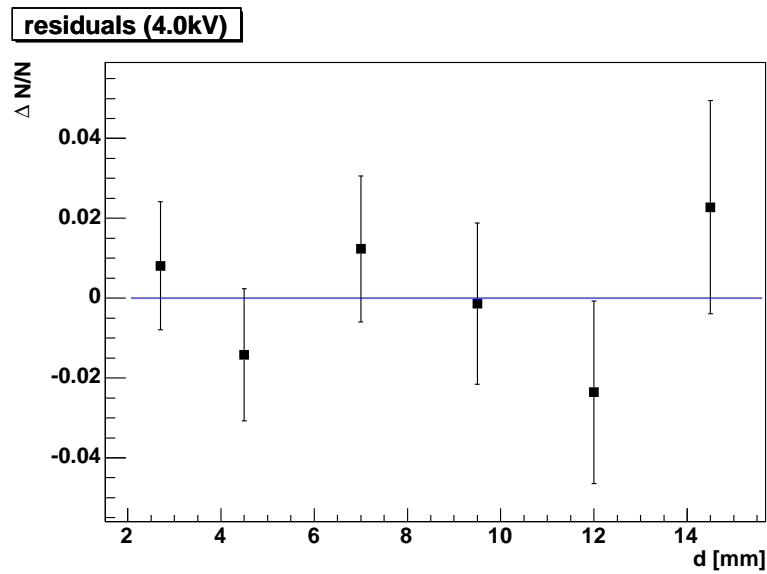


Figure C.22: Residuals (data - fit) divided by the data of the decay curve measured at $U = 4000$ V.

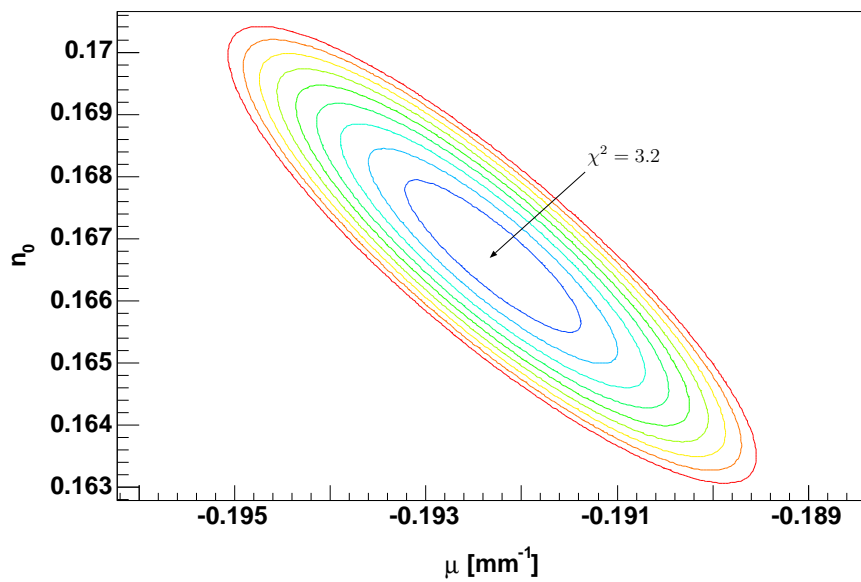


Figure C.23: $U = 4000$ V: Contour plot of χ^2 as a function of the two fitting parameters n_0 and μ . The equidistance of the contour lines is $\Delta\chi^2 = 0.2$.

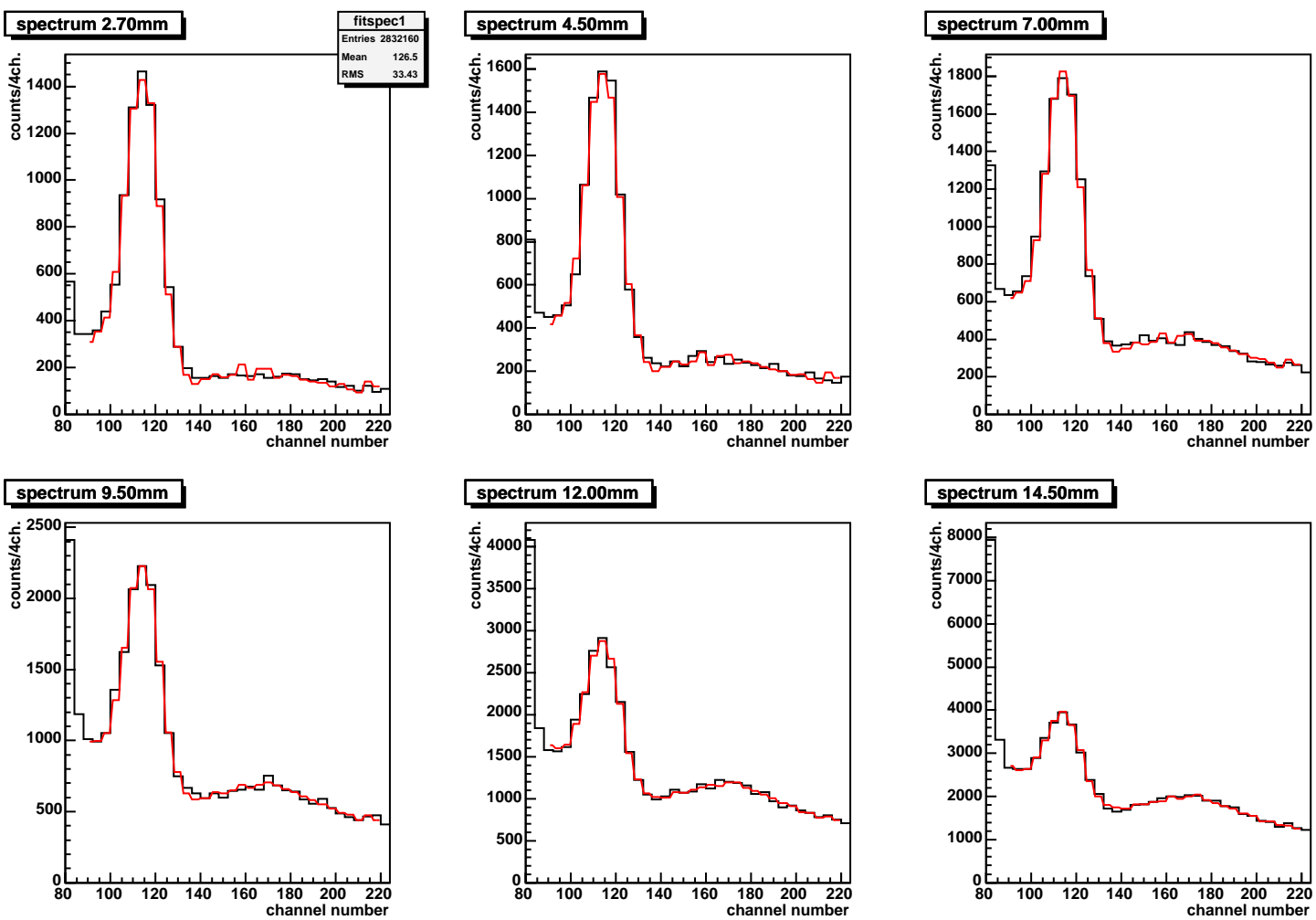


Figure C.24: Fit to the spectra recorded at $U = 4000$ V, using a linear combination of the corrected 28.0 mm background and the experimental positron line shape. The data is drawn in black, the fit function in red.

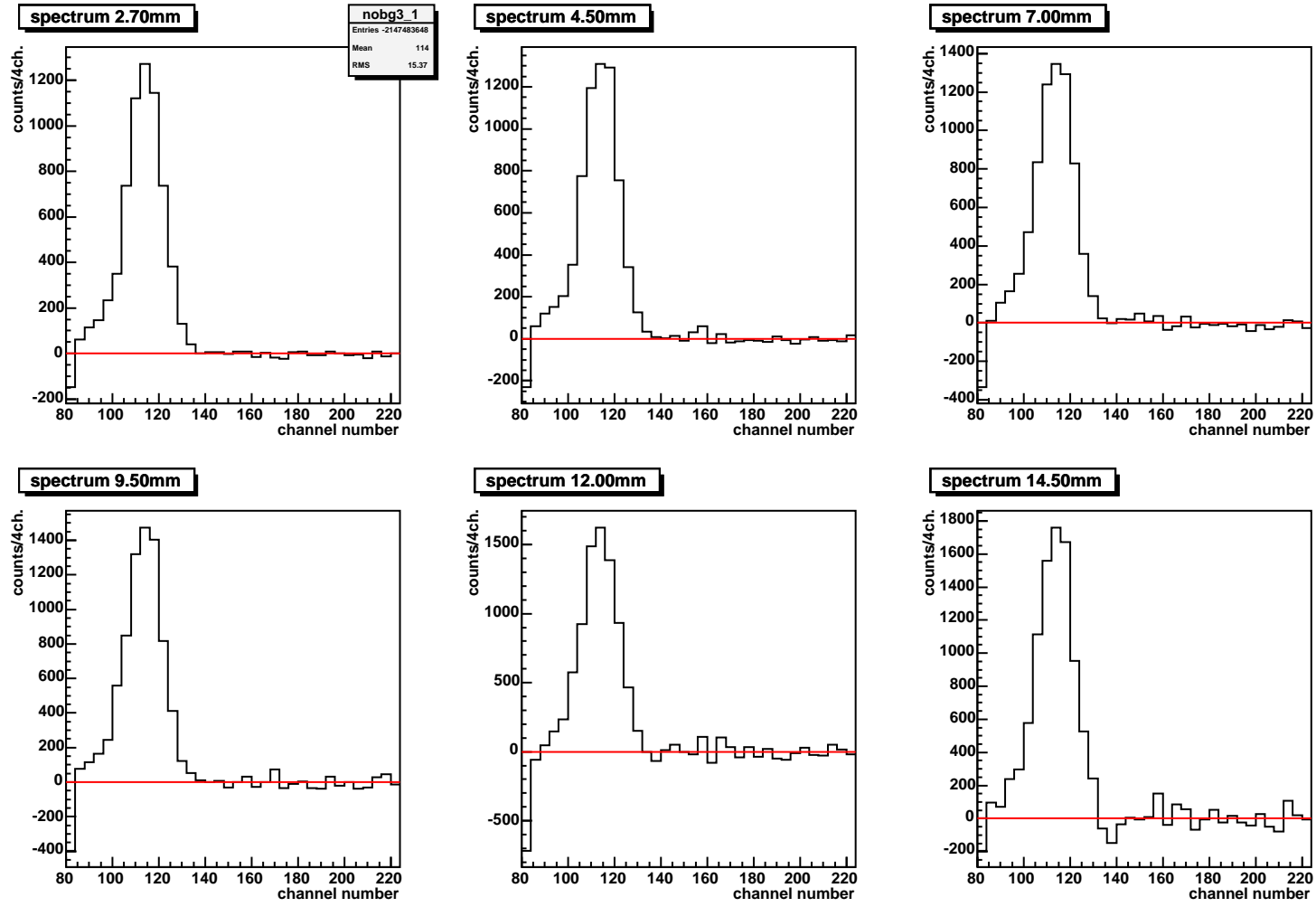


Figure C.25: The spectra recorded at $U = 4000$ V after background subtraction.

C.6 Runs #8 and #10 at $U = 4800\text{ V}$

d [mm]	time [s]	counts	bg. counts	corr.	$N_{e\text{-bg}}$	$N_{\text{bg}}^{\text{fit}}$	N/t [s^{-1}]
3.5	60154	7159 ± 85	2087 ± 46	+95	2712	2013	0.0856(16)
6.1	95326	8242 ± 91	3125 ± 56	+143	4062	3019	0.0548(11)
8.7	153770	10297 ± 101	4920 ± 70	+224	6394	4664	0.03663(77)
11.4	244490	12728 ± 113	7658 ± 88	+349	9952	7296	0.02222(56)
14.0	387317	17099 ± 131	11858 ± 109	+541	15410	11339	0.01487(42)
16.6	605811	22702 ± 151	18171 ± 135	+829	23613	17296	0.00892(32)
28.0	593918	16821 ± 130			21859		

Table C.6: Results of the measurement at $U = 4800\text{ V}$ (sum of runs 8 and 10): for each distance d the dead-time corrected measuring time, the integrated number of counts in the positron peak (before background subtraction), the number of counts in the same region of the appropriately scaled 28 mm background spectrum, the correction for the residual Ps contribution in the 28 mm background spectrum, the number of counts in the Compton electron background used for the first normalization $N_{e\text{-bg}}$, the final number of background counts under the peak as obtained from the fit ($N_{\text{bg}}^{\text{fit}}$) and the resulting Ps count rate N/t are listed.

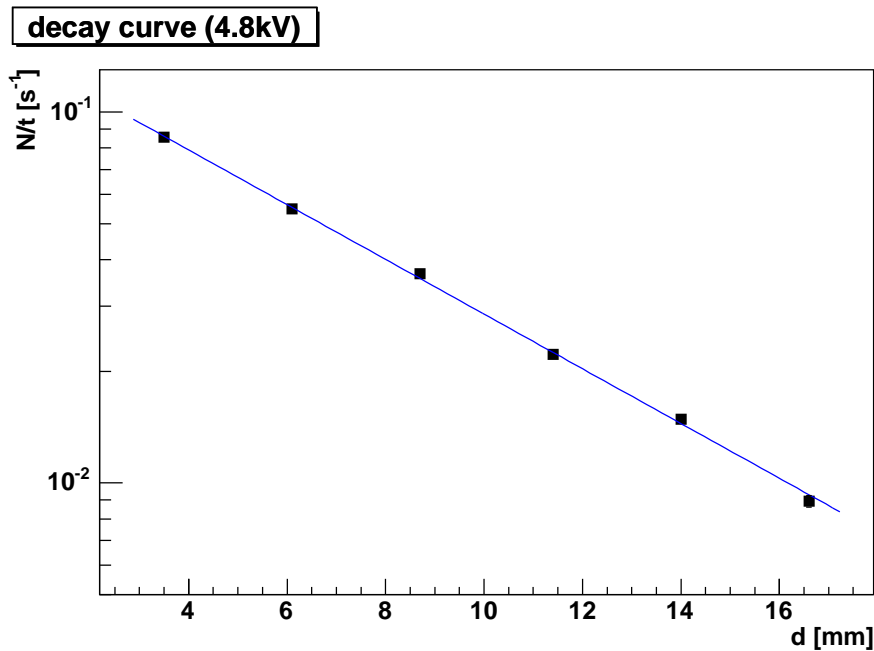


Figure C.26: Measured decay curve at $U = 4800\text{ V}$.

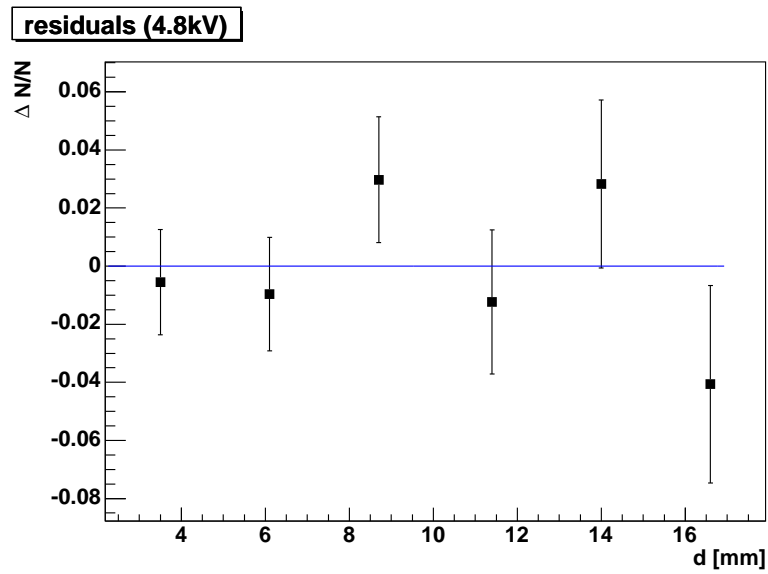


Figure C.27: Residuals (data - fit) divided by the data of the decay curve measured at $U = 4800$ V.

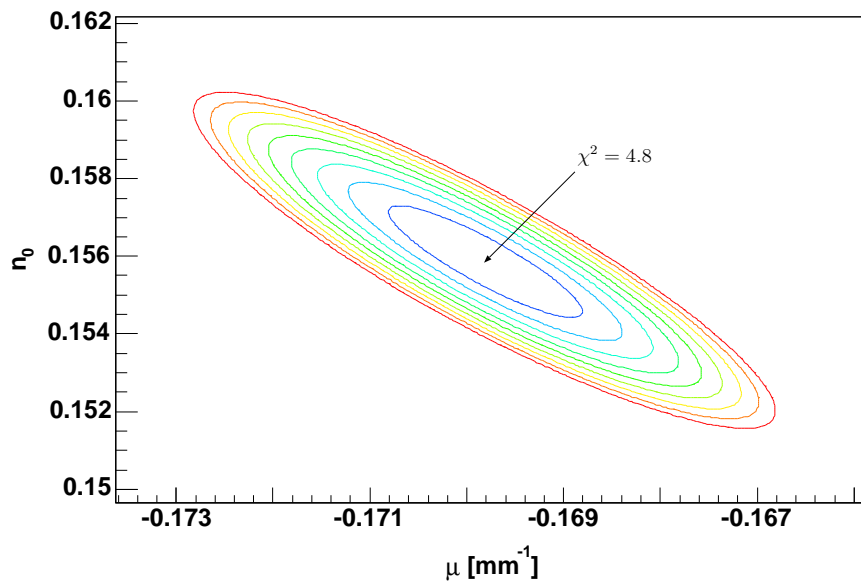


Figure C.28: $U = 4800$ V: Contour plot of χ^2 as a function of the two fitting parameters n_0 and μ . The equidistance of the contour lines is $\Delta\chi^2 = 0.2$.

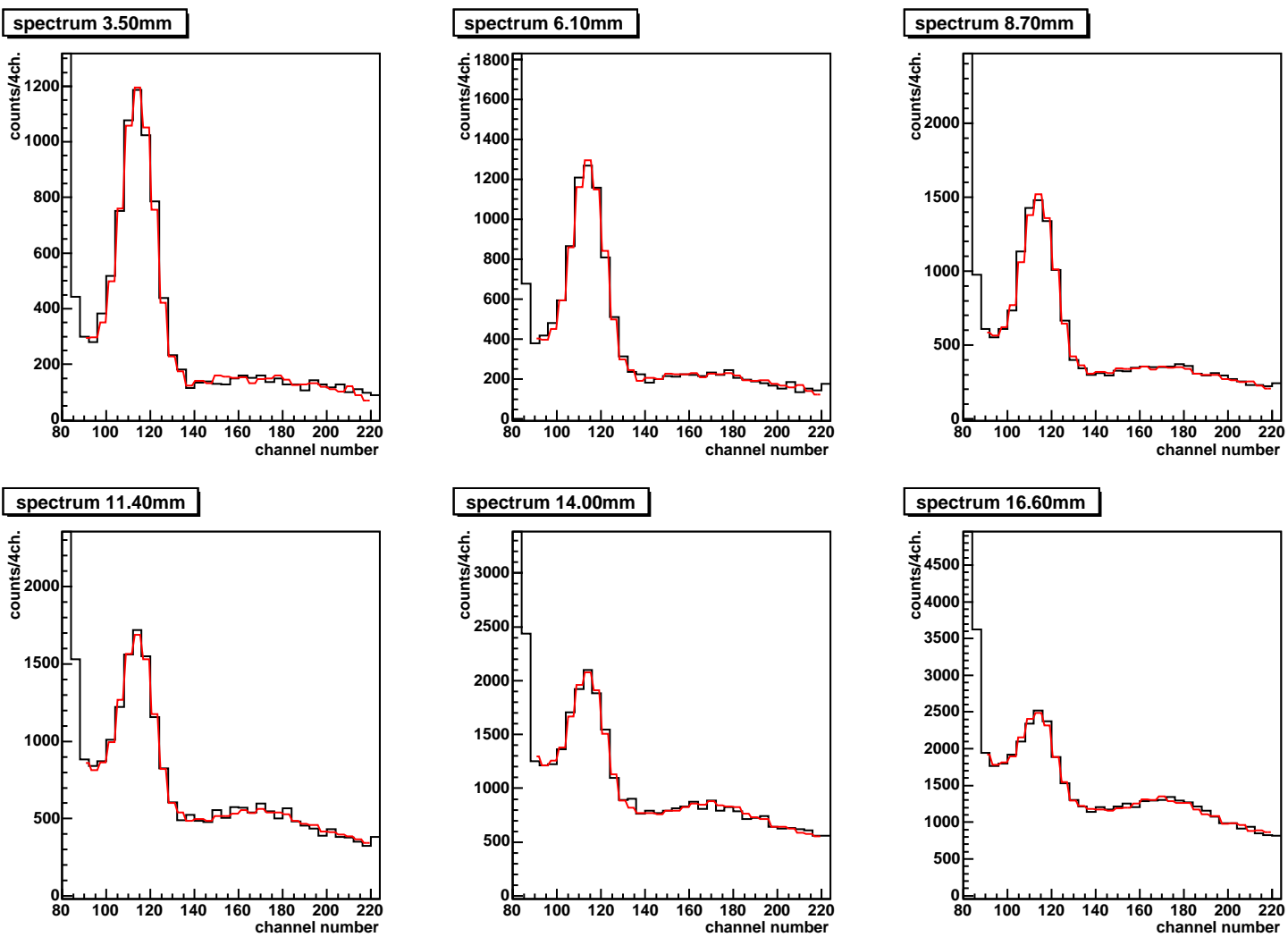


Figure C.29: Fit to the spectra recorded at $U = 4800$ V, using a linear combination of the corrected 28.0 mm background and the experimental positron line shape. The data is drawn in black, the fit function in red.

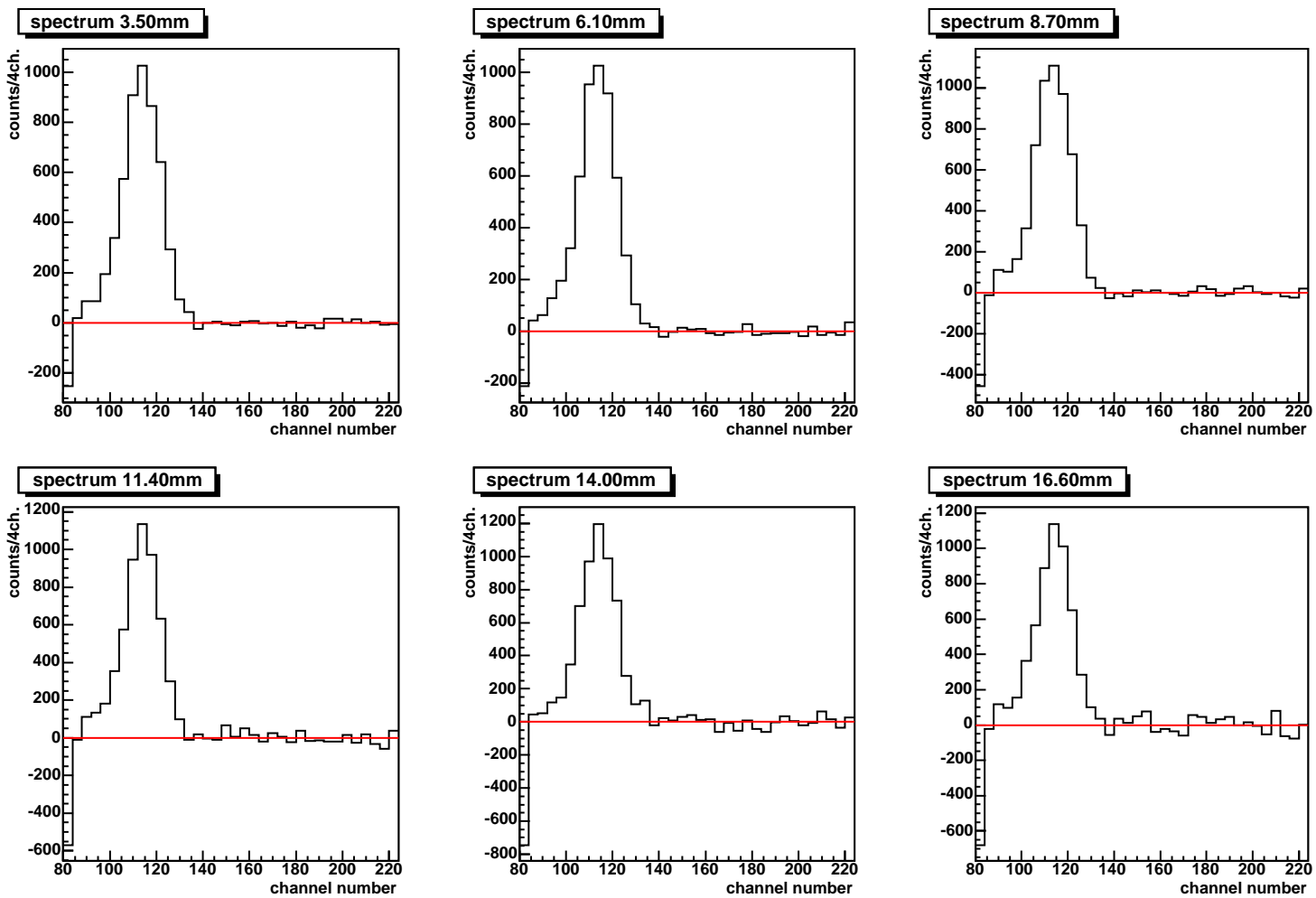


Figure C.30: The spectra recorded at $U = 4800$ V after background subtraction. The red histograms represent the corrected background approximation (cf. sec. 4.3.2).

C.7 Run #9 at $U = 3900$ V

d [mm]	time [s]	counts	bg. counts	corr.	N_{e-bg}	N_{bg}^{fit}	N/t [s^{-1}]
2.7	28864	3652 ± 60	975 ± 31	+25	1318	951	0.0936(23)
4.5	41223	4044 ± 64	1346 ± 37	+35	1819	1294	0.0667(17)
7.0	67267	4760 ± 69	2122 ± 46	+54	2868	2063	0.0401(12)
9.5	109863	5977 ± 77	3383 ± 58	+87	4573	3264	0.02470(83)
12.0	179210	8002 ± 89	5423 ± 74	+139	7330	5285	0.01516(61)
14.5	291929	11184 ± 106	8468 ± 92	+217	11446	8256	0.01003(45)
28.0	292001	7955 ± 89			10753		

Table C.7: Results of the measurement at $U = 3900$ V ((control) run 9): for each distance d the dead-time corrected measuring time, the integrated number of counts in the positron peak (before background subtraction), the number of counts in the same region of the appropriately scaled 28 mm background spectrum, the correction for the residual Ps contribution in the 28 mm background spectrum, the number of counts in the Compton electron background used for the first normalization N_{e-bg} , the final number of background counts under the peak as obtained from the fit (N_{bg}^{fit}) and the resulting Ps count rate N/t are listed.

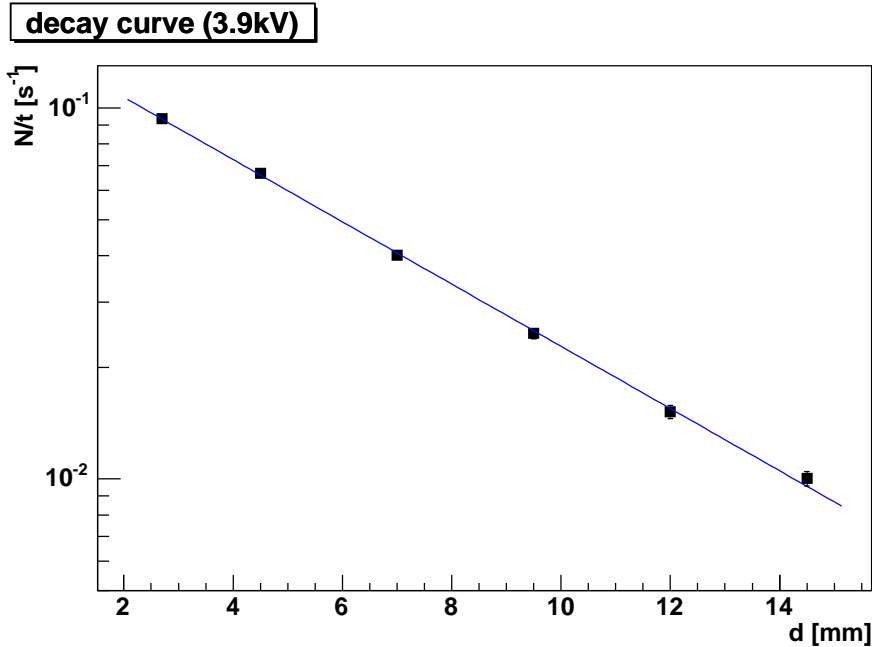


Figure C.31: Measured decay curve at $U = 3900$ V (control run).

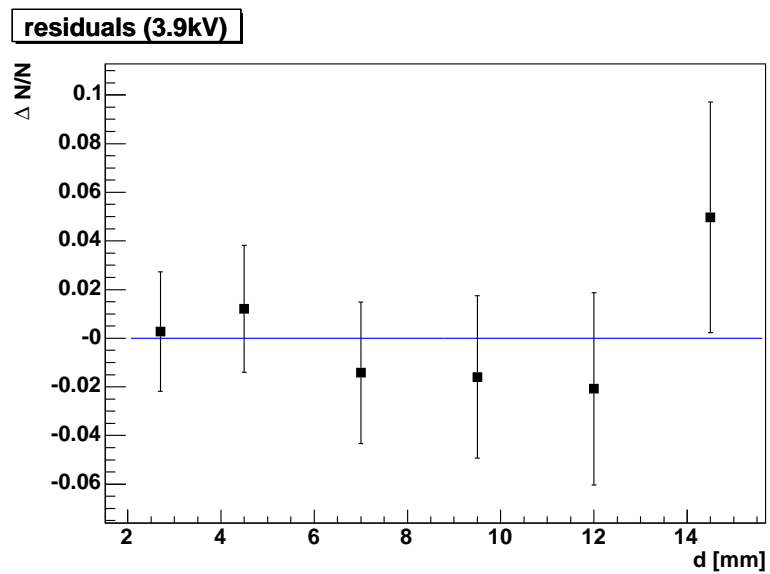


Figure C.32: Residuals (data - fit) divided by the data of the decay curve measured at $U = 3900$ V (control run).

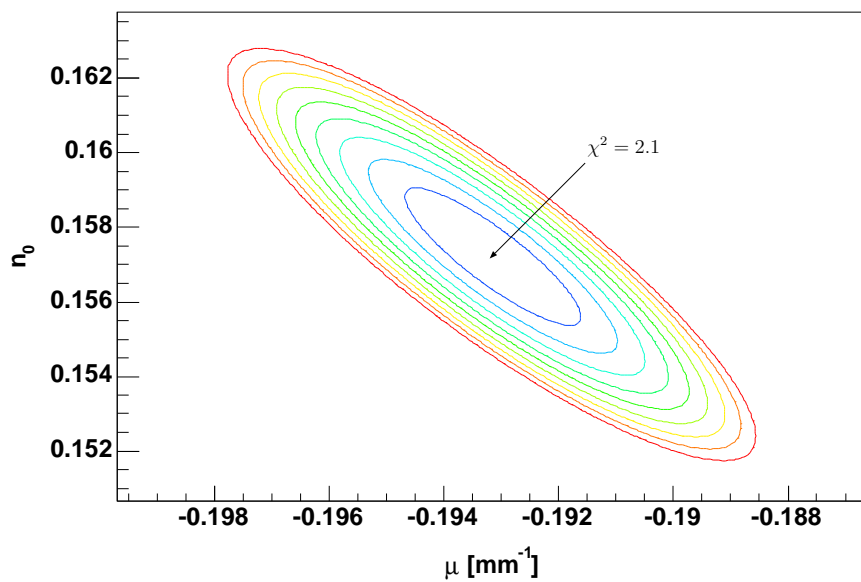


Figure C.33: $U = 3900$ V (control run): Contour plot of χ^2 as a function of the two fitting parameters n_0 and μ . The equidistance of the contour lines is $\Delta\chi^2 = 0.2$.

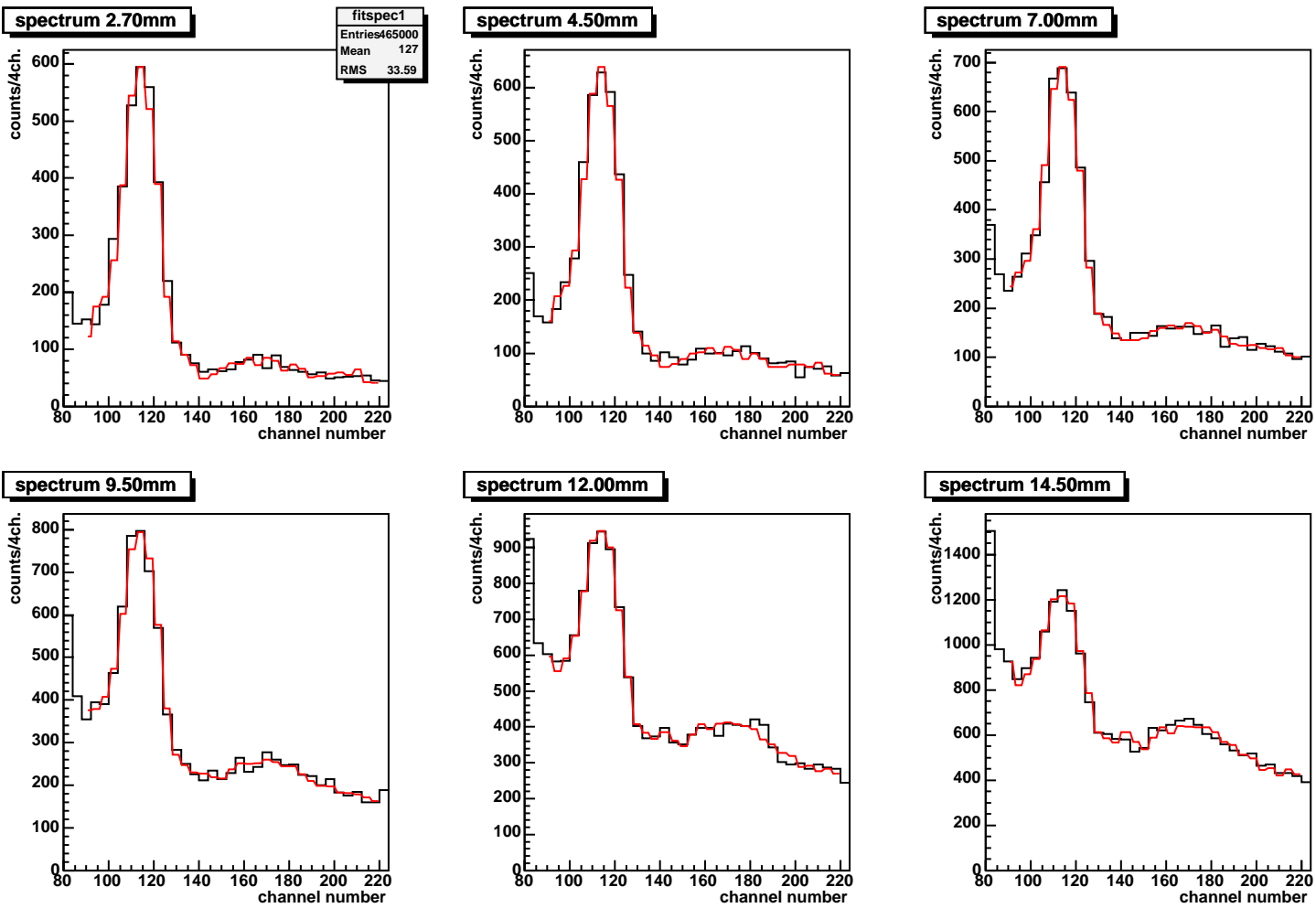


Figure C.34: Fit to the spectra recorded at $U = 3900$ V (control run), using a linear combination of the corrected 28.0 mm background and the experimental positron line shape. The data is drawn in black, the fit function in red.

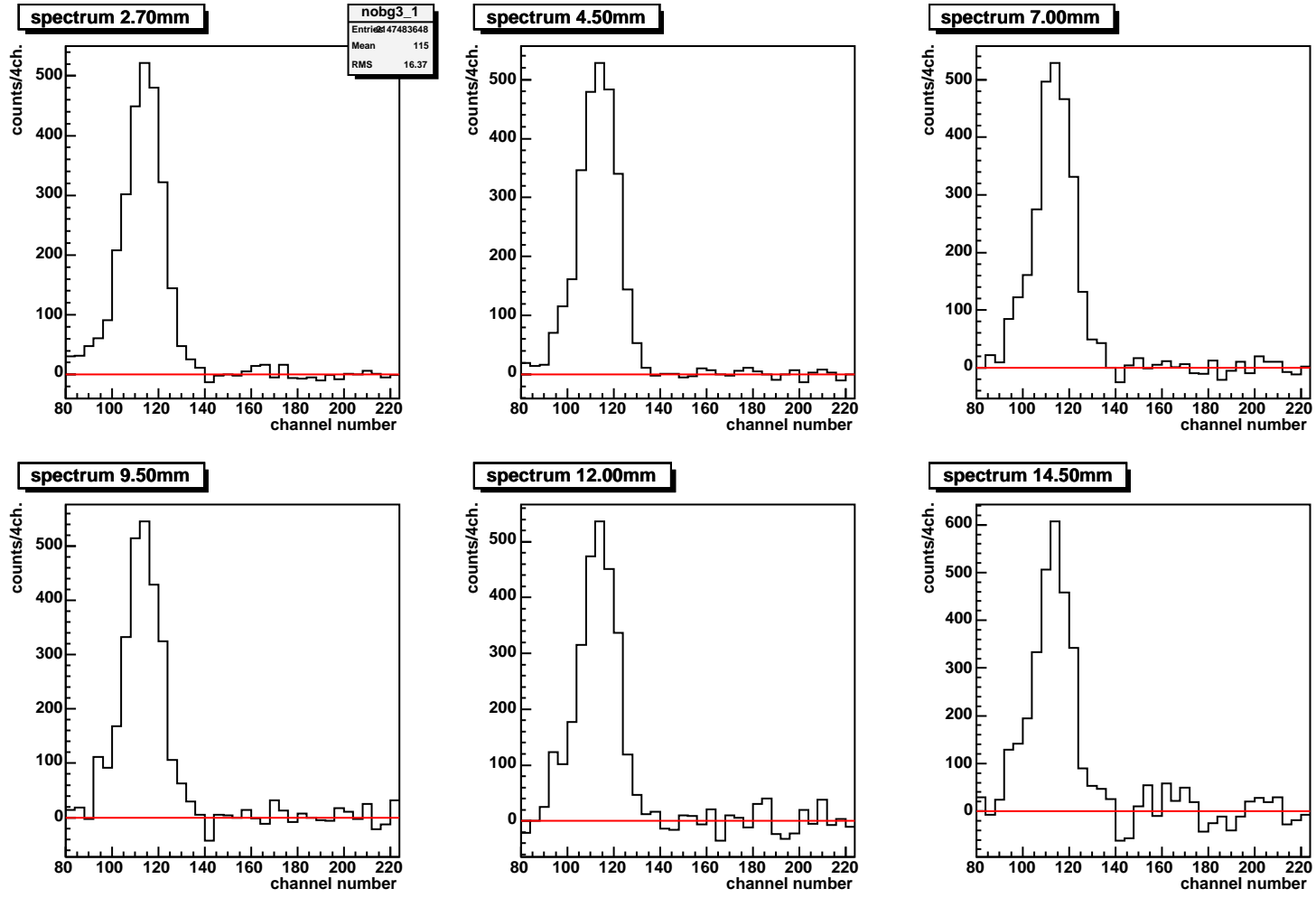


Figure C.35: The spectra recorded at $U = 3900$ V (control run) after background subtraction.

Acknowledgements

An dieser Stelle möchte ich allen, die zum Gelingen dieser Arbeit beigetragen haben, meinen herzlichen Dank aussprechen.

Zunächst einmal herzlichen Dank an Prof. Dr. Dirk Schwalm, der mir das Thema für diese Doktorarbeit angeboten hat, und der sich trotz seiner vielen anderen Verpflichtungen stets die Zeit genommen hat, mir bei meinen Fragen oder Problemen zu helfen. Dankeschön für das freundschaftliche Klima und die motivierende Begeisterung für das Ps^- -Experiment! Für die gute Zusammenarbeit möchte ich Michael Lestinsky danken, der während seiner Diplomarbeit die Messungen mit der γ -Methode durchgeführt hat.

Herzlichen Dank auch an Gerald Gwinner, der, solange er noch am MPI für Kernphysik war, stets ein offenes Ohr für meine Fragen hatte.

Ebenso gebührt den "Kernis" Dank für ihre Hilfe im Umgang mit dem MINIBALL-Detektor, der Elektronik und der Datenaufnahme. Ganz besonders hervorzuheben sind hier Heiko Scheit, Hans Boie, Jörg Fitting sowie Frank Koeck. Auch ihre Vorschläge und Ideen auf anderen Gebieten waren oft hilfreich.

Oliver Koschorreck war eigentlich immer zur Stelle, wenn irgendetwas elektronisches nicht funktionieren wollte, und er hat sich während der Vorbereitung der γ -Messung tapfer am Kampf mit den XIA-Karten beteiligt. Vielen Dank dafür!

Auf jeden Fall erwähnt werden müssen auch Doris Cerny und Helga Krieger, die immer für ein gutes Arbeitsklima in der Gruppe sorgen. Helga Krieger weiß auch stets, wen man fragen muß, um etwas schnell erledigt zu bekommen.

Vielen Dank auch an alle Mitarbeiter in den Werkstätten des MPI für Kernphysik, in der Elektronik, der Haustechnik, der Konstruktion und dem Strahlenschutz, ohne deren Einsatz und Fachkenntnisse eine experimentelle Arbeit nicht möglich wäre. Bei den Herren Mallinger, Bender, Hahn und Schlicksupp möchte ich mich dafür bedanken, daß sie es ertragen haben, daß immer wieder etwas "möglichst bis gestern" angefertigt werden mußte. Thomas Busch hat mich bei einigen obskuren Hochspannungsproblemen tatkräftig unterstützt. Von der Konstruktion sind besonders die Herren Weber und Gahn sowie Frau Grüninger zu nennen, die am Entwurf eines realisierbaren Aufbaus maßgeblich beteiligt

waren und damit den Werkstätten vermutlich einiges erspart haben. Herr Lackner und Herr Dr. Heusser haben mir sehr geholfen, wenn es um Strahlenschutzbelange ging, insbesondere beim Einbau der neuen Positronenquelle, aber auch bei vielen anderen Fragen. Dankeschön!

Herrn Vogt von der Bibliothek möchte ich dafür danken, daß er mir verschiedene Artikel besorgt hat, die ich für die Anfertigung dieser Arbeit gut gebrauchen konnte.

Der ganzen Gruppe Schwalm danke ich schließlich für die schöne Zeit und die angenehme Atmosphäre. Ganz besonders gilt dieser Dank meinen Büronachbarn und der Besetzung des mittäglichen Kaffeetischs für die gute Stimmung, den Humor and die vielen Diskussionen.

Ein großes Dankeschön geht nicht zuletzt an meine Eltern, die meine Interessen von klein auf gefördert haben und so auch die Voraussetzungen geschaffen haben, daß diese Arbeit jemals entstehen konnte.

Schließlich möchte ich mich bei meinen Freunden bedanken. Sie haben dafür gesorgt, daß ich auch die Phasen gut überstanden habe, in denen nichts so richtig zu funktionieren schien.